XIII

RECENT ADVANCES IN GEOTECHNICAL ENGINEERING PRACTICE

PROCEEDINGS

OCTOBER 8, 1982

PROCEEDINGS OF THE THIRTEENTH OHIO RIVER VALLEY SOILS SEMINAR

RECENT ADVANCES IN GEOTECHNICAL ENGINEERING PRACTICE

October 8, 1982

Holiday Inn, North
Lexington, Kentucky

sponsored by

KENTUCKY GEOTECHNICAL GROUP, ASCE

UNIVERSITY OF KENTUCKY
DEPARTMENT OF CIVIL ENGINEERING
OFFICE OF CONTINUING EDUCATION

UNIVERSITY OF LOUISVILLE
DEPARTMENT OF CIVIL ENGINEERING

and

CINCINNATI GEOTECHNICAL GROUP, ASCE

UNIVERSITY OF CINCINNATI
DEPARTMENT OF CIVIL AND ENVIRONMENTAL ENGINEERING

HOST COMMITTEE

WE GRATEFULLY ACKNOWLEDGE THE EFFORTS OF THE FOLLOWING:

Tom Gorman, Chairman
Stokely-Cheeks and Associates

David Allen
University of Kentucky

Charles Bishop
Engineering Science

Robert Deen
University of Kentucky

Vincent Drnevich
University of Kentucky

Paul Howell
Soil Conservation Service

Ron Hurt
Parrott, Ely and Hurt

Henry Mathis
Kentucky Department of Highways

Doug Zolkowski
University of Kentucky

WE APPRECIATE THE PARTICIPATION OF THE FOLLOWING FIRMS AS EXHIBITORS AND SOCIAL HOUR SPONSORS:

ELASTIZELL SYSTEMS, INC.
2434 Dryden Road
Dayton, Ohio 45439

BRANARD-KILMAN DRILLING
P.O. Box 487
Tucker, Georgia 30084

THE REINFORCED EARTH COMPANY
4100 Executive Park Drive
Suite 9
Cincinnati, Ohio 45241

ASSOCIATED PILE AND FITTING CORPORATION
P.O. Box 1043
Clifton, New Jersey 07014

CARTHAGE MILLS, INC.
EROSION CONTROL DIVISION
1821 Summit Road
Cincinnati, Ohio 45237

TROXLER ELECTRONICS LABORATORIES, INC.
P.O. Box 12057
Corwallis Road
Research Triangle Park, North Carolina 27709

CONTENTS

RELIABILITY IN GEOTECHNICAL ENGINEERING - A WARRANT

by Milton E. Harr, Professor of Geotechnical Engineering
Purdue University, W. Lafayette, Indiana
for Ohio River Valley Soils Seminar, Lexington, KY, Oct. 8, 1982

At the turn of the 19th into the 20th century an International Conference was convened in the Balkans. In attendance were many of the famous physicists of the time. The purpose of the meeting was to explore the expected role of physics in the 20th century. It was the overwhelming conclusion of the participants that the role of physics in the 20th century would be that of "refining constants"; that is, of adding another significant figure to say the speed of light. The claim was made that "all that needed to be known in physics was already known!"

Shortly after the Balkan Conference, in the years 1904/1905, a revolution took place. It happened so quickly that it is difficult to call it an evolutionary process. Once it began, physics and subsequently all sciences as well as engineering would never again be the same. Albert Einstein and Max Plank brought forth probabilistic models: Einstein in his derivation of Brownian motion and Plank in his development of quantum mechanics. It is of some interest to reflect that Einstein's and physics' first comprehensive probabilistic model was completely overlooked by him when he stated, some years later, "God does not play dice with the cosmos!" Maybe he does.

The major thrust of physics today is mainly probabilistic. Heisenberg in presenting his "uncertainty principle" demonstrated that it is impossible to determine simultaneously both the position and velocity of a particle: it can only be inferred probabilistically. The real world is casual, not causual!

It is the role of engineering to provide for the transfer of energy at levels that can be tolerated. It is the form of this energy that dictates the special branch of the engineer: electrical, mechanical, chemical, civil, etc. Within this framework, it is the function of the civil engineer to provide for the transfer of energy at tolerable levels by and for the civilian population. In this regard, professionally, all engineers are in the "filter business". In addition, unlike the scientist, who can luxuriate and bask in reflected thought concerning his problem indefinitely, the engineer must come up with a workable solution and must do so within very severe time constraints. This is the agony and the ecstasy of our profession.

In truth, the engineering profession finds itself today participating in two revolutions. In the past, each branch of engineering was formed as a "spin-off" from civil engineering, which in turn is believed by some engineers to have broken away from agricultural engineering. Until very recently it was the aim of developed procedures in each of the branches of engineering to provide solutions to problems at such a level that practitioners working at a desk with a piece of paper, a pencil and a slide rule could make assessments of their designs. Today, hand-held

calculators have rendered slide rules obsolete. An engineer has available computational capabilities that were inconceivable only a decade ago, and this technological advantage is increasing exponentially. As an example, today this writer owns a programmable calculator (that uses a magnitized slip of paper) that has far more computational capabilities than did all the computers at Purdue University when he received his doctorate degree (which wasn't that long ago). The ability of the engineer to "crunch" numbers has revolutionized present practice.

The second revolution in which we are presently participating is accommodating the uncertainties encumbent in analyses and the ability to predict performance. It is the movement from deterministic to probabilistic modeling. In common with the development of computers, this too must be described as a revolution; albeit, it is only in its beginning phase. The two are not independent revolutions; however, they are also not completely dependent. Motivating the probabilistic movement, among other things, is the type of problems that the profession is being asked to solve. Consider only a few: The decaying of America, to quote a recent issue of "NEWSWEEK" in their assessment of our highways, dams, sewer systems, etc.; the proposed MX system; groundwater pollution, perhaps the most important problem of all from a point of view of soil mechanics; foundations for nuclear power plants; stability of soil structures under high risk excavations; the use of new materials and of recycled materials; verification testing; accounting for new information in an objective manner; etc.

Consider the present civil engineering system. Many alternate forms are possible but essentially, in concept, they reduce to the metaphorical "chain" shown in Fig. 1. The metaphor is even more closely established when one considers that the polishing of only one link, say "FORMULAS", will provide the chain with a single shiny link but in doing so will also serve to weaken the system. That is, if one improves one of the components to the total disregard of the others, the system is not necessarily better. Needless to say, the link called "FORMULAS" is the easiest to alter: it can be done so while sitting at one's desk or simply by invoking "computer-power". A theoretical finite element solution, uncoupled from other considerations, does not necessarily lend more confidence to the overall process.

Consider each of the four links.

SAMPLING:

What fraction of the soil body, influenced by a structure, do we sample? Even a cursory assessment shows this to be, at best, one part in 250,000. In some structures, such as highways, it may even be one part per million. Consider that good engineering design seeks a level of performance at a level of reliability of 0.999 or a probability of failure of 1×10^{-3}. Considering the paucity of samples, this is not unlike seeking a needle in a haystack or measuring millimeters with a meter stick. The sampling process itself reeks of "the tail wagging the dog". Because rotary motion is such an efficient mode of sampling we remove cylindrical samples from the soil and these, in turn, provide the basis for most laboratory testing. (How many cylindrical soil structures have ever been built?) Suppose after carefully removing the sample from the tube and after having followed an undisturbed and very careful sampling procedure, the specimen exhibits

a crack. How does this information become part of the design process? Or, is the sample discarded because it is not the proper height to fit into the triaxial apparatus? Yet, there is little information to be obtained from a very thorough laboratory testing program that is as important as the appearance of a crack in the sample after its careful removal under "undisturbed" conditions.

LABORATORY TESTING:

All laboratory tests, irrespective of their intended use, produce results that quantify some theory. If not, how does one know what to measure? Often, the test is dictated by simplicity. Simplicity, by itself, is often a virtue; however, it may also be wrong. Consider that the triaxial test is based upon Mohr's circle, which assumes weightless and point-wise attributes and pleads the state of equilibrium at the point in question. When used in the triaxial apparatus this is reduced to assuming the cylinder as a "two-dimensional point" and considering only the major and minor principal stresses as being significant. In fact, it is always assumed that the stresses (or pressures) that one can measure are the only ones that are pertinent. Be this as it may, when used in conjunction with the other links in the chain in Fig. 1 we are indeed able to "BUILD WITH CONFIDENCE". As an additional example of the numbers of tests and "parameters" that are required, consider that the profession employs a lexicon that necessitates not only the Latin alphabet but a good part of the Greek alphabet with both upper and lower subscripts and lower case as well as capital letters (e.g., ϕ, c, E, μ, γ, σ'_o, K_o, etc.).

FORMULAS:

Present treatment of soil bodies pleads the existence of a continua. Historically, this evolved from formulations for incompressible liquids to those for compressible solids by simply introducing tangential forces into the latter. Whereas, developed formulas and procedures for incompressible fluid flow required only one parameter, the unit weight of the material, the addition of tangential forces rendered equilibrium alone to be insufficient when equating the available equations and the unknown quantities.

Early in the 19th century when metals began to gain usage in ships and railroad trains, considerable interest was directed toward the action of solid bodies under loadings. This led to the formulation of the classical "Theory of Elasticity". In its basic form, the theory presents 15 equations for the 15 unknowns, all specified at a point. In addition, assuming linearity between stresses and strains and those to be without memory, 36 (81 for some formulations) elastic constants are required! In one "fell swoop" by inventing "ISOTROPY" the 36 constants were reduced to 2: Young's modulus and Poisson's ratio. The transformation, from point-wise attributes to global, body-wise considerations, are achieved by invoking "HOMOGENEITY". Assumed in these two transformations are the existence of matter at all points within the boundaries of the medium. Hardly the real state of affairs for soils. The major differences among the various types of continua theories are in their assumed "constituitive equations". For example, theories of plasticity exist that specify the relationship between stress and strain as being time and/or nonlinearly dependent. Again, in spite of the gross simplifications,

matters are accommodated when the link of "FORMULAS" is incorporated as a proper unit within the system shown in Fig. 1.

EXPERIENCE:

In geotechnical engineering, experience is generally quantified as a tolerable or allowable minimum "factor of safety". The allowable factor of safety itself depends upon the particular design under consideration. For example, for a retaining wall a minimum allowable factor of safety of approximately 2 would be required; for slope stability, approximately 1.3; and for bearing capacity, approximately 4. Yet, in all of these problems all the other links in the metaphorical chain would be the same. As a note in this regard, the region of the upstream slope of a dam usually has the highest and lowest allowable factor of safety in geotechnical engineering: for rapid drawdown at this face a minimum factor of safety would be specified of about 1.05; whereas, an upstream blanket for a dam, in the same general location, requires a factor of safety on the order of 20!

Where did the numerical values that constitute allowable factors of safety come from? They came from the experiences of a few engineers who observed the response of geotechnical structures mainly in the time period of 1930-1960's. They witnessed the performance of a number of structures and determined the minimum allowable factors of safety required to provide (at that time) a tolerable level of failures. Consider that when these assessments were made construction conditions were very different from what they are today. The inspector on a job most likely had considerable experience, if not a bachelor's degree in civil engineering. Labor, materials, and maintenance were at different levels and mixtures of relative cost than today. Yet, the same minimum tolerable factors of safety still prevail.

An examination of current design procedures indicates that there is no relationship between allowable values for the factor of safety from one structural configuration to another; e.g., 20 vs. 1.05. In fact, there is no known scaling of the factor of safety even for a given structure. One might ask, what factor of safety should be used to double the security of a given structure? All that is truly known is that, theoretically, a factor of safety equal to unity designates incipient failure.

The four metaphorical links in the chain in Fig. 1 have been explored in some detail above. It should be noted that one of the primary benefits of "in situ" testing lies in combining the first two links of the chain. In addition, the sampling and testing procedures in laboratory work provide information relative to a soil sample that is subsequently thrown away: the soil we know the most about is not put back in the ground. Whereas, in in situ testing the soil that is tested remains as part of the structure.

The main thrust of geotechnical engineering, if not all engineering, in the future is the need to "predict the performance of things not yet done" - "PTPOTNYD". The above considerations demonstrate that the chain of events (Fig. 1) cannot do this: What factor of safety should be used for a new and untested design? Consider if we had experience only for slope stability problems, where a minimum tolerable factor of safety of 1.3 would be adequate, and had used the same measure for bearing capacity:

failures would be excessive and intolerable. What factors of safety should be specified for things for which we have no experience if we do not even know how to increase the factor of safety for structures for which we have considerable experience? Must we conduct factorial experiments over a period of many years to learn how to do new things? To be able to specify a reliability of 0.99, theoretically, one must observe the performance of at least 100 similar structures; What about a reliability of 0.999?

The answer to the question raised above is obviously "NO". Recourse must be and can only be had to probabilistic methods: the solution is to invoke the "mathematics of uncertainty". The question is: How to do so? This will first be approached in a facitious manner; however, the essentials of a very realistic and practical approach stem from this excursion.

Suppose we wish to determine the value for say the bearing capacity of a given footing such that the probability that it would not be satisfactory is at a level of performance of 1:1000 (0.1% inadequacy). One procedure would be to obtain 10,000 samples (if you want to find something at level of 1:1000 you should investigate at least 10,000 of them!), run tests on each of them and obtain their corresponding parameters ϕ, c and γ. These values would then be substituted to an appropriate bearing capacity formula to obtain 10,000 values for the bearing capacity. These could then be ordered and put into a cumulative-percentage plot, much like the grain-size distribution. We would then select the lower 10% value (10% of 10,000 equals 1,000). This is the value that we would recommend so that the likelihood it would not be adequate would be equal to or less than 0.1%. Obviously, in the real world we can't obtain 10,000 samples and run the corresponding number of tests. Realistically, we are limited to a very small number of samples. How, then, can this be accommodated?

The 10,000 samples and their results gave us a distribution of the bearing capacity of the footing. It is precisely the form of this distribution that is offered by probabilistic methods. A particular method that has considerable potential and is well within the limits of practicability was developed by Rosenblueth (1). His method when combined with the present writer's extension of the versatile Beta distribution (2) provide a distribution for any function of random variables within the order sought in geotechnical engineering problems. It is not the purpose of the present paper to present the methodology. It is the aim of the present exposition to alert the interested reader to the problem and to indicate the direction to follow to obtain its solution.

Finally, distributions can be obtained for both the "capacity" and the "demand" placed on a structure; for example, the capacity might be the bearing capacity and the demand would be the column load, which itself would be a random variable depending on live load, dead load, the position of the sun, the season, wind load, snow load, earthquakes, etc. Having the distributions of the two, a measure of the probability that the demand will exceed the capacity can be obtained: this is the probability of failure of the system. The probability that the capacity will exceed the demand is its reliability. Only through such procedures can we:

References

1. Rosenblueth, E.: "Point Estimates for Probability Moments", Proc. Nat. Acad. Sci., USA, Vol. 72, No. 10, Oct. 1975.

2. Harr, M. E.: "Mechanics of Particulate Media: A Probabilistic Approach", McGraw Hill Book Company, 1977.

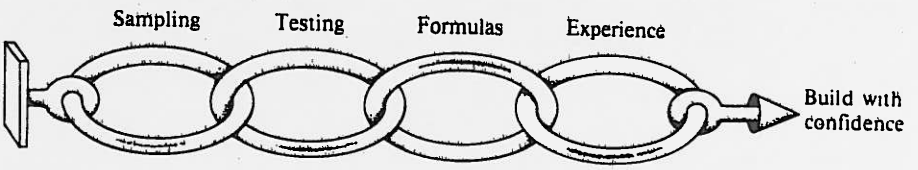

Figure 1

A NEW APPROACH FOR CONSOLIDATION SETTLEMENT ANALYSIS

BY: Chitta R. Gangopadhyay[1]

INTRODUCTION

Consolidation Settlement Analysis is conventionally done using the method by Terzaghi-Taylor or by Skempton-Bjerrum (10, 15, 18). Both the methods implicitly assume that the horizontal stresses developed in the clay become adjusted during consolidation in such a manner that the condition of zero lateral strain or one-dimensional deformation is maintained. This assumption is equivalent to the stress point (Figure 1) after undrained loading to move from point 1 to point 6 (Terzaghi-Taylor) or from point 5 to point 6 (Skempton-Bjerrum), both along the Ko-line. In actual practice, it is more common that there will be lateral deformations during consolidation, so that the effective stress path will not follow the Ko-line.

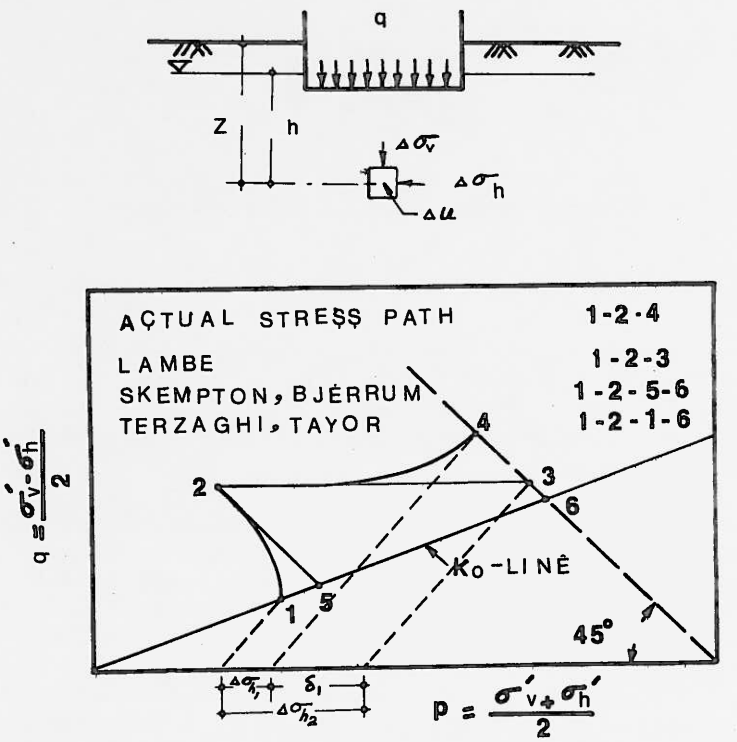

FIG. 1.- Field Stress Paths on Foundation Loading

A direct approach that can be considered to take into account the effect of lateral deformation is to first subject the sample to the initial in-situ stresses, and then to stress changes it is likely to undergo on loading in the field. This approach has been suggested by Lambe (10, 11) in his stress-path method of settlement analysis. Using this method, the assumption is that the increase in the effective stresses during consolidation is isotropic, so that the field stress path will be 2-3 (Figure 1), resulting in no change in total horizontal stress. Davis & Poulos (6) and Kerisel and Quatre (9) have suggested different forms of this approach.

In reality, however, the shear strength, the stress-strain modulus and Poisson's ratio would change during consolidation. Such changes in soil properties are unlikely to cause any significant changes in the vertical stress. However, the total horizontal stress will decrease during consolidation due to the change in soil properties by $\delta = \Delta\sigma_{h_1} - \Delta\sigma_{h_2}$ in which $\Delta\sigma_{h_1}$ = total horizontal stress increment after undrained loading and $\Delta\sigma_{h_2}$ = total horizontal stress after consolidation (Figure 1). The reduction in total horizontal stress should cause the stress point to move from 2 to 4

[1]Associate Professor of Civil Engineering Wayne State University Detroit, Michigan

(rather than from 2 to 3) during consolidation. Thus, the increase in effective stress during consolidation is not likely to be isotropic.

For a normally consolidated or lightly overconsolidated clay, field elements beneath the center of a footing may be in a near-failure state (5). The initial total horizontal stress increment, $\Delta\sigma_{h_1}$, should be such that, in conjunction with the total vertical stress increment, $\Delta\sigma_v$, the shear strength of the soil, S_u, is not exceeded. Thus, the undrained stress distribution beneath the center of the footing immediately after loading may need adjustment from values predicted by any stress distribution theory, such as by Poulos (12) or other methods (3).

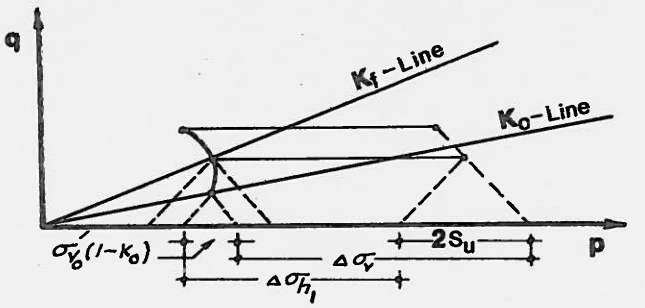

FIG. 2.- Adjusted Total Horizontal Stress Increment

Figure 2 indicates that the adjusted total horizontal stress increment $\Delta\sigma_{h_1}$ can be obtained from (4, 5, 7):

$$\frac{\Delta\sigma_{h_1}}{q} = \frac{\Delta\sigma_v}{q} - \frac{\sigma'_{v_o}}{q}\left[2\,S_u/\sigma'_{v_o} - (1-K_o)\right] \quad ---(1)$$

in which q = applied footing stress, σ'_{v_o} = present effective overburden pressure, Ko = coefficient of earth pressure at rest.

This paper presents the effects of stress path on the axial and volume strain during consolidation of an artificially sedimented, normally consolidated kaolinite. A method of consolidation settlement analysis is proposed, and then used to analyze the consolidation settlement of a model footing. The proposed method of settlement analysis considers excess pore pressure development due to undrained loading based on $\Delta\sigma_{h_1}$ determined after adjustment, as mentioned in the previous paragraph. The method considers the influence of more realistic field stress paths similar to 2-4 (Figure 1) on the consolidation settlement. The existing stress path methods involve laboratory Triaxial Tests which are difficult for routine use. The proposed method takes into account the effect of stress path on consolidation settlement in an indirect manner by using the results of routine laboratory tests in a theoretical relationship based on anisotropic elasticity.

EXPERIMENTAL PROGRAM

In order to study the effect of stress path on consolidation settlement, a series of Triaxial Tests were carried out using 1-13/16 inch diameter specimens of a normally consolidated kaolinite (L.L. = 52.8%, P.L. = 4 .1%, clay fraction = 25.4%). The kaolinite was deposited in a sedimentation tube at a water content equal to twice the liquid limit. After sedimentation, the soil was first one-dimensionally consolidated to 12.5 psi in the tube, and then transferred to the triaxial apparatus. The samples were then consolidated under Ko-condition with a back pressure of 30 psi to vertical effective stress (σ'_{v_o}) levels of 30, 45, 5 and 60 psi. Two series of tests were then performed using the same initial vertical stress level, σ'_{v_o}, and the same vertical stress increment, $\Delta\sigma_v$, for each series.

Series A - Samples were first subjected to vertical and horizontal stress increments ($\Delta\sigma_v$ and $\Delta\sigma_h$, respectively) under undrained conditions to simulate stress path 1-2 (Figure 1) of the undrained loading stage beneath a foundation. Then the samples were allowed to consolidate along different stress paths (similar to 2-4 (Figure 1)). To achieve this, the vertical stress was maintained constant and the cell pressure was

slowly lowered so that the final effective stress increment ratios, $\Delta\sigma_3'/\Delta\sigma_1'$, after consolidation were 1.0, 0.75, 0.62 and 0.5. It may be noted that the samples in this series approximately represented hypothetical field elements at different depths when the rate of loading was fast.

Series B - In this series, the samples were subjected from the initial Ko-state to drained compression along different stress paths. The cell pressures were adjusted to obtain effective stress increment ratios, $\Delta\sigma_3'/\Delta\sigma_1'$, of 0, 0.2, 0.4 and 0.5. The Series B tests show rate of loading with no appreciable pore pressure development.

Prior determination of the value of Ko for this test program was made by running a series of constant stress ratio drained tests. The specimens for these tests were prepared in the sedimentation tube with a vertical one-dimensional consolidation pressure of 6.25 psi. These samples were first consolidated to an all-around pressure of 3 psi in a triaxial cell, and then the cell pressure and the deviator stress were gradually adjusted so as to follow a path of constant ratio. The value of Ko was determined, by interpolation, to be the effective stress ratio at which the ratio of axial strain ϵ_1 to the volumetric strain ϵ_v was equal to 1. The value of Ko was found to be 0.5. All the tests were carried out under "free end" conditions using lubricated end platens. The loads were measured inside the triaxial cell with a load transducer. A strain rate of 0.025 mm per minute was used for the drained tests. The pore pressure was monitored, and both the axial and volume strains were measured.

TEST RESULTS

Ko-Consolidation - Figure 3 shows the vertical effective stress versus void ratio relationship obtained from these tests. Also plotted on this figure are the results of an oedometer test on the same kaolinite. It is seen that a straight line relationship is obtained on the semi-logarithmic plot for the two types of tests. The value of compression index C_c is found to be 0.335.

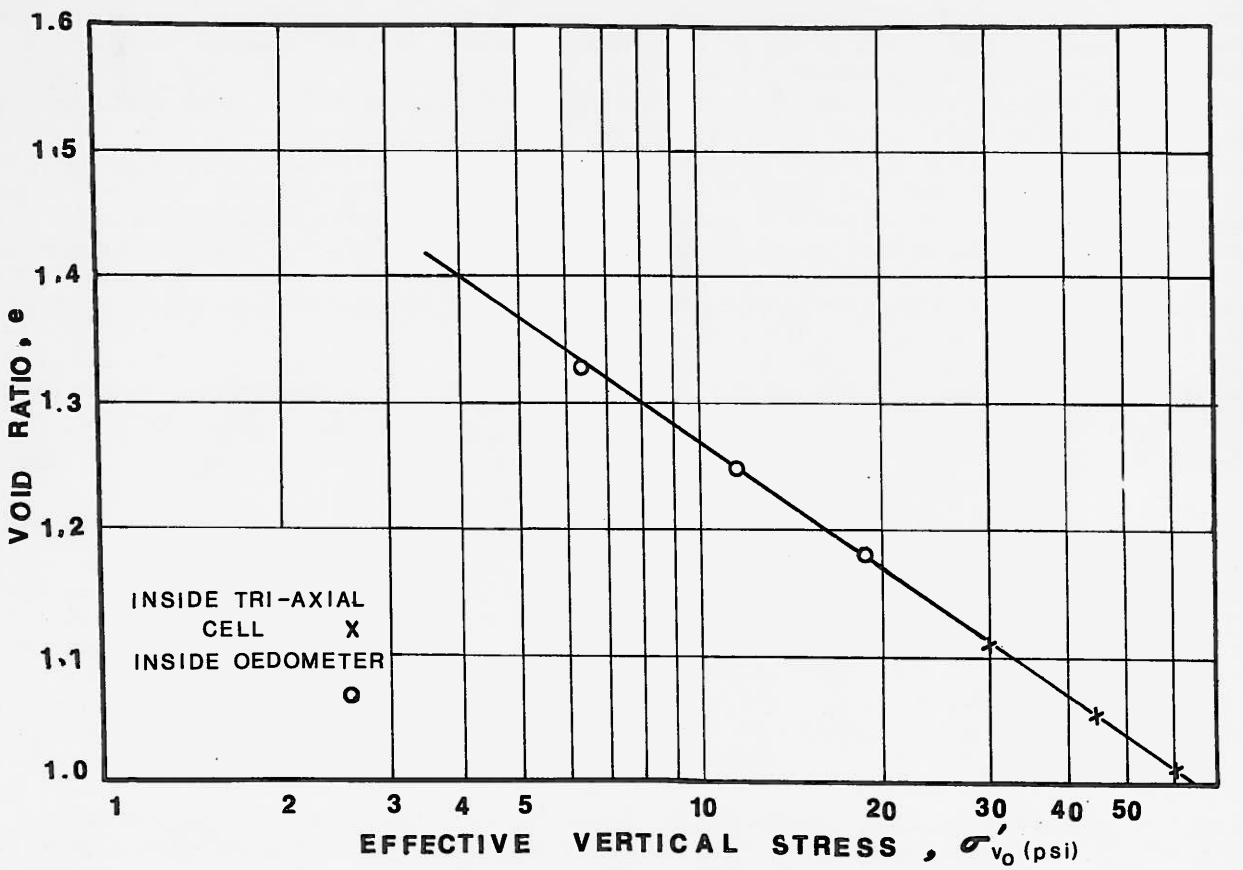

FIG. 3.- e Versus Log σ_{v_o} Curve from One-dimensional Consolidation Tests

Stress Paths - Figure 4 shows the effective stress paths followed by samples of Series A and B tests with the initial vertical effective stress $(\sigma_v')_o$ of 30 psi. Similar stress paths were obtained for other values of $(\sigma_v')_o$. In Series A tests, the rate of lowering the cell pressure cannot be synchronized precisely with the rate of pore pressure dissipation. Stress increment ratios ($\Delta\sigma_3'/\Delta\sigma_1'$) calculated for Series A samples as 1.0, 0.75, 0.62 and 0.5 shall, for further discussion, mean the stress ratio that was obtained at the end of consolidation. In Series B tests, however, the stress increment ratio was constant throughout the drained compression.

Axial Strain - Figure 5 shows a plot of the ratio axial strain to volumetric strain (ϵ_1/ϵ_v) versus $\Delta\sigma_3'/\Delta\sigma_1'$ for all samples under Series A and B. As the normalized vertical stress increment $\Delta\sigma_1'/(\sigma_1')_o$ at the end of consolidation was almost the same for all the samples, this plot, in effect, indicates the influence of lateral stress increments on ϵ_1/ϵ_v. It is seen that two curves are obtained for the two series - the curve for Series A lying above that of Series B. The results of constant stress ratio drained tests performed to determine the value of Ko are also plotted on Figure 5. It is seen from Figure 5 that the points from these tests also lie on the curve for Series B, although the initial stress ratio with reference to which the axial and volumetric strains were calculated were different for each sample. It appears, therefore, that if there is no undrained loading prior to consolidation, the ϵ_1/ϵ_v versus $\Delta\sigma_3'/\Delta\sigma_1'$ relationship is independent of the initial stress ratio. On the other hand, if consolidation is preceded by undrained loading (Series A), the values of ϵ_1/ϵ_v are always higher than the corresponding values for Series B tests. The value of ϵ_1/ϵ_v for isotropic stress increase ($\Delta\sigma_3'/\Delta\sigma_1'$ equal to 1) is 0.4 for Series B tests and 0.48 for Series A tests. Thus, the samples of Series A were more anisotropic than the samples of Series B. This is because in Series A tests, a part of the lateral stress increase during consolidation was actually a recompression following the decrease of lateral stress during loading. Experimental curves shown in Figure 5 can be compared with the theoretically computed curves based on (a) isotropic elasticity (10), (b) anisotropic elasticity (16).

(a) Isotropic Elasticity - The relationship between the ratio of axial strain, ϵ_1, to volumetric strain ϵ_v, defined herein as strain ratio $\lambda = \epsilon_1/\epsilon_v$ and the incremental stress incremental ratio $K' = \Delta\sigma_3'/\Delta\sigma_1'$ can be obtained for axial stress symmetry from the following relationship due to Lambe (10):

$$\lambda = \epsilon_1/\epsilon_v = \frac{1 + \bar{K}o - 2\,\bar{K}o\,K'}{(1-\bar{K}o)\,(1 + 2K')} \quad \ldots (1)$$

in which $\bar{K}o$ = the value of K' for one-dimensional strain. The two curves indicated by dotted lines shown on Figure 5 are plots of equation (1) using $\bar{K}o = 0.5$ for Series B tests and 0.66 for Series A tests. It can be seen that the correlation with the measured relationship for both the Series is not particularly good because the assumption of isotropy is really not valid for the soil.

(b) Anisotropic Elasticity - Simons & Som (16) defines a relationship between λ and K' based on anisotropic elasticity as given below:

$$\lambda = \epsilon_1/\epsilon_v = \frac{1 - 2n\,\nu_2'\,K'}{1 + 2\nu_3'\,(K'/\bar{K}o - 1) - 2n\,\nu_2'\,K'} \quad \ldots (2)$$

in which ν_2' = the effect of horizontal strain on vertical strain.

ν_3' = the effect of vertical strain on horizontal strain.

n = ratio of drained elastic modulii in the vertical and horizontal directions = E_h'/E_v'. The effect of one horizontal strain on the other horizontal strain (i.e. ν_1') is automatically included in the term Ko. For predicting the relationship between λ and K' from equation (2), only three parameters - Ko, ν_3' and ($n\,\nu_2'$) are to be known.

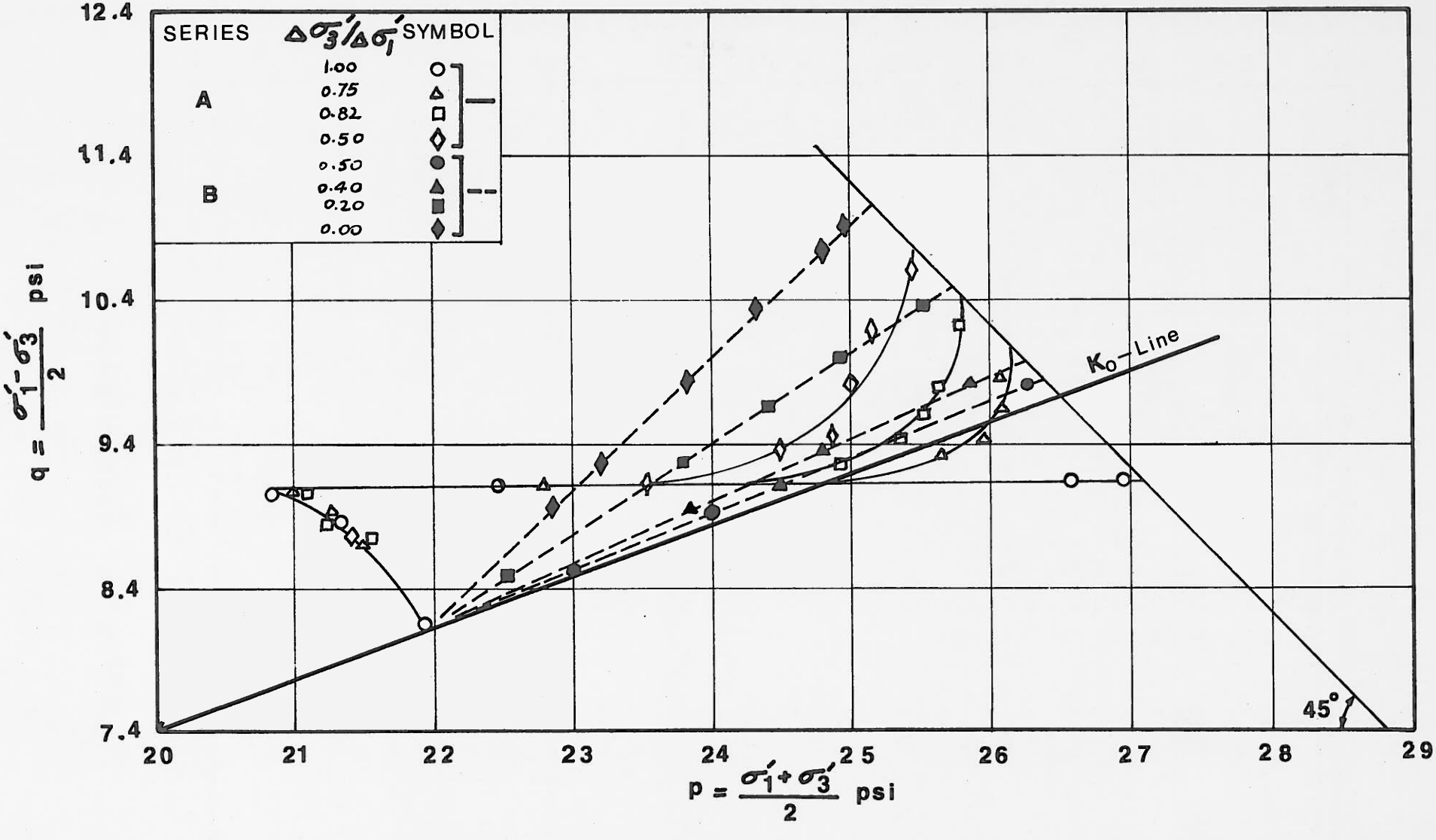

FIG. 4.- Effective Stress Paths at $\sigma_{vo}' = 30$ psi

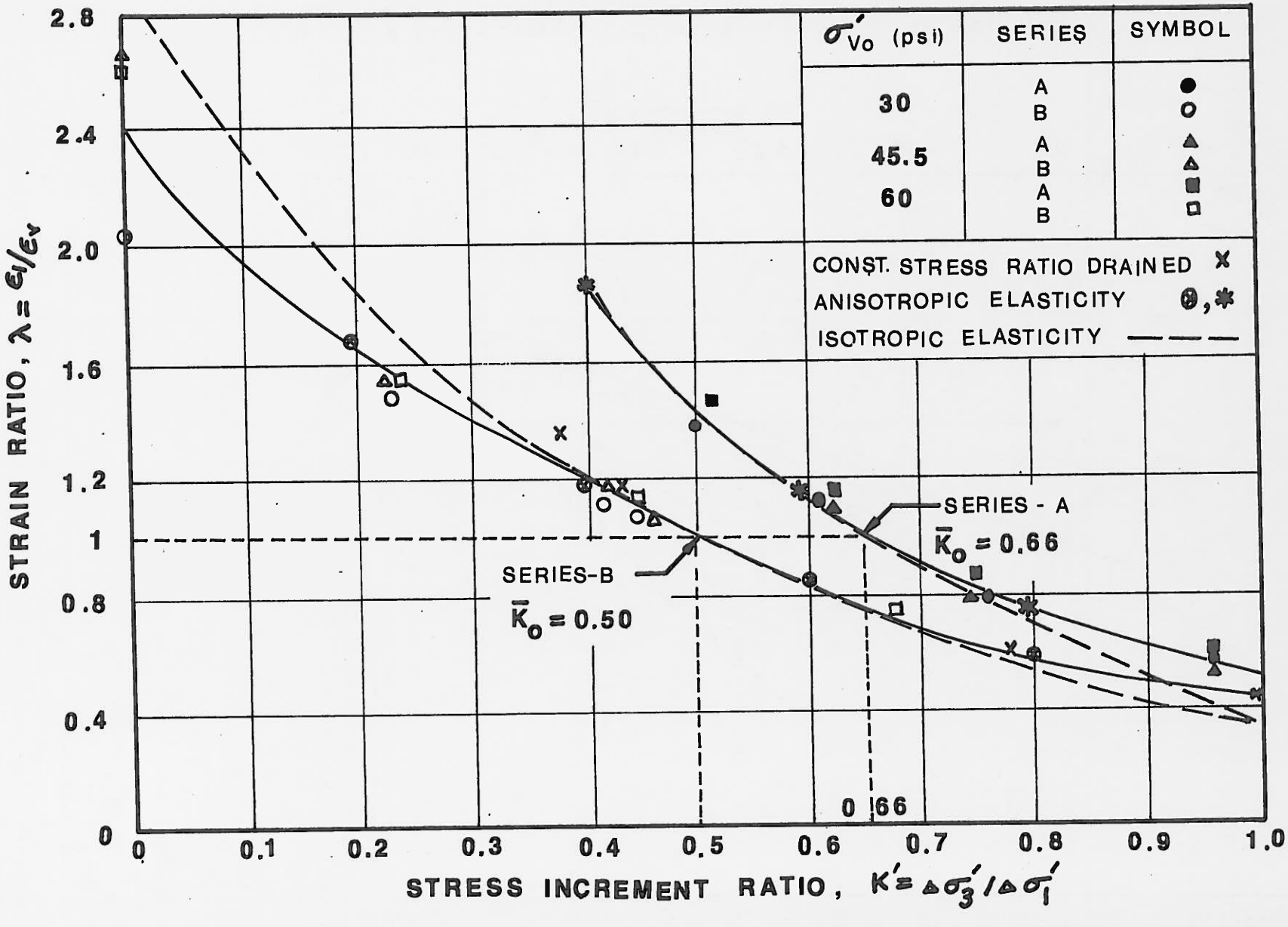

FIG. 5.- Strain Ratio, λ Versus Stress Increment Ratio, $\Delta\sigma'_3/\Delta\sigma'_1$

Using the results of a conventional drained triaxial test ($K' = 0$) and an isotropic consolidation test ($K' = 1$), the corresponding $\epsilon_1/\epsilon_v = 2.44$ and 0.4 for Series B tests (Figure 5). For the Series A tests, $\epsilon_1/\epsilon_v = 1.45$ for $K' = 0.5$ and $\epsilon_1/\epsilon_v = 0.48$ for $K' = 1$.

Using $\overline{K}o = 0.5$ for Series B tests, equation (2) becomes:

$$\epsilon_1/\epsilon_v = \frac{1 - 0.606K'}{1 + 0.59\ (2K'-1) - 0.606\ K'} \quad \ldots\ldots (3)$$

For Series A tests, $\overline{K}o = 0.66$, and the relationship from equation (2) becomes:

$$\epsilon_1/\epsilon_v = \frac{1 - 0.564\ K'}{1 + 0.92\ (1.515K'-1) - 0.564\ K'} \quad \ldots\ldots (4)$$

The curves obtained from equations (3) and (4) have also been plotted on Figure 6, and they are found to agree almost exactly with the respective experimental data.

PROPOSED METHOD OF SETTLEMENT ANALYSIS

A method of analysis of consolidation settlement is proposed herein which takes into account the influence of stress path. A general expression for vertical settlement is given by (16):

in which $\rho_c = \int_0^z \lambda\,(m_v)_3\,\Delta u\,dz \quad \ldots\ldots\ldots\ldots\ldots\ldots\ldots\ldots (5)$

λ = strain ratio ϵ_1/ϵ_v which is a function of K';

$K' = \Delta\sigma_3'/\Delta\sigma_1'$ during consolidation;

Δu = pore pressure developed during loading;

$(m_v)_3$ = volumetric compressibility corresponding to three-dimensional strain;

z = the thickness of clay stratum

The value of λ can be determined from experimentally-determined relationships shown on Figure 5. It can be seen that this relationship depends on the stress history of the soil. The curve for drained compression is different from the case where consolidation is preceded by undrained loading. To be realistic, the latter should be considered for use in the settlement analysis. But this curve would be different for different depths, and the test procedure is somewhat complicated for routine use. However, the difference between the two curves reduces considerably as the ratio $\Delta\sigma_3'/\Delta\sigma_1'$ approaches unity (K' ranges between Ko and 1 during consolidation in the field). The curves for drained compression can be obtained either from constant stress ratio consolidation tests or from theoretical relationship based on anisotropic elasticity, using data from some simple tests like standard drained Triaxial Tests and Isotropic Consolidation Tests. For some soils, the difference between the two curves can be investigated from laboratory tests. However, in the present investigation, the relationship between ϵ_1/ϵ_v versus $\Delta\sigma_3'/\Delta\sigma_1'$, as obtained from drained compression (the lower curve in Figure 5), has been used to study the settlement behavior of model footings.

Many researchers have found that the volume change of clays is governed primarily by the major principal effective stress, the other stresses exerting little or no influence (2, 14). Thus, the value of $(m_v)_3$ can be determined from oedometer tests. However, some clays have shown that the volume change may be a function of the average principal effective stress (1, 8, 13). The kaolinite used indicated some dependence of $(m_v)_1$ on the stress increment ratio K', where $(m_v)_1$ is the volumetric compressibility based on the major principal effective stress (7). However, the effect of such dependence on settlement was small.

The complete procedure for the proposed method of analysis for an inelastic soil medium is enumerated below:

1. Divide the compressible stratum into a number of layers.

2. Compute the vertical and horizontal stresses at the center of each layer. The stresses immediately upon loading ($\Delta\sigma_v$ and $\Delta\sigma_{h_1}$) may be obtained by adjustment from elastic theory (as in Figure 6). The horizontal stresses reached at the end of consolidation ($\Delta\sigma_{h_2}$) may be approximately taken as that originally obtained from elastic analyses prior to adjustment.

3. Calculate the excess pore pressure, Δu, at the center of each layer from the relationship(17):

$$\Delta u = \Delta\sigma_{h_1} + A(\Delta\sigma_v - \Delta\sigma_{h_1}) \quad \ldots\ldots\ldots\ldots \quad (6)$$

The value of the pore pressure coefficient A may be determined from laboratory tests or estimated from the stress history and the probable strain level.

4. The increase of effective vertical stress, $\Delta\sigma_v'$, during consolidation will be equal to Δu. Compute the increase in effective horizontal stress, $\Delta\sigma_h'$, from $\Delta\sigma_h' = \Delta u - \delta$ in which $\delta = (\Delta\sigma_{h_1} - \Delta\sigma_{h_2})$ = decrease in horizontal total stress during consolidation.

5. Compute volume strain of each layer from:

$$d\epsilon_v = (m_v)_1 \Delta\sigma_v' \quad \ldots\ldots\ldots\ldots \quad (7)$$

6. Compute $K' = \Delta\sigma_h'/\Delta\sigma_v'$; using the relationship between K' and λ (obtained either experimentally or from expression for anisotropic elasticity). Find the value of $\lambda = \epsilon_1/\epsilon_v$.

7. Compute the vertical deformation of each layer from either of the expressions:

$$\Delta\rho_c = (m_v)_1 \Delta\sigma_v' dH \quad \ldots\ldots\ldots\ldots \quad (14)$$
$$(15)$$

in which dH is the thickness of each layer.

8. The consolidation settlement, P_c, is now obtained as:

$$\rho_c = \sum \Delta\rho_c \quad \ldots\ldots\ldots\ldots \quad (16)$$

If the loading and the soil condition is such that elastic theory can be used for computing stresses (that is, overconsolidated clays with small load increments), then K can be directly obtained from theoretical considerations (Reference 18).

MODEL TESTS

The applicability of the proposed method of settlement analysis was verified in large size instrumented model footing tests. Both vertical and horizontal stress distributions were measured using pressure cells, and excess pore pressures were measured using small pore pressure pick-ups (5). The settlement of a circular footing of 7.48 in. (190 mm) effective diameter resting on a normally consolidated bed of kaolinite of about 30 in. (762 mm) thick was measured. A surcharge load of 6.4 psi (equal to the vertical effective stress at consolidation) was placed over the entire area of the soil in order to keep it in a normally consolidated condition. Two tests, designated as tests A_1 and A_2 were performed at different footing pressures [q = 6.58 psi, i.e. $q/\sigma_{vo}' = 1.03$ for test A_1 and q = 5.10 psi, i.e. $q/\sigma_{vo}' = 0.8$ for test A_2] . Figure 6 presents the results of measured and computed stress distributions beneath the model footing. It can be seen from this figure that the horizontal stresses decreased with consolidation.

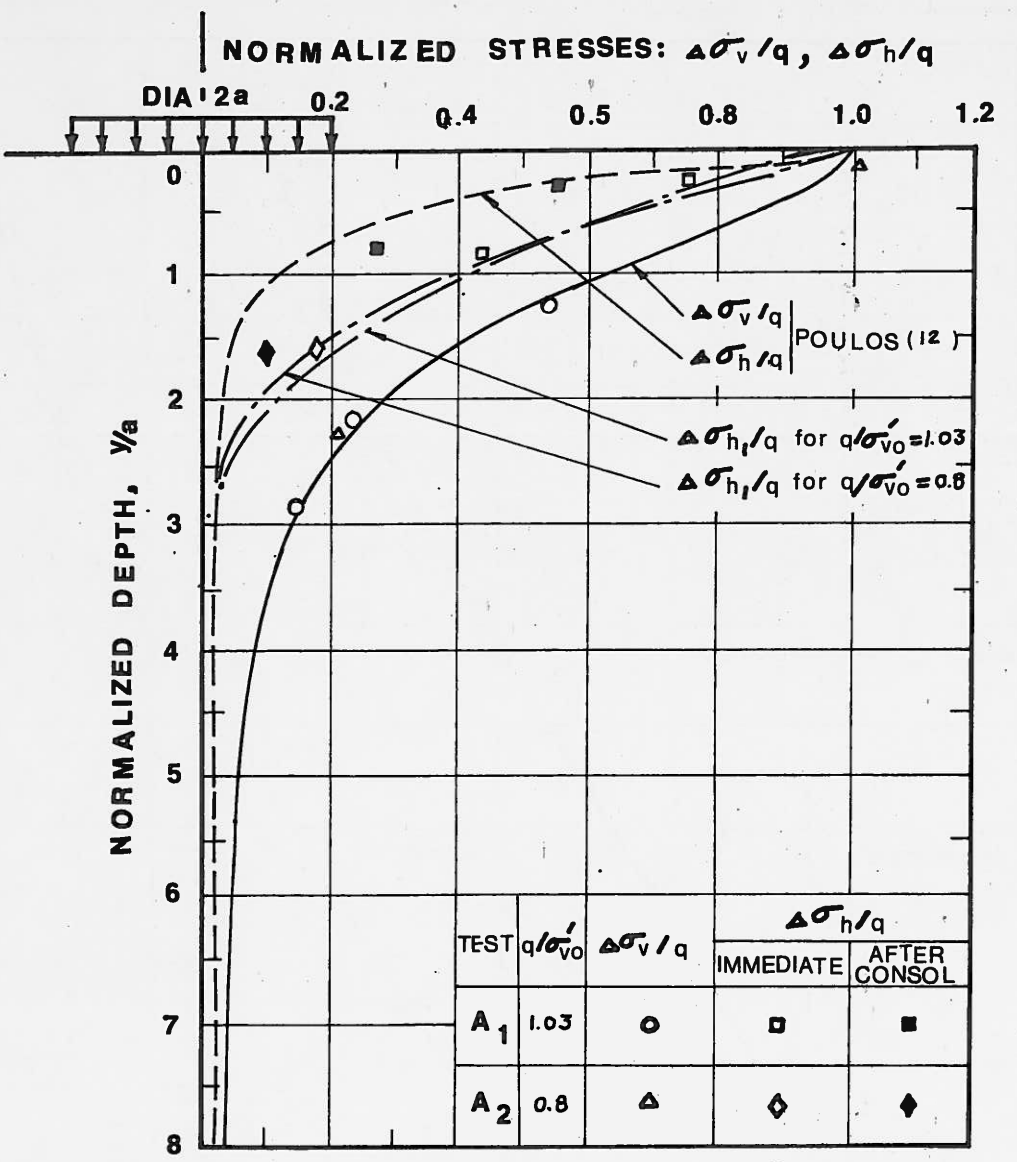

FIG. 6.- Computed and Measured Stress Distribution

This might be possible due to the decrease of Poisson's ratio from 0.5 (undrained value) to its fully drained value. With consolidation, the clay gains in shear strength. If the vertical stresses do not change during consolidation, then the horizontal stresses required to keep the stress difference within the yield limit will decrease. The resulting distribution of stresses may bring the horizontal stresses much closer to those obtained from elastic analyses with $\nu = 0.5$. This was observed in the model tests (Figure 6).

The settlement data are presented in Figure 7. Separation of immediate and consolidation settlement by log-time fitting method gave the results shown in Table 1.

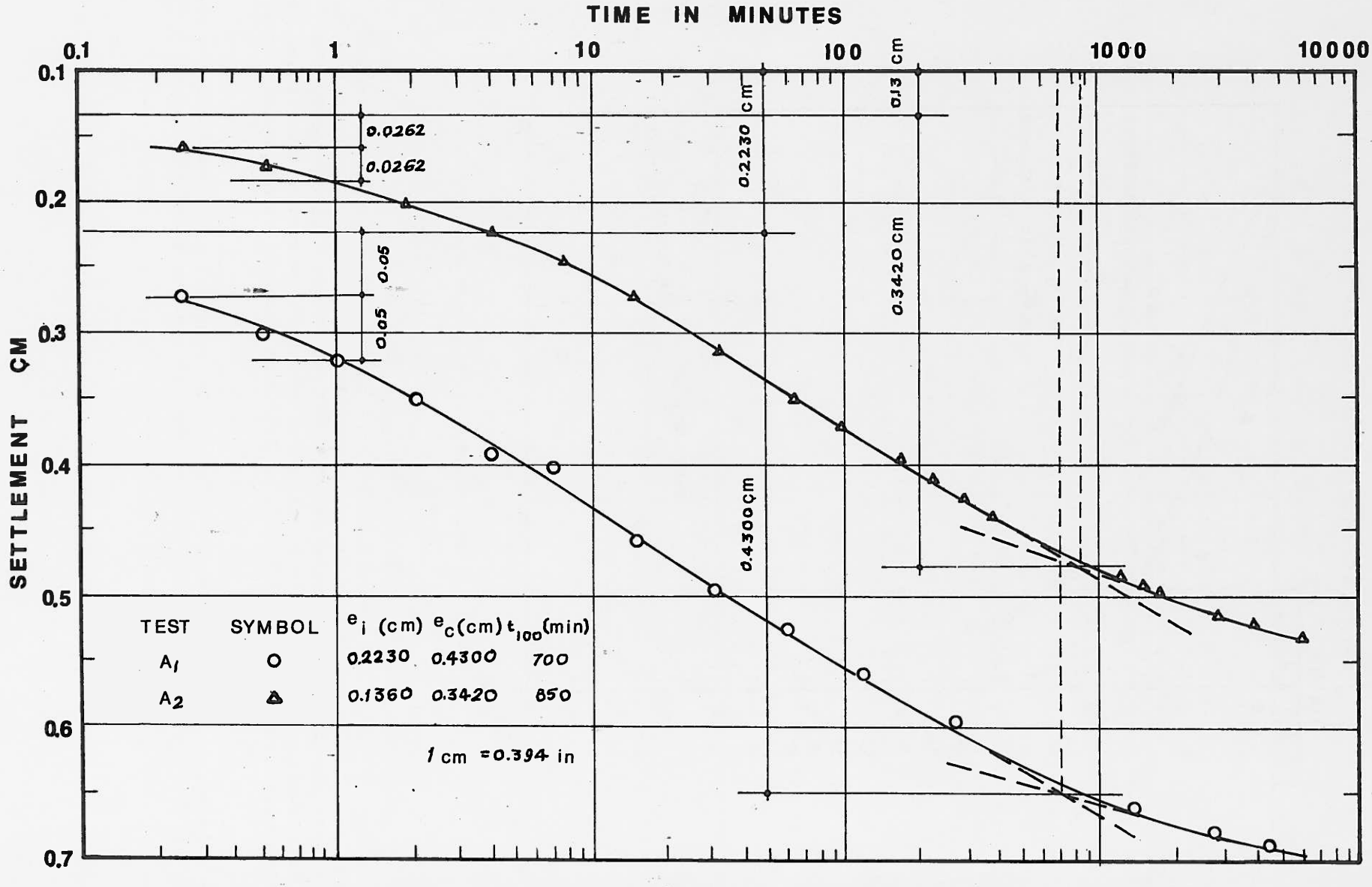

FIG. 7.- Time-Settlement Curve from Model Tests

TABLE 1 - SETTLEMENT DATA FROM MODEL TESTS

Test No.	Footing Pressure, In Pounds Per Square Inch	q/σ_{vo}'	Immediate Settlement, ρ_i, In Inch	Consolidation Settlement, ρ_c, In Inch
A_1	6.58	1.03	0.088	0.17
A_2	5.10	0.80	0.054	0.135

PREDICTED VERSUS MEASURED SETTLEMENT

The consolidation settlement of the model footing described above was analyzed by Terzaghi-Taylor method, Skempton-Bjerrum method, and by the stress path method proposed herein. The relationship between λ and K' was taken as those obtained for Series B in Figure 6. Separate calculations were made with measured stresses, stresses obtained by adjustment from measured stresses (Figure 6) and Boussinesq stresses.

In the settlement analyses, the pore pressure coefficient A was taken as 0.85. This was obtained as the weighted average of the measured values. Table 2 gives a comparison of the settlements calculated by the different methods with those measured in the model test. It can be seen that the proposed stress path method gives a much better prediction of the settlement than by the methods in current use.

TABLE 2 - COMPARISON OF PREDICTED AND MEASURED SETTLEMENTS

Test No.	Stress-Distribution	Calculated Settlement, In Inch			Measured Settlement, In Inch
		Terzaghi-Taylor Method 1	Skempton-Bjerrum Method 2	Proposed Stress-Path Method	
A_1	Measured	0.27	0.26	0.14	0.17
	Adjusted from Poulos (Figure 7)	0.26	0.24	0.18	
	Boussinesq (3, 4)	0.25	0.23	0.11	
A_2	Measured	0.22	0.20	0.11	0.135
	Adjusted from Poulos (Figure 7)	0.20	0.19	0.12	
	Boussinesq (3, 4)	0.20	0.18	0.08	

Table 2 shows that the result of settlement analyses depends on the assumed stress distribution. When the analysis is made with the measured distribution and the proposed method, calculated settlement is only slightly less than the measured value. Methods 1 and 2, on the other hand, grossly overestimate the settlements. Stress distribution obtained by adjustment from Poulos is almost the same as the measured distribution, and consequently, this adjustment method could yield very good prediction of settlement by the stress path method. Also note that when Boussinesq stresses are used, the stress path method considerably underestimates the settlement.

CONCLUSIONS

1. The deformation of soil elements in the field depends largely on the stress path followed during loading and consolidation.

2. A relationship between the strain ratio ϵ_1/ϵ_v, and the stress increment ratio $\Delta\sigma'3/\Delta\sigma'1$ for drained deformation can be obtained from properly performed Triaxial Tests or can be theoretically computed from consideration of anisotropic elasticity.

3. A method of settlement analyses (the stress-path method) has been proposed wherein the effect of stress path during consolidation is taken into account. The volume strain is calculated using the data obtained from oedometer tests. The axial strain or the consolidation settlement is then obtained from this volume strain using a properly determined relationship between ϵ_1/ϵ_v and $\Delta\sigma'3/\Delta\sigma'1$. This method has been found to give much better prediction of consolidation settlement of the model footings studied herein than by the methods in current use, provided the stress distribution is correctly estimated.

REFERENCES

1. Akai, K. and Adachi, T., "Study of One-dimensional consolidation and the shear strength characteristics of Fully Saturated Clay in terms of Effective Stresses", Proceedings 6th. International Conference on Soil Mechanics and Foundation Engineering, Vol. 1, Montreal, Canada, 1965, pp. 146-150.

2. Bjerrum, L., "Theoretical and Experimental Investigation on the Shear Strength of Soils", Norwegian Geotechnical Institute, Oslo, Norway, Publication No. 5, 1954.

3. Boussinesq, J. V., "Application des Potentials a Latude de L'Equilibre et du Movement des Solides E'Lastiques", Gannthier-Villers, Paris, France, 1885.

4. Das, S., "Predicted and Measured Values of Stresses and Displacements During Loading and Consolidation Under a Circular Footing Resting on a Saturated Clay Medium", thesis presented to Jadavpur University at Calcutta, India in 1975 for the degree of Doctor of Philosophy.

5. Das, Subhas C., and Gangopadhyay, Chitta R., "Undrained Stresses and Deformations Under Footings on Clay", Journal of the Geotechnical Engineering Division, ASCE, Vol. 104, No. GT 1, Proc. Paper 13463, January, 1978, pp. 11-25.

6. Davis, E. H. and Poulos, H. G., "The Use of Elastic Theory for Settlement Prediction Under Three-dimensional Conditions", Geotechnique, London, England, Vol. 18, No. 1, 1968, pp. 67.

7. Gangopadhyay, Chitta R., Das, S. and Som, N., "Stress Path Influence on Drained Deformations of Clay", Journal of the Geotechnical Engineering Division, ASCE, Vol. 106, No. GT 11, Proc. Paper 15807, November, 1980, pp. 1243-1260.

8. Henkel, D. J., "The Correlation Between Deformation, Pore Water Pressure and Strength Characteristics of Saturated Clay", thesis submitted to University of London for the degree of Doctor of Philosophy, 1958.

9. Kerisel, J. and Quartre, M., "Settlement Under Foundations - Calculations Using Triaxial Apparatus", Civil Engineering and Public Works Review: Part I (May, 1968) and Part II (June, 1968).

10. Lambe, T. W., "Methods of Estimating Settlement", Journal of the Soil Mechanics and Foundations Divisions, ASCE, Vol. 90, No. SM5, Proc. Paper 4060, September, 1964, pp. 43-67.

11. Lambe, T. W., "The Stress-Path Method", Journal of the Soil Mechanics and Foundations Divisions, ASCE, Vol. 93, No. SM6, Proc. Paper 5613, November, 1967, pp. 309-331.

12. Poulos, H. G., "Stresses and Displacements in an Elastic Layer Underlain by Rough Rigid Base", Geotechnique, London, England, Vol. 17, No. 4, December, 1967, pp. 378-410.

13. Roscoe, K. S., Schoffield, A. N., and Wroth, C. P., "On Yielding of Soils", Geotechnique, London, England, Vol. 8, No. I, 1958, pp. 22-53.

14. Rutledge, P. L., "Relation of Undisturbed Sampling to Laboratory Testing", Transactions, ASCE, Vol. 109, 1944, pp. 1155-1185.

15. Seed, H. B., "Settlement Analysis - A Review of Theory and Testing Procedures", Journal of the Soil Mechanics and Foundation Division, ASCE, Vol. 91, No. SM2, Proc. Paper 4275, March, 1965, pp. 39-48.

16. Simons, N. E. and Som, N., "The Influence of Lateral Stresses on the Stress-Deformation Characteristics of London Clay", Proceedings 7th. International Conference on Soil Mechanics and Foundation Engineering, Mexico, 1969, Vol. 1, pp. 369-377.

17. Skempton, A. W., "The Pore Pressure Coefficients A and B", Geotechnique, London, England, Vol. 4, 1954, pp. 143-147.

18. Skempton, A. W. and Bjerrum, L., "A Contribution to the Settlement Analysis of Foundations on Clay", Geotechnique, London, England, Vol. 7, No. 4, December, 1957, pp. 168-178.

NOTATION

The following symbols are used in this paper:

A = Skempton's pore pressure coefficient;

a = footing radius;

E' = drained modulus of elasticity;

E_h' = drained modulus in horizontal direction;

E_v' = drained modulus in vertical direction;

H = thickness of soil medium;

K_o = Coefficient of earth pressure at rest;

K' = stress increment ratio, $\Delta\sigma_3'/\Delta\sigma_1'$;

$\bar{K}_o$ = stress increment ratio for one-dimensional strain;

q = footing load per unit area;

S_u = undrained shear strength;

Δu = increment of pore water pressure;

γ = unit weight of soil;

γ_w = unit weight water;

δ = decrease in horizontal total stress during consolidation;

ϵ_1 = axial or vertical strain;

ϵ_v = volumetric strain;

λ = strain ratio ϵ_1/ϵ_v;

ν' = drained Poisson's ratio;

ρ_i = immediate settlement;

ρ_c = consolidation settlement;

$(\sigma_1)_o', \sigma_{vo}'$ = effective vertical stress at consolidation/vertical overburden pressure;

σ_{v1}' = effective vertical stress at the end of undrained loading;

σ_{h1}' = effective horizontal stress at the end of undrained loading;

$\Delta\sigma_v$ = increment in vertical total stress;

$\Delta\sigma_h$ = increment in horizontal total stress;

$\Delta\sigma_3'$ = effective stress increment in horizontal or lateral direction; and

$\Delta\sigma_1'$ = effective stress increment in vertical or axial direction.

INSTRUMENTATION OF SHEET PILE COFFERDAM AT LOCK AND DAM 26 REPLACEMENT SITE

Christopher B. Groves
Shannon & Wilson, Inc.
St. Louis, Missouri

Brian Kleber
U.S. Army Corps of Engineers
St. Louis District

INTRODUCTION

The replacement lock and dam is presently under construction approximately 11,000 feet downstream of the existing Lock and Dam 26 on the Mississippi River and about 25,000 feet upstream of the confluence with the Missouri River. The new lock and dam will replace the aging existing lock and dam which was constructed in 1938. Of significant importance will be the new 1200 by 110 foot lock which will replace the existing 600 by 110 foot lock through which barge traffic on the upper Mississippi and Illinois rivers must travel to reach the lower Mississippi, Missouri and Ohio rivers.

The new lock and dam will be constructed entirely in the dry using a three stage cofferdam. The first stage cofferdam will permit construction of the first six and one-half gate bays on the Missouri side of the river. Each will support a tainter gate 110 feet wide. These gate bays will be constructed in a cofferdam measuring 1200 feet by 800 feet (Figure 1). The second stage cofferdam will permit construction of the lock and the half gate bays on each side of the lock and will measure 2100 feet by 500 feet. The third stage cofferdam will permit construction of the gate bays on the Illinois side of the river and the balance of the dam and will be the smallest cofferdam.

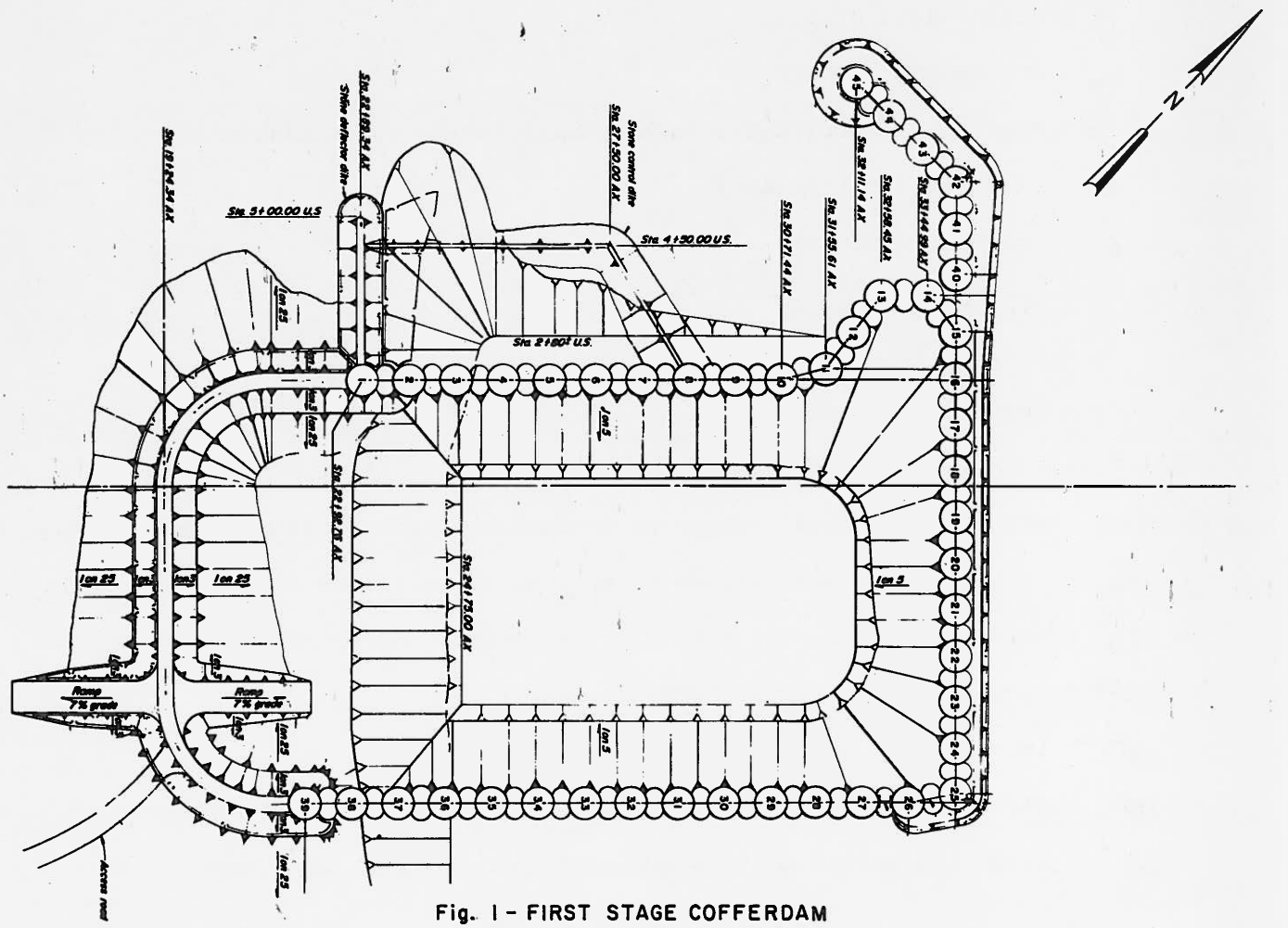

Fig. 1 - FIRST STAGE COFFERDAM

Because of the great expense in construction of cofferdams of this size, it was decided to instrument the first stage cofferdam in order to develop site specific information useful in the design of the second and third stage cofferdams.

MONITORING CRITERIA

The primary objective of the instrumentation program was to monitor hoop tension in the common wall between the circular cells and the connecting arc (Figure 2) and at the wye pile. The design called for 63-foot diameter circular cells on 86.5-foot centers with connecting arcs of 16-foot radius. With this configuration, the Tennessee Valley Authority (TVA) secant formula would predict hoop tensions on the common wall about 56 percent higher than elsewhere on the circular arc (Figure 2). Such hoop tensions required the use of high strength sheet piles (PSX32) at considerable expense due to difficulties in rolling these high strength sheet piles.

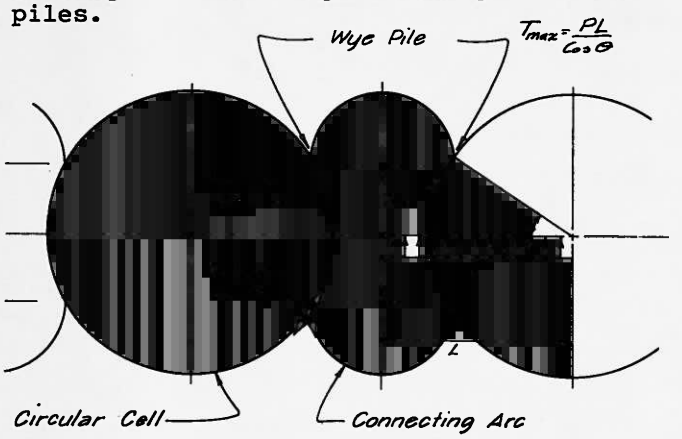

Fig. 2 - PLAN OF CELLS

Other more general objectives included monitoring the overall behavior to confirm the parameters and method of analysis. Such monitoring is distributed around the cell and takes the form of displacement, strain, and pressure measurement. Deflection measurements are also included to determine if the interior berm makes a significant impact on cell stability as well as control of interlock tension.

GAGE PLACEMENT

The cofferdam is about 60 feet high from a river bottom at about elevation 370 to a top elevation of 430. The cells were filled with dredged river sands and an interior stabilizing berm of dredged sands was also placed to about elevation 395 (Figure 3). Two circular cells were selected for monitoring. The instrumentation program was layed out so that a set of redundant data would be obtained. The instrumentation layout is symmetric about the connecting arc as shown in Figure 4. All instrumentation was mounted on the selected sheet piles at the St. Louis District Corps of Engineers service base, then transported to the site and the sheet piles installed. A total of 26 sheet piles received some form of instrumentation.

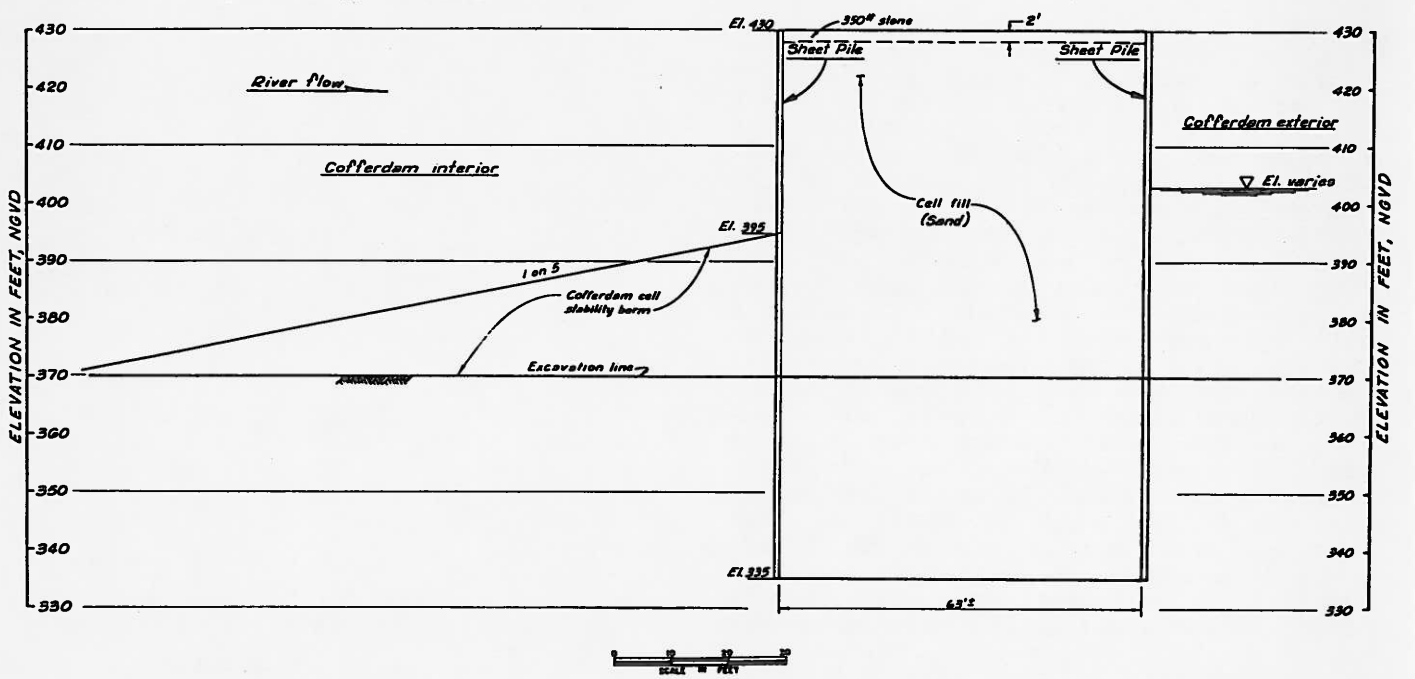

Fig. 3 - COFFERDAM SECTION

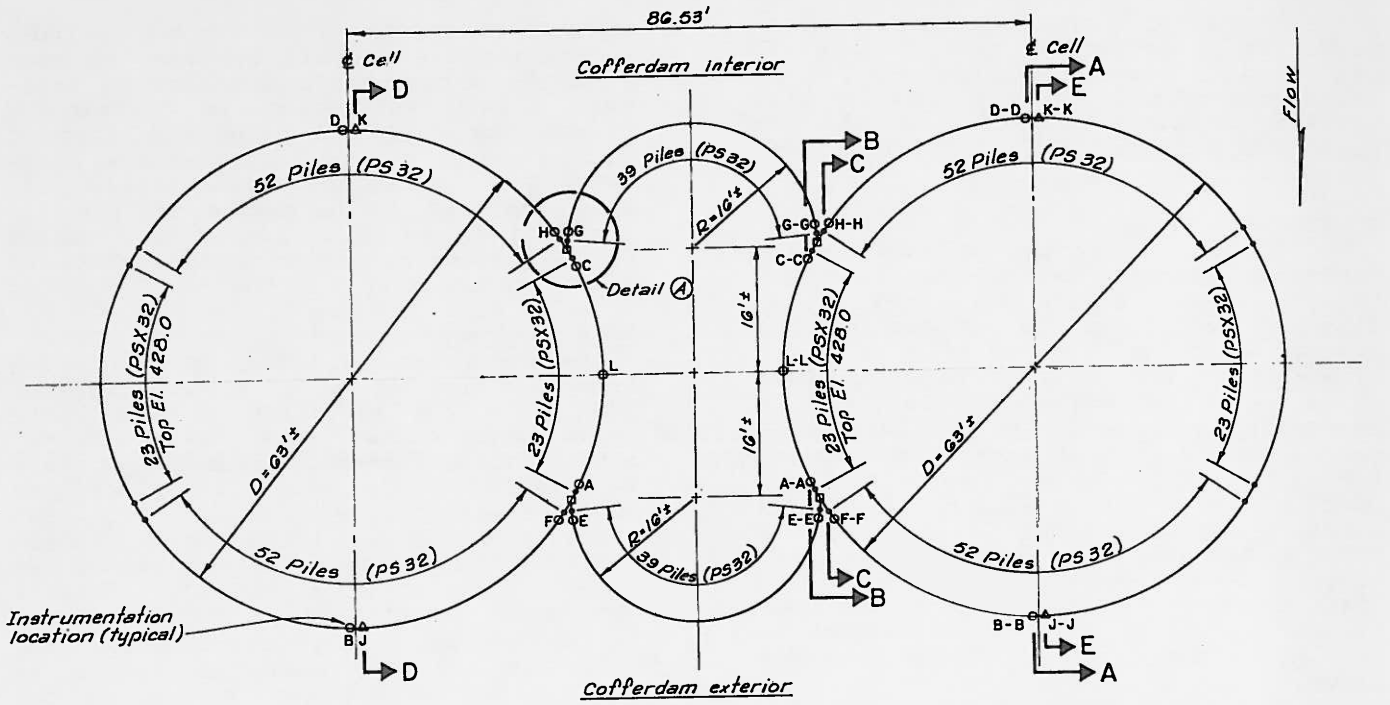

Fig. 4 - PLAN OF INSTRUMENTED CIRCULAR CELLS AND CONNECTING ARCS

SCALE IN FEET

LEGEND:
- o - Sheet pile with strain gage instrumentation.
- Δ - Sheet pile with plastic inclinometer casing, piezometer and pressure cell instrumentation.
- □ - Sheet pile with steel tube inclinometer casing.

Strain gages were selected to monitor hoop tension, axial pile loads and vertical as well as horizontal bending. The strain gages were mounted on sheet piles around the circumference of the circular cell at the maximum inboard and outboard points, in the center of the common wall and on each of the three sheet piles adjacent to the wye pile. This distribution was selected to provide some indication of how hoop tension varies about the circumference of the cell and to permit analysis of forces at the wye pile. Hoop tension on the connecting arc was not instrumented except at the wye pile. The vertical distribution of the gages varied from pile to pile, but were generally at five-foot intervals from about 20 to 30 feet below the top of the cell to about 10 feet into the river bottom (Figure 5). Vertical strain gages were placed less frequently. Strain gages were more closely placed where sheet pile loads were expected to be the highest and spread out nearer the ends of the piles. A total of 18 sheet piles were instrumented with strain gages.

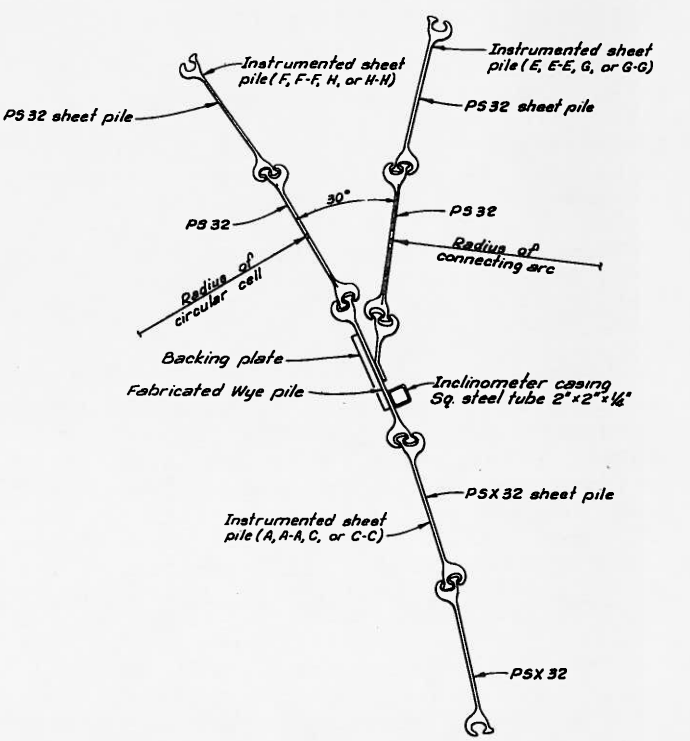

DETAIL A
N.T.S.

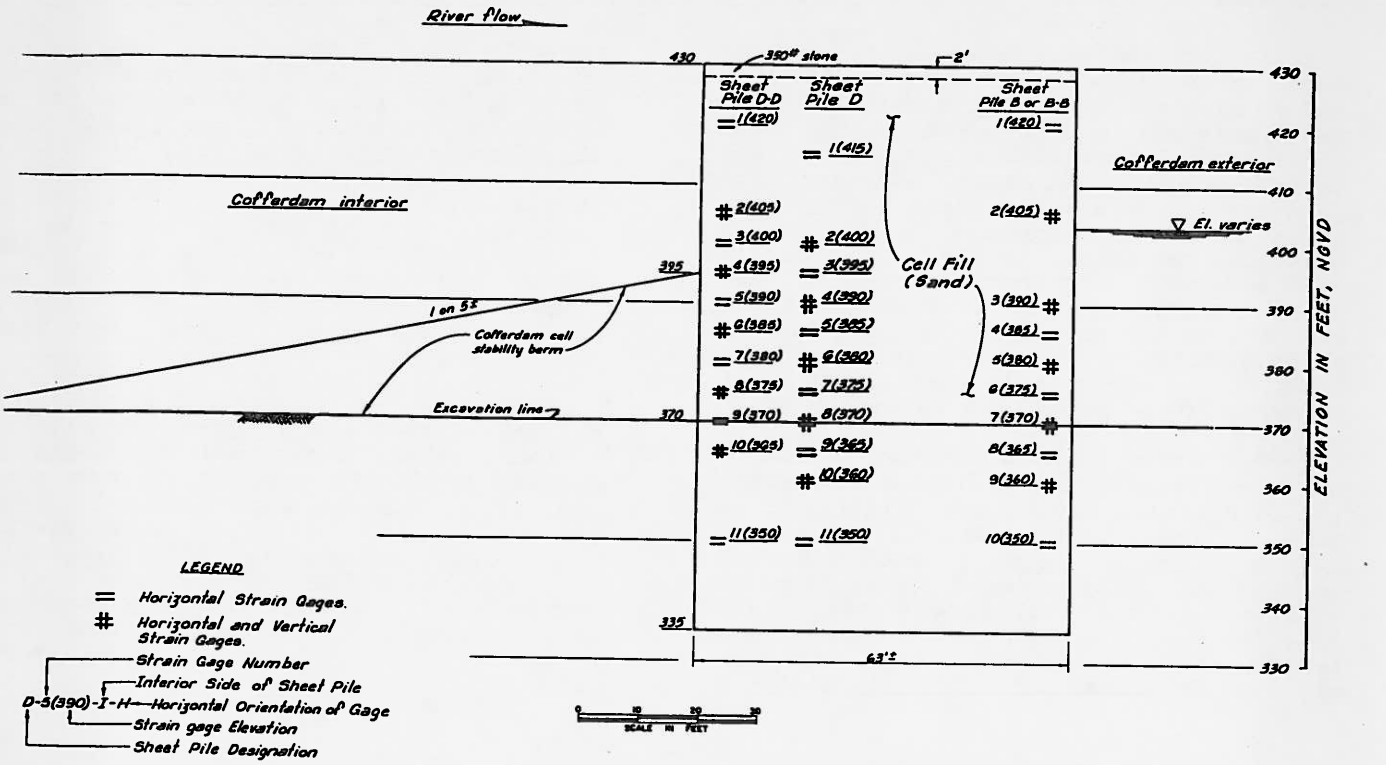

Fig. 5 - LOCATION OF STRAIN GAGES

Deformation measurements were made in inclinometer casings. These casings were mounted in eight sheet piles. Casings were placed on the maximum inboard and outboard points on the circular cells as well as on each of four wye piles for a total of eight inclinometer casings. The casings extended from elevation 340, five feet above the tip of the pile to the top of the cell. Inclinometer casings were selected because with them the distribution of deformation with elevation could be accurately determined, thus making it possible to determine the magnitude and elevation of maximum bulge, the existence of any racking or torsional deformation, movements at the wye pile as a result of arc cell filling and the magnitude of deformation as passive pressures are developed against the interior berm.

Total earth pressure cells were selected to measure the lateral earth pressures against the sheet piles. Four sheet piles were selected for these measurements which consist of the maximum inboard and outboard piles of the circular cells. These were also piles instrumented with inclinometers. The earth pressure cells were placed at a 10-foot vertical interval from 410 to 360 in the inboard side and 390 to 360 on the outboard side. Two pressure cells were placed on the exterior side of the inboard sheets to measure passive pressures from the interior stabilizing berm. As with the strain gages, the total earth pressure cells were placed through the zones where the maximum earth pressures were expected. In order to measure water levels, several piezometers were installed in the sheet piles also instrumented with inclinometers.

As a separate measurement of cell displacement, trilateration monuments were placed on the tops of each sheet pile which included inclinometers. The trilateration benchmarks were located on the levee on the Illinois side of the river several thousand feet from the cofferdam.

DETAILING OF INSTRUMENTATION

Strain Gages. Of the most concern, was the mounting of strain gages to insure the greatest survivability. The bonded electrical resistance strain gage was selected. All strain gage mounting activities were conducted by personnel of the Corps of Engineers Waterways Experiment Station. The program, as developed, called for mounting 410 full bridge strain gages on 18 sheet piles, each 95 feet in length in a period of only several weeks in August of 1981. All gages were mounted while the piles were laying on a work barge near a barge mounted crane used to handle the piles. A tent was used to cover the work barge while mounting gages. When in the sun, the surface temperature of the steel frequently reached 120° Fahrenheit.

All gages were mounted in a full bridge configuration, two active and two dummy gages on a sheet metal carrier, with the bridge completed at the gaging point to prevent temperature dependent resistance changes in the long lead wires from affecting the gage response.

Prior to gage mounting, webs of the steel sheet piles were cleaned of rust and mill scale by grinding with an electric grinder. After exposing the bare white metal, the surface was cleaned and degreased with a chemical solvent. The quantity of chemical solvent used in the cleaning and degreasing process was minimized to reduce the amount of chemical residues left on the metal. The gage was then epoxied in position using AE 10 epoxy with a bonding pressure of approximately 10 to 15 pounds per square inch. The electrical wires were connected and the gages were waterproofed.

Waterproofing is recognized as probably the single most important factor in determining the survivability of a gage. The waterproofing procedures varied slightly during the project. Initially, Gagekote No. 1 (a product of Bill Bean) was applied over the active gage as well as the dummy gage. The second coat of waterproofing consisted of Nitrile Rubber. A final coat of Gagekote No. 5 completed the waterproofing. To provide mechanical protection, a small piece of steel channel was welded to the pile over the gage. Later the procedures were altered so that a bead of Nitrile rubber was placed around the gaging position to seal Gagekote No. 1 before covering with Gagekote No. 5. A thick coat of Wall-Nu epoxy was then placed over the installation to supplement mechanical protection, and the steel channel was welded in place (Figure 6).

Leads from the gages were extended to the top of the pile adjacent to gage positions. The leads were encased in Wall-Nu epoxy and covered with a steel angle for mechanical protection. Leads for each pile were sealed in a plastic canister to prevent moisture from coming in contact with the ends and being drawn down to the gage by capillary tension. All canisters containing leads were stored in metal boxes at the top of the piles until the gages were read.

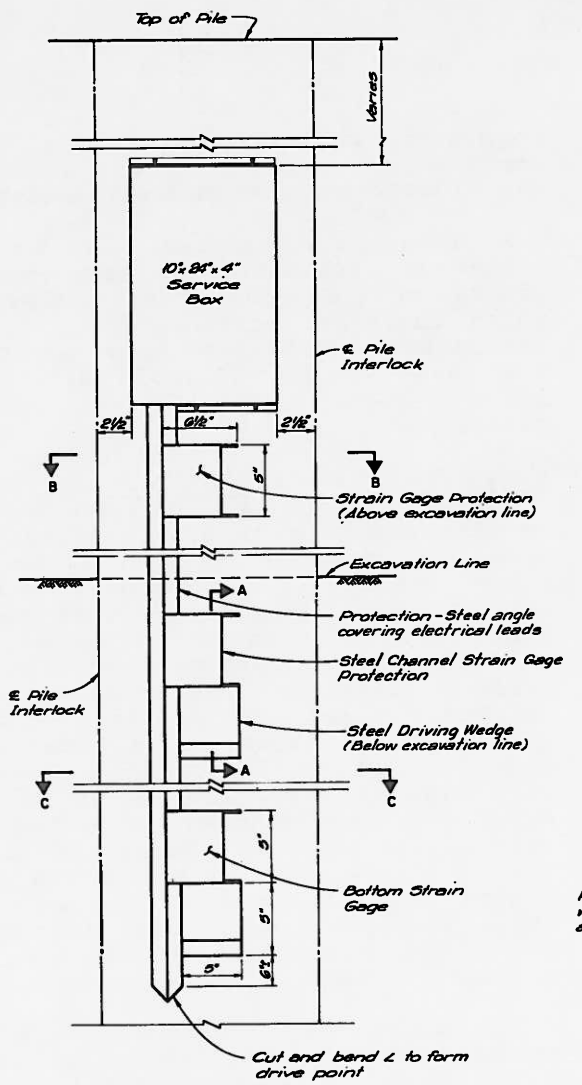

FACE OF PILING

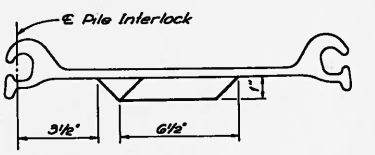

SECTION B-B

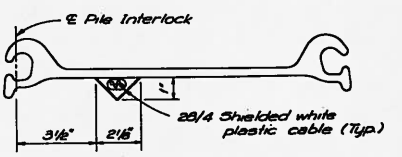

SECTION C-C

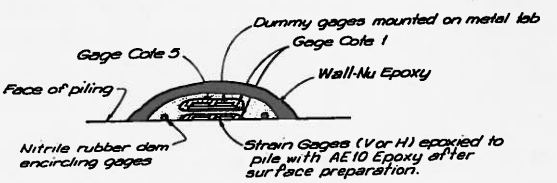

PROFILE OF STRAIN GAGE WATER PROOFING

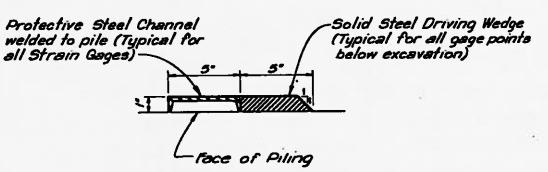

SECTION A-A

Fig. 6 - STRAIN GAGE DETAILS

Earth Pressure Cells. The earth pressure cells consisted of a specially fabricated, fluid filled Glötzl-type earth pressure cell manufactured by Petur Instruments of Seattle, Washington. These cells have a diaphragm approximately 7 inches wide by 11 inches long by 0.125 inches thick mounted on a 9 by 13-inch backing plate. The cell and backing plates were made of type 304 stainless steel. The backing plate is approximately 0.19 inch thick. The edge of the cell was fabricated from 0.19 inch diameter stainless rod which was welded to the backing plate and to the diaphragm cover. A small tubing connects the top of the pressure cell to a pneumatic transducer. The transducer senses the fluid pressure within the pressure cell and converts it to a gas pressure for measurement at the top of the pile (Figure 7).

The cell was filled with a 50-50 mix of water and ethylene glycol which was de-aired and internally pressurized by the gage manufacturer. This pressurization is provided to permit the cell to read low applied pressures at reduced temperature. As the temperature drops, the fluid within the cell contracts and the pressure drops. Since the transducer is unable to read negative fluid pressures, the initial positive pressurization helps in preventing negative pressures from forming in the cell at low temperatures.

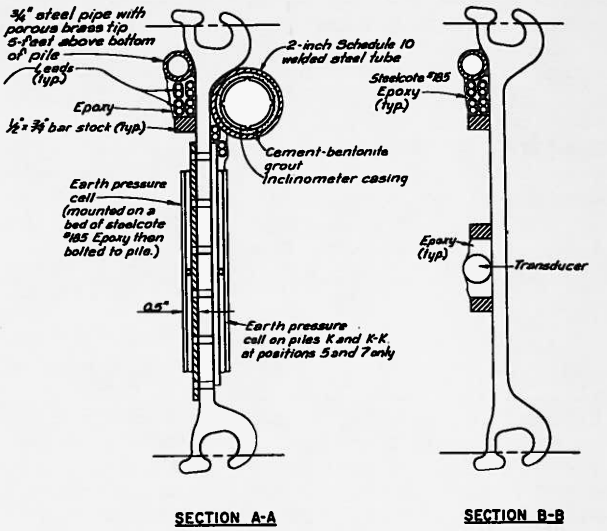

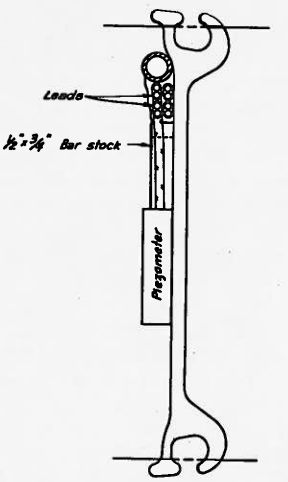

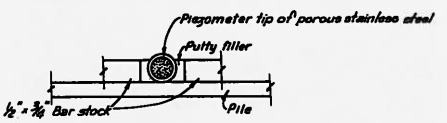

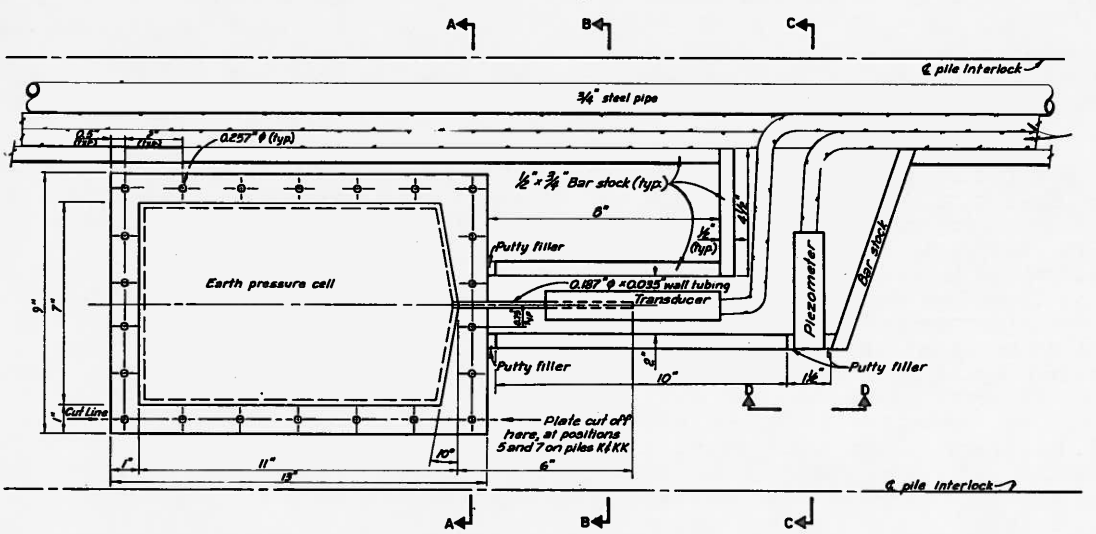

Fig. 7 - EARTH PRESSURE CELL AND PIEZOMETER INSTALLATION

The pressure cells are of rather heavy construction and as such are susceptible to internal pressure changes as a result of pile bending. In order to develop correction calibration to account for pile bending, a series of pile flexure tests were conducted on a pile while the apparent pressure changes of the gage were recorded. The pile curvature was determined by measuring pile deflection at several points near the pressure gage. It was found that the change in gage pressure was approximately linear with the inverse of the radius of bending.

The piles instrumented with pressure cells were also instrumented with inclinometer casings making it possible to compute the radius of pile bending after installation of the sheet pile and thus apply a correction to the earth pressure cell reading. Pile bending in the horizontal plane was not measured in the field nor were the pressure cells calibrated for bending in that plane.

Piezometers. Pneumatic piezometer transducers similar to those used on the earth pressure cells were also used to measure the water level at selected locations. Transducers and leads were protected in the same manner as the earth pressure cell transducers. A vertical standpipe was provided on each pile with pneumatic piezometers so that soundings of the water level could also be made.

The body of the pneumatic piezometers were held in position by encasement in epoxy. The porous tip of the piezometer was positioned so that it penetrated an opening in the bar stock which formed the epoxy dam. The edges of the opening were filled with putty to prevent the epoxy from leaking or coming in contact with the porous tip.

Inclinometers. Two types of inclinometer casings were mounted on the sheet piles. The first type consisted of a 1.9 inch diameter ABS plastic casing in a protective steel tube. The second type consisted of a two-inch square steel tube.

The ABS plastic inclinometer casing was mounted inside a two inch schedule 10 steel tube for protection during driving. The small inclinometer casing was selected to minimize the projection of the casing from the face of the pile, to minimize the cross-sectional area at the top, and thus to minimize the effect on the drivability of the sheet pile. This tubing was positioned on the outside of the pile (relative to cell) and tack welded in place. The tack welding caused a camber in the sheet pile of about three to six inches. No difficulties in driving these sheet piles were reported. A drive shoe cut from a piece of circular billet steel was welded to the bottom of the pile to protect the tubing during driving.

After the inclinometer casing was assembled and installed, pipe fittings were attached at both ends of the steel tube, and the annular space between the inclinometer casing and the steel tube was packed with caulking at the upper end. A cement-bentonite grout was then pumped into the annular space between the inclinometer casing and the steel tube.

The second type of inclinometer casing consisted of a two by two-inch steel tube with 1/4-inch walls welded to the web of the wye pile. A special splice detail and drive shoe for the bottom were also developed. These casings were mounted by the cofferdam contractor.

SCHEDULE OF READINGS

Readings were scheduled to obtain initial sets of data after the piles were driven and before the cells were filled. Subsequent readings were keyed to significant changes in loading as construction proceeded. Such a schedule permits a determination of instrument response to each change in loading conditions. Readings were obtained as follows in the period prior to dewatering.

Data	Readings Obtained and Construction Status
10/14 thru 10/16/81	Sheet piles for Cell 34 driven and initial readings taken.
10/30/81	Sheet piles for Cell 33 driven and initial readings taken.
11/03/81	Second set of initial readings for Cell 33.
11/12/81	Readings on Cell 34 filled with sand. Connecting arc on Missouri side in place and also filled with sand.
11/17/81	Readings on Cell 33 filled with sand. Connecting arc between Cells 33 and 34 in place but not filled.
11/23 thru 11/24/81	Readings on both Cell 33 and 34 after connecting arc filled. Five-foot water head inside cofferdam due to dredging activity.
12/1 thru 12/2/81	Readings on both Cells 33 and 34. Berm in place and eight-foot water head inside cofferdam.
1/27 thru 1/28/81	Readings on both Cells 33 and 34.
2/10 thru 2/11/82	Readings on both Cells 33 and 34.

2/24 thru 2/25/82	Readings on both Cells 33 and 34 during a high river crest at elevation 416.

Subsequent readings were scheduled as follows:

1. During dewatering;
   a. immediately prior,
   b. at three intermediate points during dewatering,
2. Monthly for the next 12 months;
3. At low tail water; and
4. At high water level (during flood conditions).

PERFORMANCE OF INSTRUMENTATION

When the instrumentation program was developed, it was recognized that the instrumented piles would be subject to hard driving in a harsh environment and that a substantial number of instruments might become inoperable during installation or over the extended project period. A degree of redundancy was, therefore, incorporated into the instrumentation program by monitoring two adjacent cells. After reviewing the performance of all the instruments, it is concluded that most of the instruments continue to perform satisfactorily.

Strain Gage

Of the 410 strain gage bridges, over 90 percent of the gages remained operable after nine months of service. Seven percent of the operable gages are suspect because of their low resistance to ground. Low resistance to ground can be an indication that moisture is getting to the gage and starting to ground it out. When this happens, the bridge is unbalanced and misleading apparent strains recorded. A detailed review of the strain gage data indicates that some of the readings may be questionable, but in general, most strain gages appear to be consistent to approximately plus or minus 0.3 kips per inch (kpi) of force. This performance meets the project requirements. It has been noted that the gates which have failed generally indicate progressively lower strains prior to actual failure. This can be due to debonding from the pile or moisture getting to the gage as discussed above.

Earth Pressure Cells

Twenty-four Glötzl-type earth pressure cells were included in the instrumentation program to supplement the strain gage data. During development of the instrumentation program, it was recognized that data scatter and inherent inaccuracies with this type of device are common, and therefore, a large number of pressure cells were included. The pressure cells on the average indicate lower lateral soil pressures than those which appear to be present based on the strain gage measurements. Several cells indicate effective pressures near zero. It is believed that some pressure cell data may be in error due to insufficient calibrations for the low temperatures experienced during the winter or due to leakage of the cells. Low temperature calibrations are planned to correct the data. Some cells appear to respond to change in load, but decrease with time as they might if leaking.

Inclinometers

Inclinometer casings were included in the instrumentation program to monitor the deformation of the cells during filling and dewatering. In most cases, the casings have performed very well. Inclinometer readings obtained before and after cell filling have made it possible to monitor deformations of the cells as a result of cell filling in a manner as yet not observed on other projects. With initial deflected shape, the tilt of the pile prior to cell filling, as a result of driving, may be subtracted from the post filling measurements to accurately determine the deformation as a result of filling (Figure 8 and 9). Some difficulty has been encountered in extending the inclinometer probe to the bottoms of two casings. Small radius deformations near the point of pile fixity in conjunction with the small diameter casing have caused obstructions. This possibility was anticipated during development of the instrumentation program; however, the small casings were used to minimize the effect of the casing on the driving of the pile. The accuracy of the inclinometer data is approximately plus or minus 0.5 inch at the top of the casing, and this meets the project requirements.

The initial trilateration survey was not established until after the cells were filled. In general, the direction and magnitude of subsequent movements measured by the trilateration surveys agree with the inclinometer surveys. The accuracy of the trilateration surveys is considered to be approximately equal to that of the inclinometer surveys.

Piezometers

Data from the pneumatic piezometers installed inside instrumented cells have agreed well with the water levels observed in the river and interior of the cofferdam, and the piezometers appear to be operating properly. Data from several open-system piezometers do not agree with the pneumatic piezometers or water levels observed in the river, and the open-system piezometers are considered questionable. It is suspected that the porous brass tips on several of the open-system piezometers were plugged during pile driving.

DISCLAIMER

This paper is the opinion of the authors and not the U.S. Army Corps of Engineers.

ACKNOWLEDGEMENTS

Support for this investigation was provided by the U.S. Army Corps of Engineers, St. Louis District who also took part in the development of the instrumentation program and the mounting of gages. Additional assistance was provided by G. Wayne Clough and W. L. Schroeder.

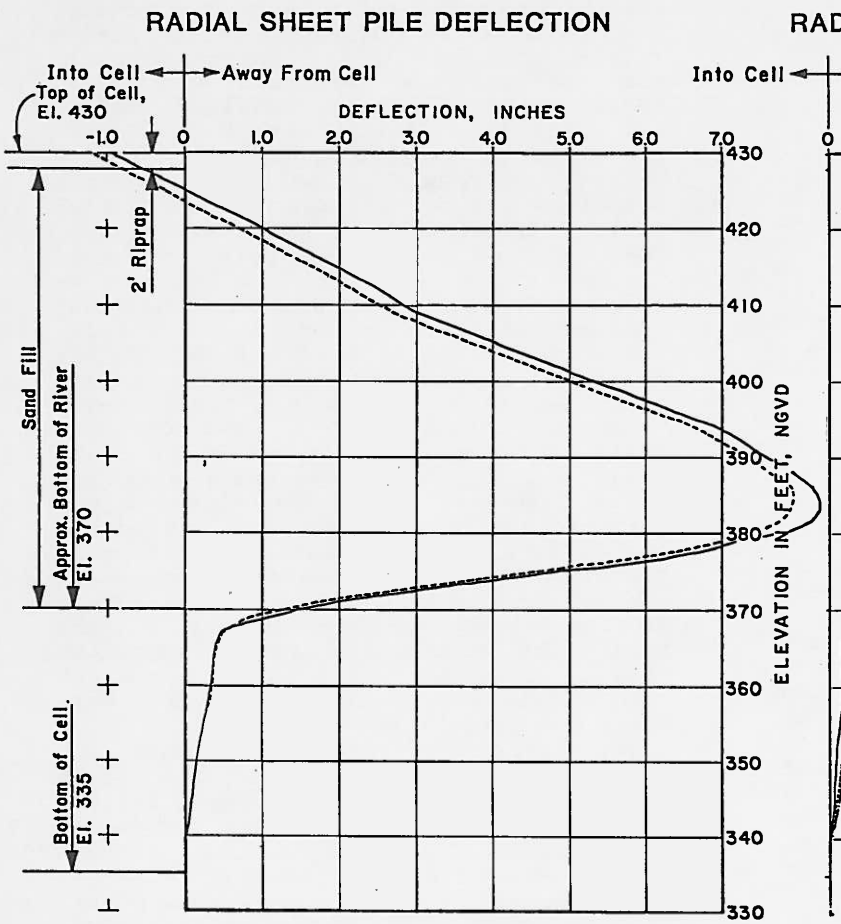

Fig. 8 - DEFLECTIONS OF INCLINOMETER CASING SHEET PILE J

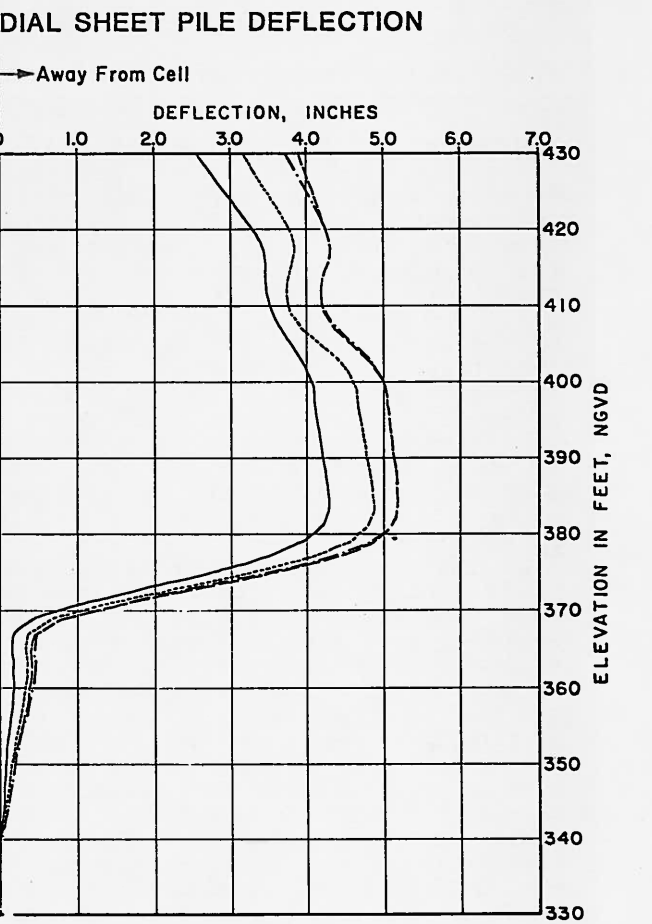

Fig. 9 - DEFLECTIONS OF INCLINOMETER CASING SHEET PILE J-J

LEGEND:

———	11/12/81	(Cell and connecting arc on Missouri side filled)
------	11/23/81	(Connecting arc to Cell 33 filled; 5-ft. inboard cofferdam head)
– – –	12/2/81	(8-ft. inboard cofferdam head)
– – –	1/28/82	(Neutral head)

LEGEND:

———	11/17/81	(Cell filled, connecting arc not in)
.....	11/24/81	(Connecting arcs filled, 5-ft. inboard cofferdam head)
– – – –	12/2/81	(8-ft. inboard cofferdam head)
—·—·	1/27/82	(Neutral head)

PROBLEMS ASSOCIATED WITH CONSTRUCTION OF A ROCKFILL EMBANKMENT

By James E. Paris
U. S. Army Corps of Engineers
Nashville, Tennessee

HISTORY

Rockfill embankments came of age in the decade of the 1960's when vibrating compaction construction equipment was developed to a degree to provide sufficient compaction. Previously, the height of rockfill embankments was limited because of compaction equipment, more precisely vibratory compaction equipment, was not available. Rockfill embankments are not like other embankments in several ways; the main difference is the zoning required to construct an impermeable stable dam. Being different from a dam constructed of materials predominatly one type or similar size material, rockfill dams may have many sizes or types of materials located in various zones through the cross section. Rockfill dams may be central core, sloping core, or all rockfill with an impermeable barrier on the upstream face. This paper will concentrate on the central core type of rockfill dam. A rockfill dam is usually designed in areas where sufficient rock, quality and quantity wise, is available either from required excavation or quarry operations to construct the embankment. Rockfills generally allow for steeper slopes than do earthfill embankments. In some instances a shortage of locally available impermeable materials suggest the design and construction of rockfill embankments.

ZONING

The internal zones consist of a central impervious core and filter-transition zones both upstream and downstream of the core. The outer shells of large rock material provide bulk and stability. The central impervious core provides the water retention capability of the dam and is the most critical element of the rockfill dam. The core is relatively thin and must function as an impermeable barrier to the passage of water; therefore, it is critical that the dam be designed and constructed to prevent movement of the core material through erosion and piping. The filter zones are designed in such a manner to provide internal drainage control but retain the embankment materials. Properly designed and constructed filters will also act to heal the core if internal cracking should occur from settlement or displacement of the embankment or foundation. The relatively thin filter zones require that the internal tolerances within the rockfill embankment be maintained by good construction practices. Proper control insures that widths of the various materials within the zones are maintained. Figures 1 and 2 show cross sections of a typical rockfill dam. Figure 1 is on overburden with an inspection trench to rock and Figure 2 shows the embankment founded on rock.

COMPACTION

Rockfill embankments are by necessity constructed of different sizes and types of materials; each must be compacted by equipment compatible with the type material involved in order to obtain the optimum density to limit settlement and meet design assumption as to strength and drainage characteristics. Test fills are the general method used to develop the design parameters for stability studies and evaluate lift thickness in conjunction with types and weights of compaction equipment. Test fills were conducted on the core materials to determine the correct number of passes of a tamping roller to develop at least 95% density as determined by the standard proctor test. Vibratory rollers were evaluated with lift thicknesses for the rockfill and filter material to determine the optimum combination for use in constructing the prototype. Based on previous experience some types and weights of compactors could be eliminated from consideration. A test quarry and screening operation was used in conjunction with the test fill so a guide could be developed for breakdown into size range of the rock. This range was evaluated as the final zoning of the embankment was developed in order to best use the material in the embankment.

For the embankment discussed herein the core material is a low plasticity clay compacted in nine-inch loose lifts by a tamping or sheepsfoot roller. The filters are eight feet wide with the filter adjacent to the core placed in 12-inch lifts compacted by a vibratory roller and having a gradation ranging from a No. 4 to No. 100 standard sieve size. The filter between the large rock and the fine filter is placed in 12-inch lifts, compacted by the vibratory roller, and ranges in size from four inch to No. 4. The outer shells are placed in 24-inch lifts compacted by the vibratory roller with the material ranging from a maximum of 16 inches to 3 inches. Because of the breakdown in the rock under steel tracked equipment the hauling and spreading equipment was limited to rubber tired.

PLACING

Placing should come before compaction; but, for the purpose which this paper is being written it is more convenient to discuss placement at this time. Placement in this case became a most critical factor in the construction of the embankment. The core and filter-transition zones should always lead the outer shell-rockfill portions of the embankment; but never far enough to cause sluffing or spilling of the leading zones

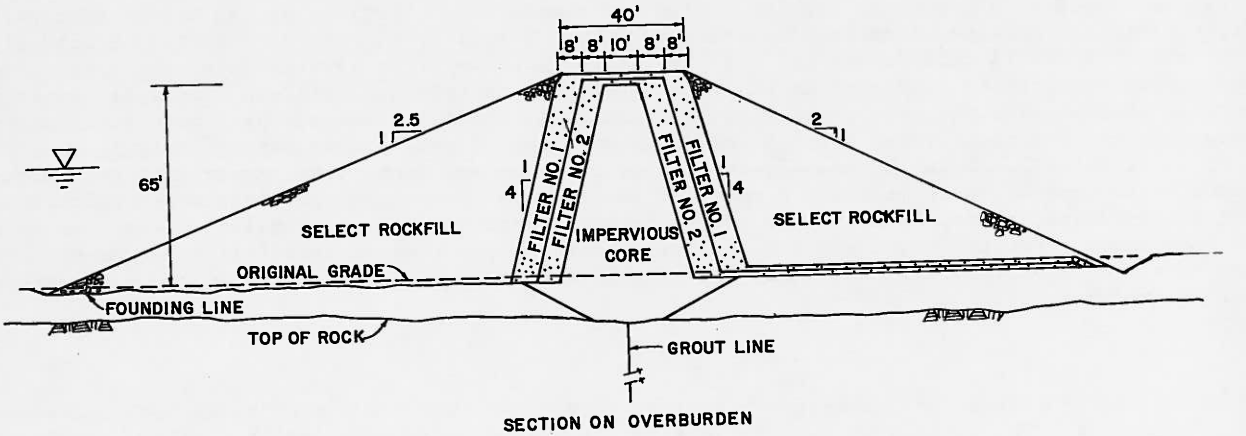

SECTION ON OVERBURDEN

FIG. 1

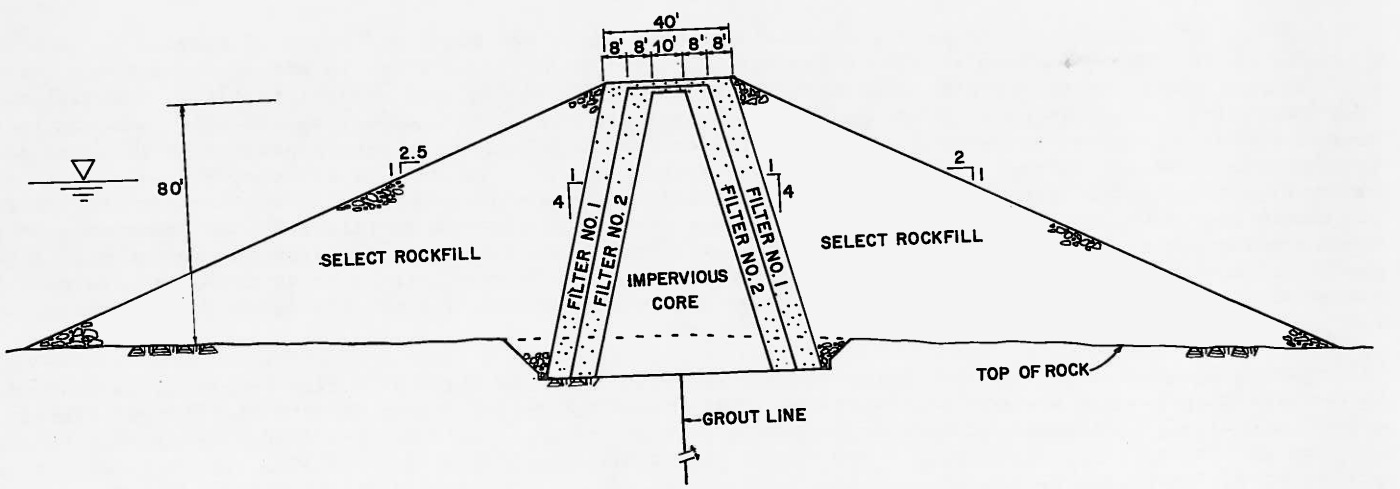

SECTION ON ROCK

FIG. 2

over those lagging. Proper alignment control is also important during placement of the zoned fill. The thin zones designed to approximate equipment width for working purposes allow very little flexibility in alignment deviation. The total embankment should proceed as near level (horizontal) as possible. Various parts of the embankment constructed separately require special emphasis at tie-ins to prevent built in potential failure surfaces or problem areas. Rockfill placement should be carefully controlled during spreading and leveling so the larger material is being spread away from zones containing smaller material. The larger rocks tend to be carried along the outer face of the lift. This creates a situation, when the larger material is pushed toward the inner zones, of clusters or nesting of larger rocks in pockets against the zones of smaller material. This invalidates the purpose of the filter zones. Clusters or nests of larger material contain larger voids which would allow the smaller material of the filter zones to pipe.

THE PROBLEM

Site visits during early construction discovered that there were larger rock clusters or pockets adjacent to the filter zone. This indicated that a problem in proper fill placement existed. The potential problem developed because of relaxing the restrictions on the finer zones leading the coarser zones and keeping the zones at generally the same level. The contractor was producing rock for the rockfill and filter at a faster rate, from the required excavation, than the core could be placed because of adverse weather conditions, to provide specified placement of the materials. Rather than stockpiling the processed rock the contractor was allowed to place the rockfill leaving steps in each subsequence lift as it proceeded up, stepping away from the filters. When filling in the lifts between the filter and inplace rock the spreading operation caused the clustering of large rock.

INVESTIGATION

The surface indication was a substantial amount of clustering or segregation was occurring. In order to determine the extent of the clustering, test pits at several random locations were excavated in the completed embankment at the large rockfill, coarse filter contact. The test pits extended through at least fifteen feet or down to the original ground surface whichever occurred first. The pits were approximately 30 feet square.

As the pits were being excavated, photographs and mapping were being accomplished to document the adequacy or inadequacy of the fill placement and compaction operations. Density tests were also taken to compare with densities taken in the mass fill and to compare the results with the densities used during design. Gradation tests were conducted to compare inplace gradation with that outlined in the specifications. As the pits proceeded down it became apparent that spill over of the coarse filter had occurred in numerous places as the embankment was being constructed. Trenches were then extended from some of the pits through the two filter zones into the impervious core. This trench had the purpose of evaluating the construction control during placing and compacting the filters and interface between the core and filter material. Density tests were also run on the various filters. Density tests were taken in the core material near the contact to evaluate the compaction of the impervious material.

RESULTS

The excavation in the rockfill portion of the embankment revealed that filling in between the steps in the rockfill and the coarse filter had caused segregation of the rockfill. This resulted in an excessive amount of larger rock adjacent to the filter. There were numerous zones of large rock in all the test pits adjacent to the coarse filter. The voids in these zones, due to the absence of finer rock, would allow movement of the coarse filter into the rockfill probably producing piping. Because of the voids the densities were not within the range of expected densities. The compaction equipment could not adequately compact the large rocks where there was point contact with other large rock and little or no fines. Also divulged in the excavation of the rockfill was that the 24-inch lift thickness requirement had not been adhered to as shown by the thin layer of fines generated on the surface of each lift during compaction.

The excavation through the filter zones into the impervious core brought to light the most disturbing aspect of the entire investigation. The filters were designed to be eight feet wide with 4 Vertical and 1 Horizontal slopes. The designed widths, slopes, and relative position in the embankment are shown in Figures 1 and 2. The designed position of the filters was staked at the top of the excavation. Lines were painted on the walls of the excavations to correctly evaluate the placement technique. As the excavation proceeded it became quite apparent that the filter zones and impervious-fine filter contact were not in any manner controlled during the dumping and spreading operations. Figures 3 and 4 are sections of a wall of two excavations. Each figure has the designed filter position shown by the dashed near vertical lines.

Figure 3 shows what one would expect from an alluvial flood plane deposit, a complete mixture and overlapping of the various zones. Filter number 2 or the fine filter area is generally taken up by the impervious core. There is some filter number 2 near the top third and bottom third. Filter number 1 or coarse filter zone is almost entirely occuppied by filter number 2. Filter number 2 shows up in the rockfill design area. The most disturbing aspect of this section is the breaching of the zones by the impervious core and coarse filter. This in effect places the clay core material adjacent to the No. 4 to 4-inch size material. Near the bottom a finger of fine filter, the No. 4 to No. 100 size material, extends into the area where the large voids existed in the rockfill. This is paramount to building in a failure mechanism to produce piping.

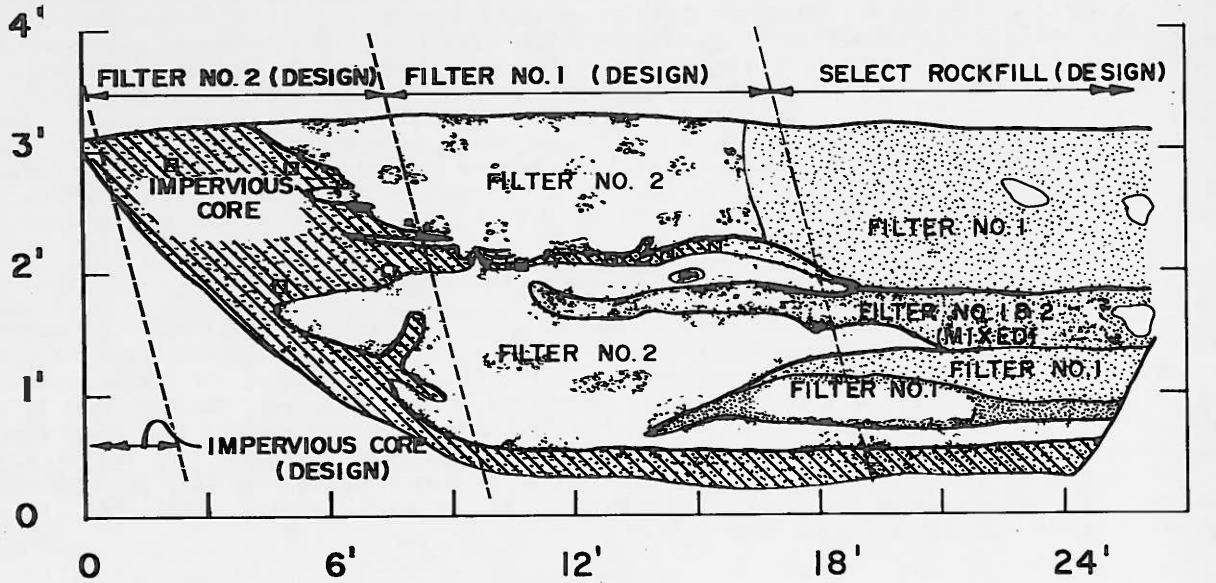
4'
3'
2'
1'
0
FILTER NO. 2 (DESIGN)
FILTER NO. 1 (DESIGN)
SELECT ROCKFILL (DESIGN)
IMPERVIOUS CORE
FILTER NO. 2
FILTER NO. 1
FILTER NO. 1 & 2 (MIXED)
FILTER NO. 2
FILTER NO. 1
FILTER NO. 1
IMPERVIOUS CORE (DESIGN)
0
6'
12'
18'
24'

FIG. 3

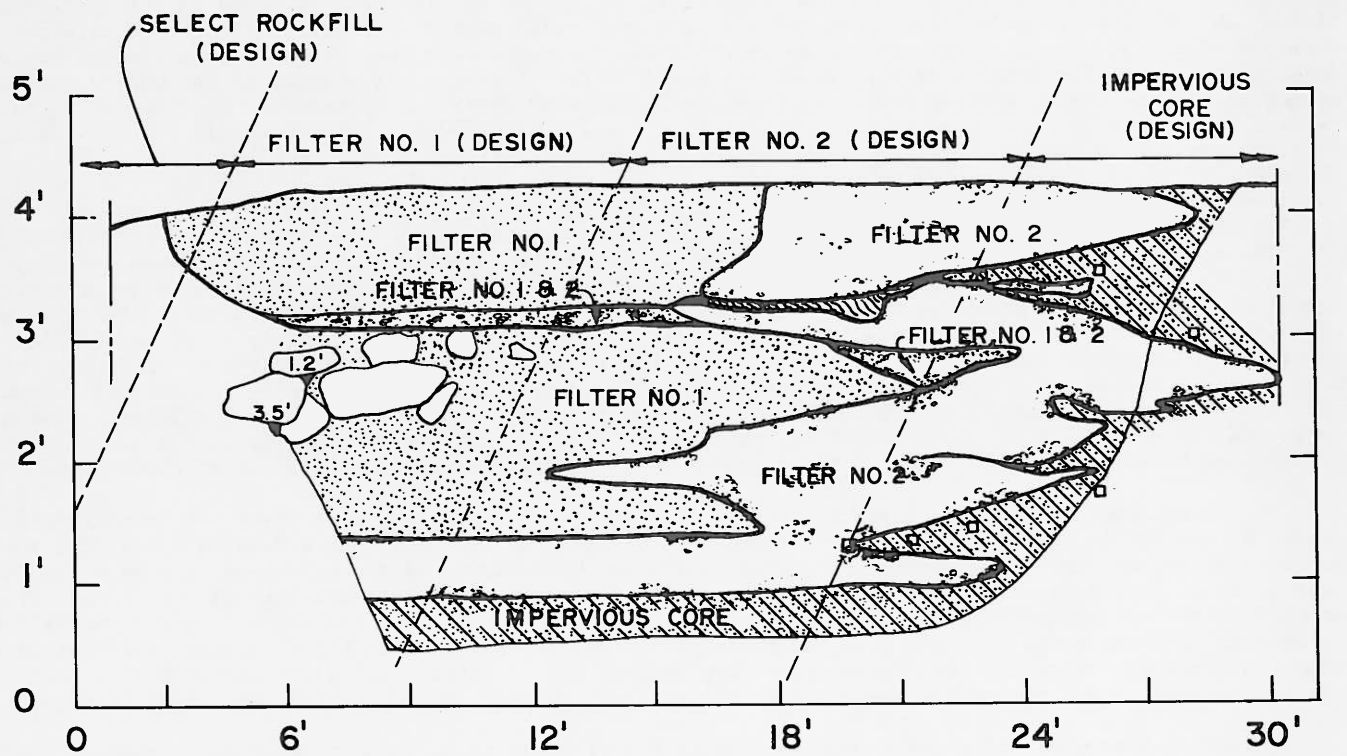
SELECT ROCKFILL (DESIGN)
IMPERVIOUS CORE (DESIGN)
5'
4'
3'
2'
1'
0
FILTER NO. 1 (DESIGN)
FILTER NO. 2 (DESIGN)
FILTER NO. 1
FILTER NO. 2
FILTER NO. 1 & 2
FILTER NO. 1 & 2
1.2'
3.5'
FILTER NO. 1
FILTER NO. 2
IMPERVIOUS CORE
0
6'
12'
18'
24'
30'

FIG. 4

Figure No. 4 is similar to figure No. 3 but shows the opposite effect. The actual inplace material is moving into the area designed for the impervious core. In the Filter No. 1, or coarse filter zone, one can see large rock Filter No. 2, or fine filter material, and zones of mixing of the various rock materials. In Filter No. 2 zone there are both filters inter-fingering and once again the impervious material breaching the fine filter designed to protect against fines movement. Both of the sections are of the downstream area of the embankment. The upstream was not examined since the elevation of the embankment at the time of investigation was still below the permanent pool elevation. No water fluctuation would occur to cause fines movement therefore no upstream investigation.

CONCLUSIONS:

1. The filter transition zones were not constructed in the proper place as designed and shown on the plans. The embankment zones had not been constructed within specified tolerances. The actual in-place location of the zones and the width deficiencies made these zones unacceptable.

2. The rockfill was badly segregated adjacent to the coarse filter.

3. The rockfill was not as dense as would be expected for rockfill placed to specification gradation and lift thickness. Voids in the rockfill were much larger than would be expected for a well compacted, well-graded mass.

4. The condition of intermingled and overlapping filter and core zones combined with the loose segregated zone adjacent to the coarse filter rendered the embankment in place unacceptable.

ACTION TAKEN

The downstream filters were removed. A portion of the rockfill adjacent to the coarse filter was removed. The improperly placed or contaminated core material was removed. The materials were replaced at the specified placement techniques. Continuous vertical and horizontal control was maintained to insure proper zone contact configuration. Also care was exercised to insure contamination or spillover of one material onto or into another did not occur.

For the continued construction the zones were constructed as near level as possible with the interior leading the outer zones. Continuous monitoring of the proper location for the zones was maintained.

REFERENCES

1. Dept. of Army, Corps of Engineers "Seepage Control" Engineering Manual 1110-2-1901. Feb. 1952
2. Sherard, ET AL, Earth and Earth Rock Dams, John Wiley & Sons, Inc., 1963
3. Terzaghi, Karl & Peck, Ralph B., Soil Mechanics in Engineering Practices, John Wiley & Sons, Inc., 1967
4. Bush, Randy, U. S. Army Corps of Engineers. Some of the data for this paper was derived from reports written by Mr. Bush, who has relocated.

THE FOLLOWING PAPERS WERE NOT RECEIVED IN TIME FOR PUBLICATION:

UNDISTURBED AND IN SITU TESTING OF FINE SAND FROM MISSISSIPPI RIVER POINT BAR DEPOSITS

By Richard W. Peterson and Victor H. Torrey, III

GEOTECHNICAL ENGINEERING PROPERTIES OF A POORLY GRADED SANDY GRAVEL

By Richard W. Peterson

THREE-DIMENSIONAL SLOPE STABILITY

by

C. W. Lovell
Professor of Civil Engineering
Purdue University
W. Lafayette, IN 47907

ABSTRACT

The paper presents principal findings of a recently completed research project which provided the Indiana Department of Highways with a method of analysis for real (i.e., 3-D) slope instabilities. The potential sliding body is divided into vertical columns, and as in the 2-D method of slices, simplifying assumptions about the internal side forces permit the calculation of a factor of safety.

The 3-D factor of safety (F_3), is nearly always greater than the comparable 2-D one (F_2), but values of the ratio (F_3/F_2) are instructive in defining the degree of conservatism in the conventional 2-D analysis. The paper describes the effects of slope angle, soil parameters, and pore water conditions on the (F_3/F_2) ratio, and thus helps to define the circumstances under which a three dimensional analysis is justified.

BACKGROUND

About 10 years ago, a research program in slope stability analysis began. It was sponsored by the Indiana Department of Highways (IDOH) and administered in the School of Civil Engineering of Purdue University by the Joint Highway Research Project (JHRP) between Purdue and IDOH. The program has been enormously successful, primarily because of the talented and energetic graduate students attracted to it.

In 1975 an extremely versatile 2-D analysis (STABL) was completed (Siegel, 1975). This program contained two routines (BLOCK and RANDOM) which allowed computer search and analysis of potential sliding surfaces of other than a simple analytic shape (such as circles, log spirals, parabolas, etc.). Computer generation of complex (but kinematically acceptable) sliding surfaces had not been reported to that time. Within a year, STABL was online at the IDOH and has been used routinely by them since that time.

STABL2 came into being two years later (Boutrup 1977), and a further refinement (STABL3) is expected to be complete later this year (Goodman, 1982). In the meanwhile, the program has been reported in the literature (Siegel et al., 1978; Boutrup et al., 1979; Boutrup and Lovell, 1980; Siegel et al., 1981) and has been adopted by perhaps several hundred companies and agencies all over the world. It has even been converted for operation on a 16K Model 1, Level 2, TRS-80 microcomputer (Rooney et al., 1982). Since all real slope failures are 3-D, the 2-D analysis is used with the assumption that there is additional safety in the real case. In the load and reduction factor design (LRFD) approach, this is equivalent to setting the analysis factor at greater than unity. The validity of this assumption is examined later.

3-D MODELS

Figures 1 and 2 schematically illustrate two failure possibilities. The first is sometimes observed at the abutment end of a fill, and tends to have a spoon shape. The second is a case of sliding at a contact between soil and bedrock and is roughly a translational movement of a block. These two cases were chosen for attention in the first 3-D analysis research (Chen, 1981). They were treated differently, in that the tendency for block movement was considered in the traditional three pieces, viz., central block, upslope active wedge and downslope passive wedge, while the spoon shape was treated as a series of 3-D slices or columns. As shown in Figure 3, the ends of the wedge can be tilted in or out, and the width of the wedge can vary in simple ways.

A circular or spoon shape body of sliding, divided into columns, is shown in Figure 4. For purpose of analogy with the 2-D methods of slices analysis, the element face in the YZ plane becomes the interslice face, while that in the YX plane becomes the intercolumn face.

To accommodate circular failures which are wider than that of Figure 4, a mixed shape was introduced. In the central portion the sliding surface has a cylindrical (roller) shape, while the ends are ellipsoids. As shown in Figure 5, a variety of shapes can be accommodated by assigning appropriate values to the length of the cylinder and to the geometry of the ellipsoid.

Model BLOCK3

The code developed to treat the translational

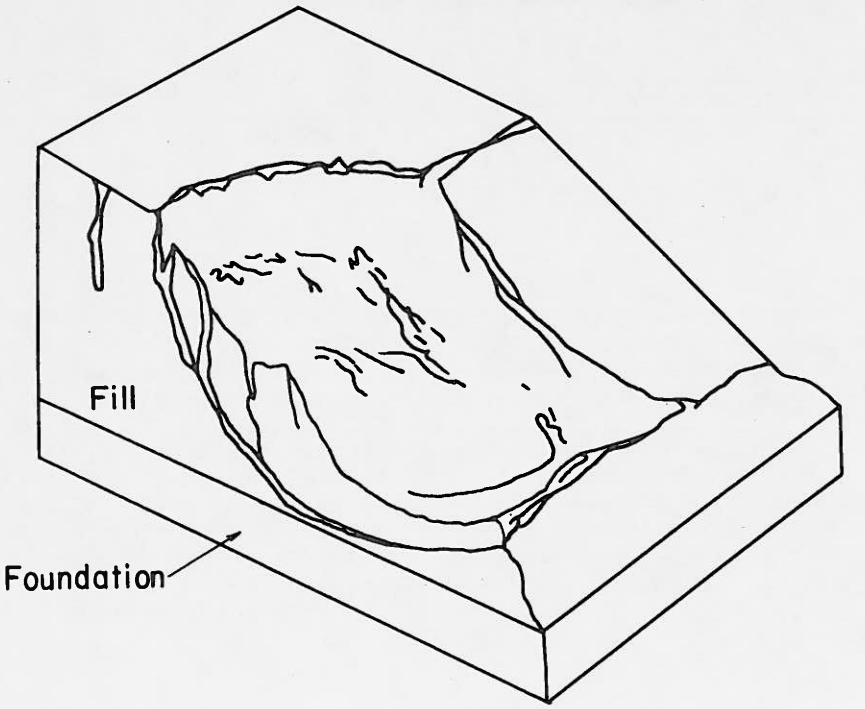

Figure 1 Spoon Shaped Failure in Fill

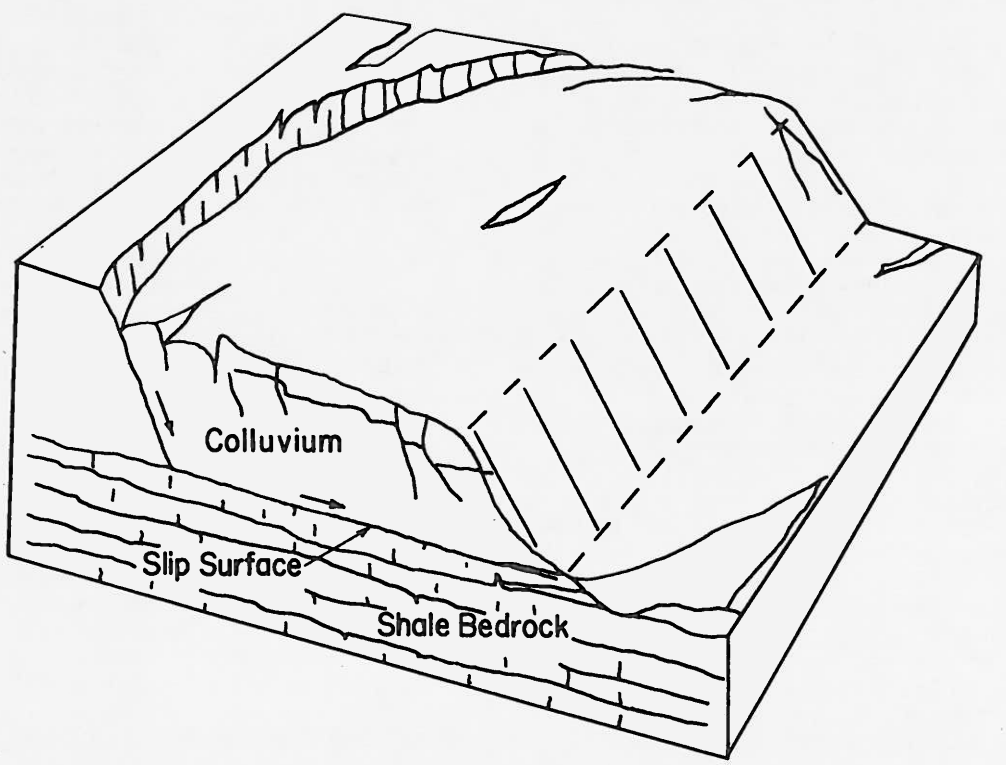

Figure 2 Sliding Failure at Contact of Colluvium and Shale

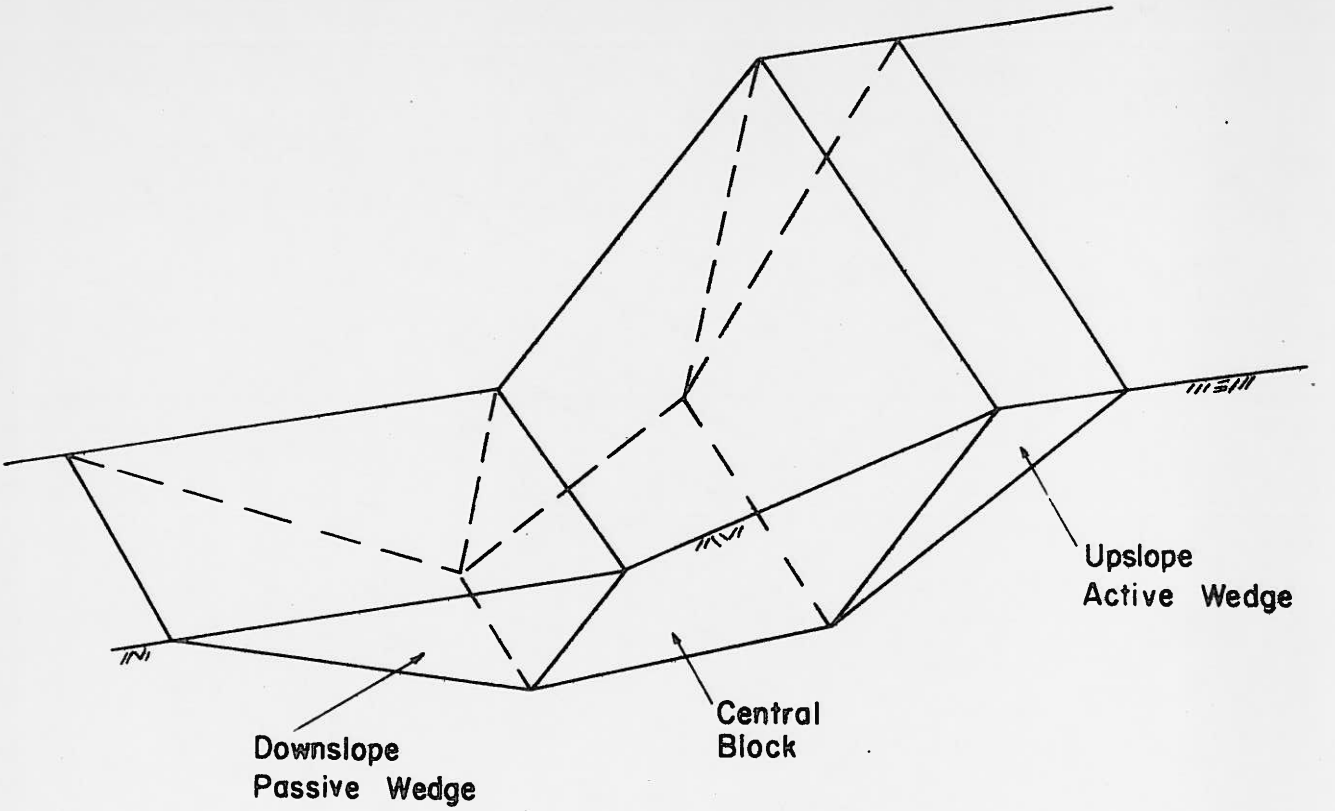

Figure 3 Schematic Model of BLOCK3

sliding case was named BLOCK3. (BLOCK and BLOCK2 are routines in STABL, where, incidentally, the analysis is a method of slices.) In its present version, Figure 3, the boundaries and subsurface geometries are simple (Chen, 1981), but these can be relaxed with additional attention to the model.

Model LEMIX

The program to solve the mixed shape of Figure 5 by a method of columns was designated LEMIX (limit equilibrium, mixed shape). In solving this problem, it was not desired to ignore the forces along the sides of the columns. To do this would produce a solution analogous to the ordinary method of slices in 2-D analysis.

The individual column with interface forces is shown in Figure 6a. In a collection of n slices and m columns, there are 12mn-5m+5n unknown forces and distances ... and only 6mn equations of equilibrium. Insertion of safety concept will introduce at least one more unknown.

The matrix of unknowns has not been successfully simplified by any rigorous means; although the effort has been made. Rather, a solution has been effected by making assumptions which seem intuitively correct. A complete listing of these is given in Chen (1981), and the major ones are repeated here.

(1) The failure mass is symmetrical in the Z direction (Figure 6a).

(2) Movement will occur in the XY direction only, and shear stresses in the YZ direction are, accordingly, zero. See Figure 6b.

(3) Intercolumn resultant shear forces are parallel to the column base (Figure 6c). These forces are a function of their position, being a maximum at the ends of the slide mass and zero at the central section where there is no relative moment.

(4) Interslice resultant forces have the same inclination (θ) throughout a given row of slices (Z=constant). See Figure 6d.

Meaning of the Safety Factor

A common technique for producing a suitable level of conservatism in civil engineering designs is the load and reduction factor design (LRFD) strategy. Although little used in slope stability solutions, it affords a logical definition of the safety factor. In this approach, a reduction factor (SRF<1) is applied to the estimated strengths; an increase factor (LF>1) is multiplied by the loads; and an analysis factor (AF) is applied to the comparison of driving and resisting values, so as to make the solution more conservative.

For example, in a comparison of driving moments (ΣM_d) and available resisting moments (ΣM_{ar}), the factors enter in a linear fashion, so that,

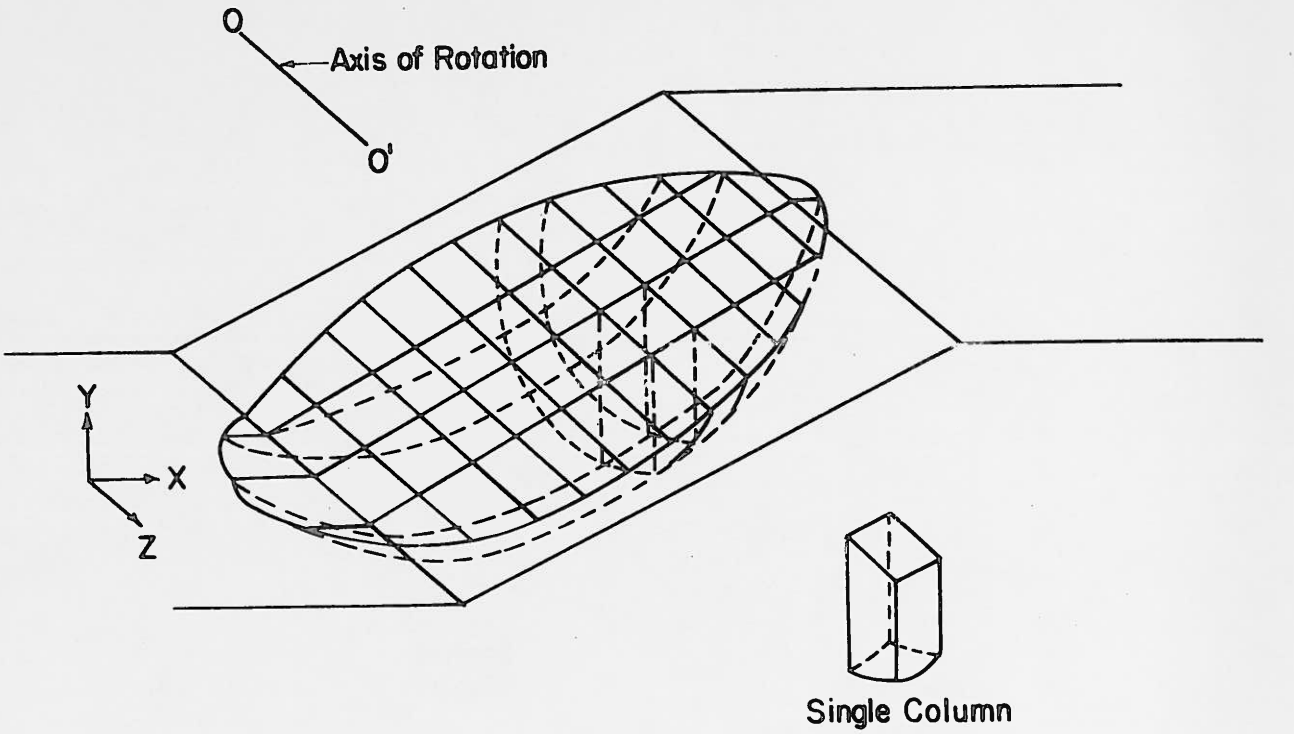

Figure 4 Spoon Shaped Failure Divided into Columns

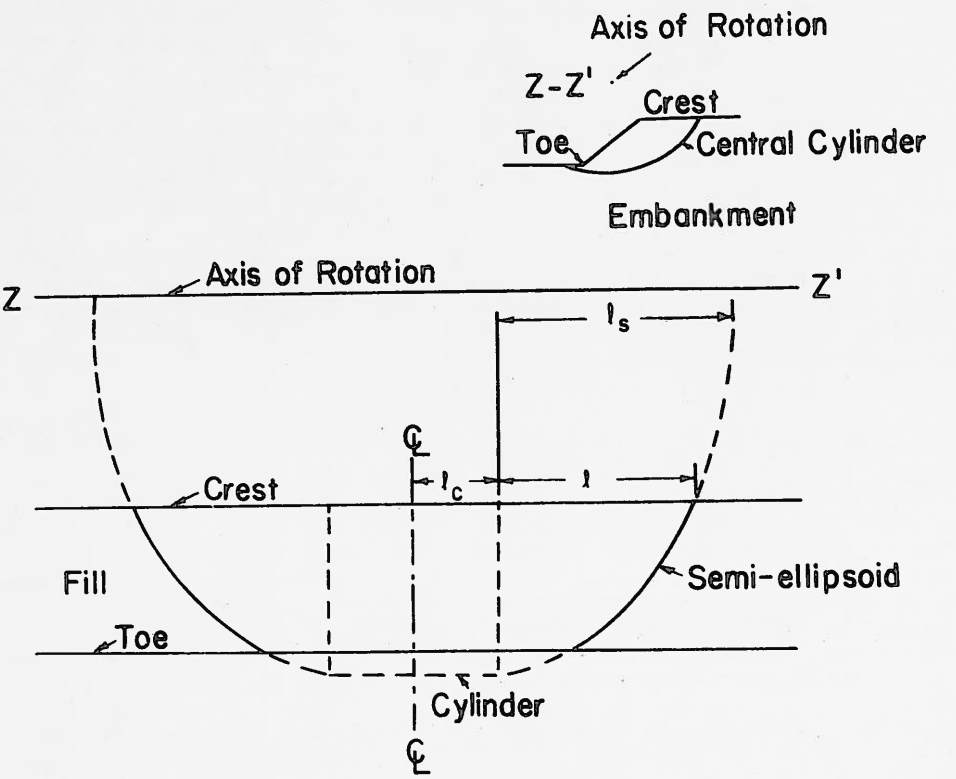

Figure 5 Front View of a Mixed Type of Failure Surface

$$SRF\ (\Sigma M_{ar}) = (AF>1)(\Sigma M_d)LF.$$

The resulting total safety factor is

$$\frac{\Sigma M_{ar}}{\Sigma M_d} = \frac{(AF>1)(LF>1)}{(SRF<1)}$$

where $\frac{1}{SRF} = F$ = the most commonly accepted definition of the factor of safety. The AF can logically be viewed as the factor operating to produce a more conservative design when a 2-D solution is applied to a 3-D problem. Where the subscripts denote a 2-D or a 3-D analysis, $F_3=F_2 \cdot AF$. Accordingly, the results of the 3-D analysis are presented in the next section as F_3/F_2 vs. the appropriate independent variables. The values of this ratio may then be interpreted as an analysis factor, i.e., the degree of conservatism involved in using a 2-D analysis to solve a 3-D problem.

For the class of practical problems involved, viz., transportation facilities, there is little data to input for available soil strength. For the embankment in Figure 1, there would normally be no values of strength for the compacted soil; presumptive values would be input into the analysis. For the cut slope of Figure 2, the engineer might have a single value of strength for the colluvium, perhaps a single one for the shale, but none at all for the weak layer at the soil-rock contact. Statistical data for these cases are practically unheard of.

RESULTS

BLOCK3 analyses were undertaken for a model of an embankment soil overlying a foundation soil which contains a thin weak layer. Most of the variables are shown in Figure 7, which is sample output. In this figure, c, ϕ represent both the embankment and foundation soil, and c_w is the strength of the weak layer.

Chen (1981) reached several conclusions from the analyses, as follows (see Figure 7).

(1) The F_3/F_2 ratio is usually greater than unity. At small values of L/H, the 3-D effect is more significant for cohesive soils than for cohesionless soils.

(2) For all soils, cohesive or cohesioness, a lower strength of the weak layer may cause a higher F_3/F_2 ratio.

(3) As the block ends are tilted away from the vertical, the end areas will increase and higher F_3/F_2 ratios are obtained.

(4) As the block shape approaches a wedge, "a" becomes small in Figure 7, and the F_3/F_2 may become less than unity, i.e., the 2-D case is safer than the 3-D one.

LEMIX rotational analyses were studied for various values of l_c and l_s in Figure 5, as well as for various strength values for an embankment soil and a foundation soil and selected pore pressure parameters. The cross section of the central cylinder was selected as the most critical circle searched by the 2-D computer program STABL2. Figure 8 is sample output for a single embankment-foundation soil, a central cylinder which is short, a pore pressure ratio (r_u) greater than zero and a variety of slope angles (β).

Major conclusions reached by Chen (1981) included the following. (See Figure 8).

(1) For gentle slopes, the F_3/F_2 ratio is higher for soils of high cohesion intercept and low friction angle.

(2) Pore water pressures may cause the F_3/F_2 ratio to be increased.

(3) As the length of the potential sliding surface increases, the F_3/F_2 ratio changes very little. The practical implication is that the length of the failure mass is very difficult to predict.

(4) The usual value of F_3/F_2 is greater than unity, but for soils of low cohesion intercept and high friction angle, the value may be slightly less than unity.

The combinations of variables which produce small values of F_3/F_2, ie., approaching unity (or even less than unity), are of greatest interest. In these cases, there is no significant additional conservatism in applying a 2-D analysis to a potential 3-D failure. The analysis factor in the LRFD has become unity.

Several checks of the 3-D analyses, particularly LEMIX, have been performed. Solutions for very long instabilities approach the 2-D case, allowing verifications at that limit. In addition, a 3-D finite element program FESPON was developed and used to produce good checks on the F_3 values by an independent approach (Chen, 1981). These checks are not general but are for specific cases involving particular levels of the variables.

SUMMATION

The acceptance of the versatile 2-D method of slices stability analysis (STABL) in geotechnical practice has encouraged Purdue University researchers to expand the same limiting equilibrium approach into 3-D analysis. The first step in this effort has produced a translational model BLOCK3, and a rotational model LEMIX, involving a central cylinder and ellipsoid ends. The latter program uses a method of columns, and intuitive assumptions about the forces on the column faces.

Output from these programs has been examined as a ratio of F_3/F_2, which is analogous to an analysis factor in a LRFD approach. As this ratio is significantly greater than unity, there is implied conservatism in applying a 2-D analysis to the (real) 3-D problem. As the ratio is large, use of the 2-D analysis is likely too conservative; as it is unity or less, the 2-D analysis may not be sufficiently conservative. The ratio serves to identify the combinations of variables which justify the practical use of a 3-D program.

The existing models have been used to examine simple problems involving specified surfaces. LEMIX output has been independently verified by a finite element solution. The results are sufficiently promising to encourage further research.

ACKNOWLEDGMENTS

The graduate students responsible for the slope stability research are R. A. Siegel, Eva Boutrup and R. H. Chen. The work was sponsored by the Indiana Department of Highways. Important contributions have been made by the author's colleagues W. D. Kovacs and J.-L. Chameau.

REFERENCES

1. Siegel, R. A. (1975). "Computer Analysis of General Slope Stability Problems." Joint Highway Research Project Reports 75-8 & 75-9, School of Civil Engineering, Purdue University, W. Lafayette, Ind. 216 pp.

Figure 6 Column Forces

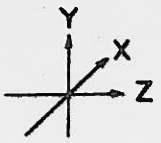

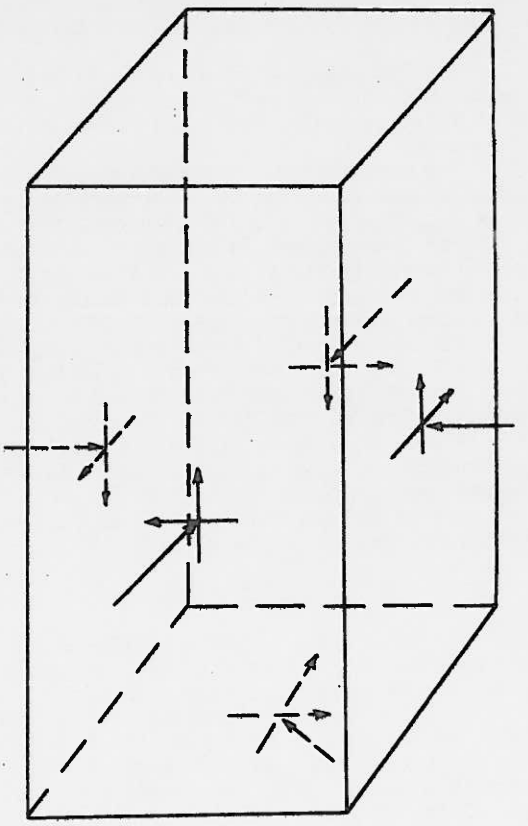

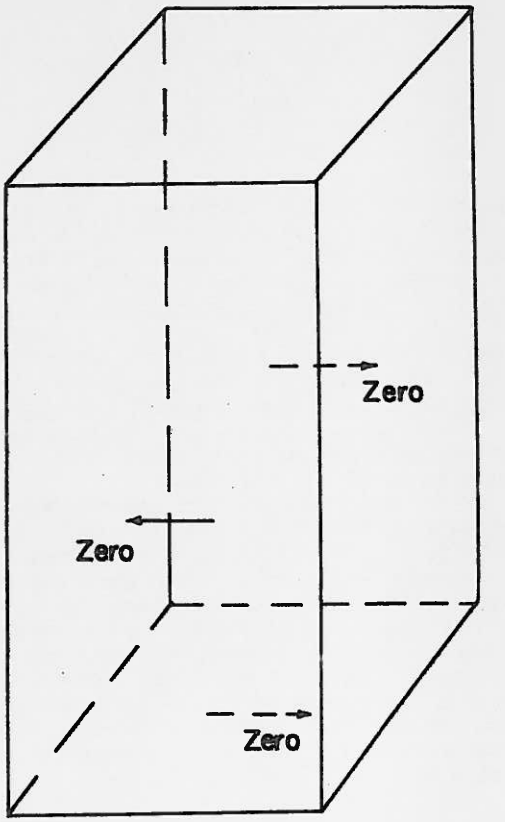

a. Upper Left, b. Upper Right,
c. Lower Left, d. Lower Right

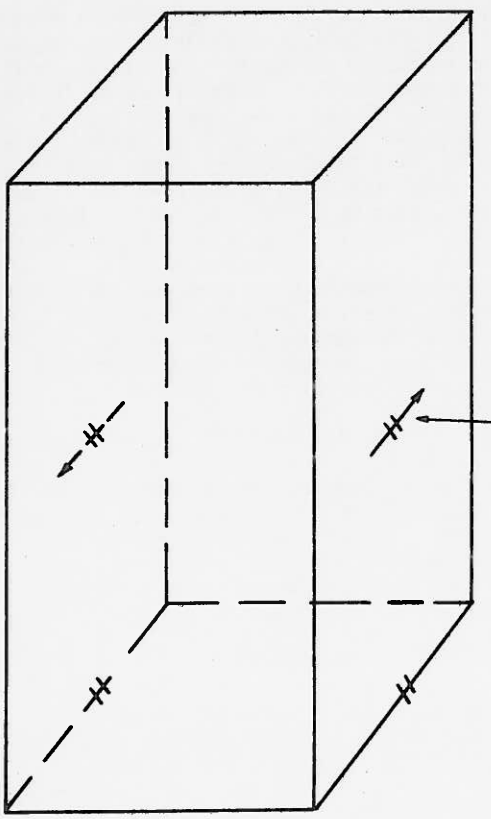

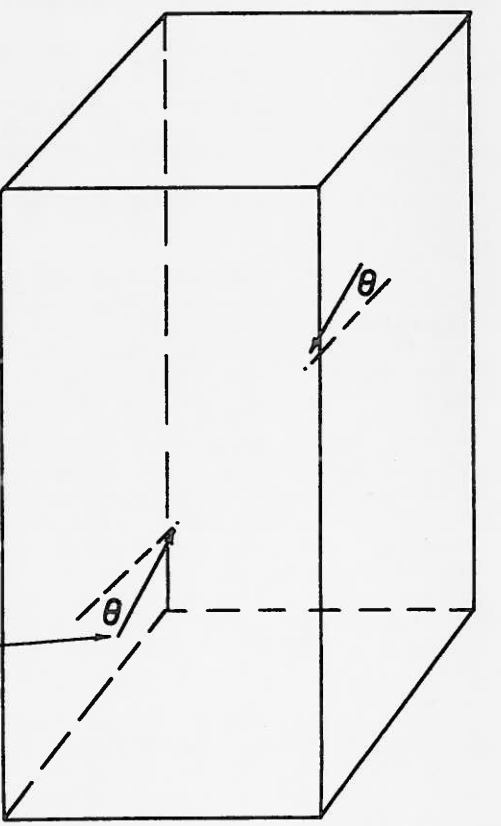

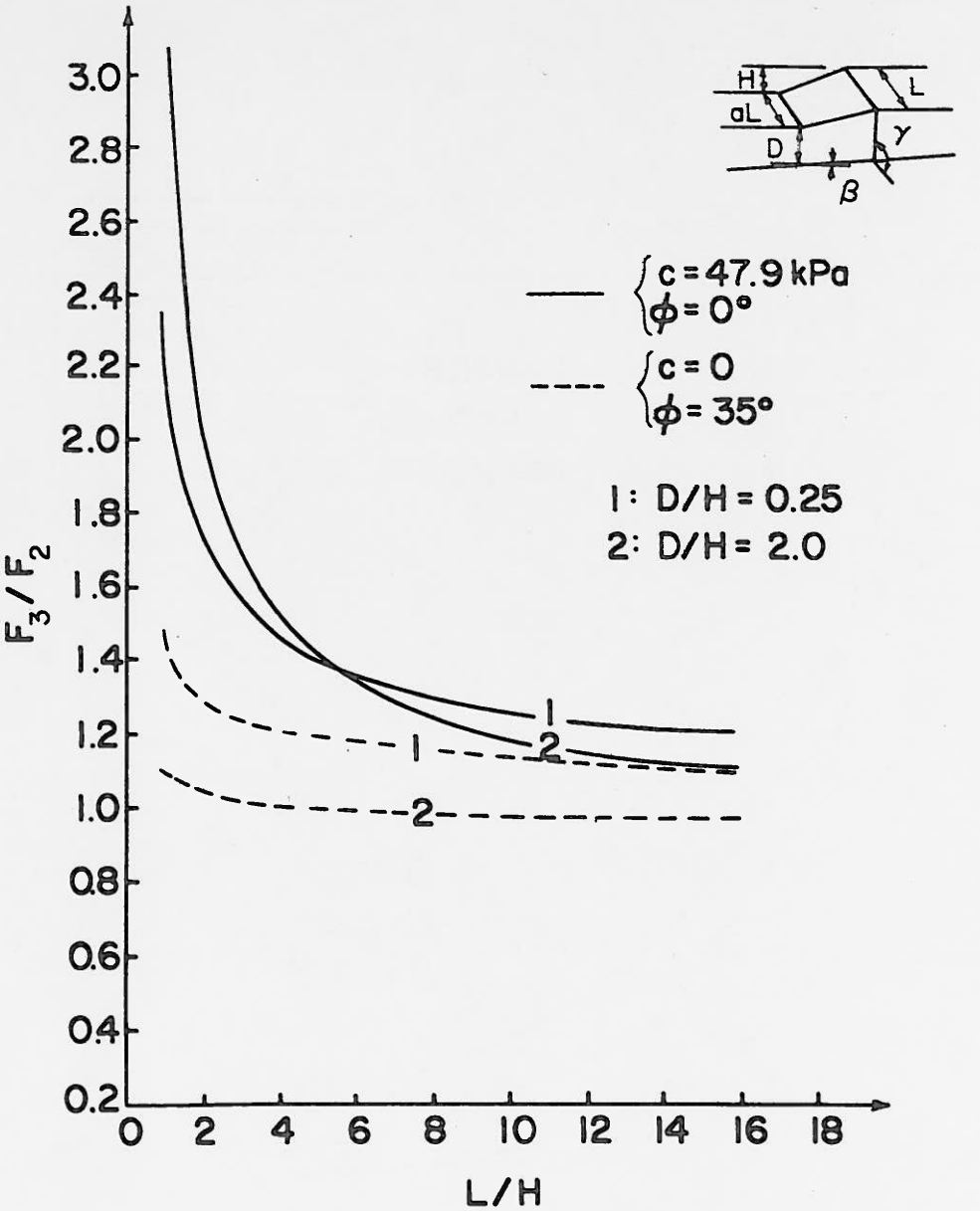

Figure 7 F_3/F_2 vs. L/H for Various D/H and Soil Parameters (at a = 0.8, $\beta = 0^o$, $\gamma = 90^o$, and c_w = 9.6kPa)

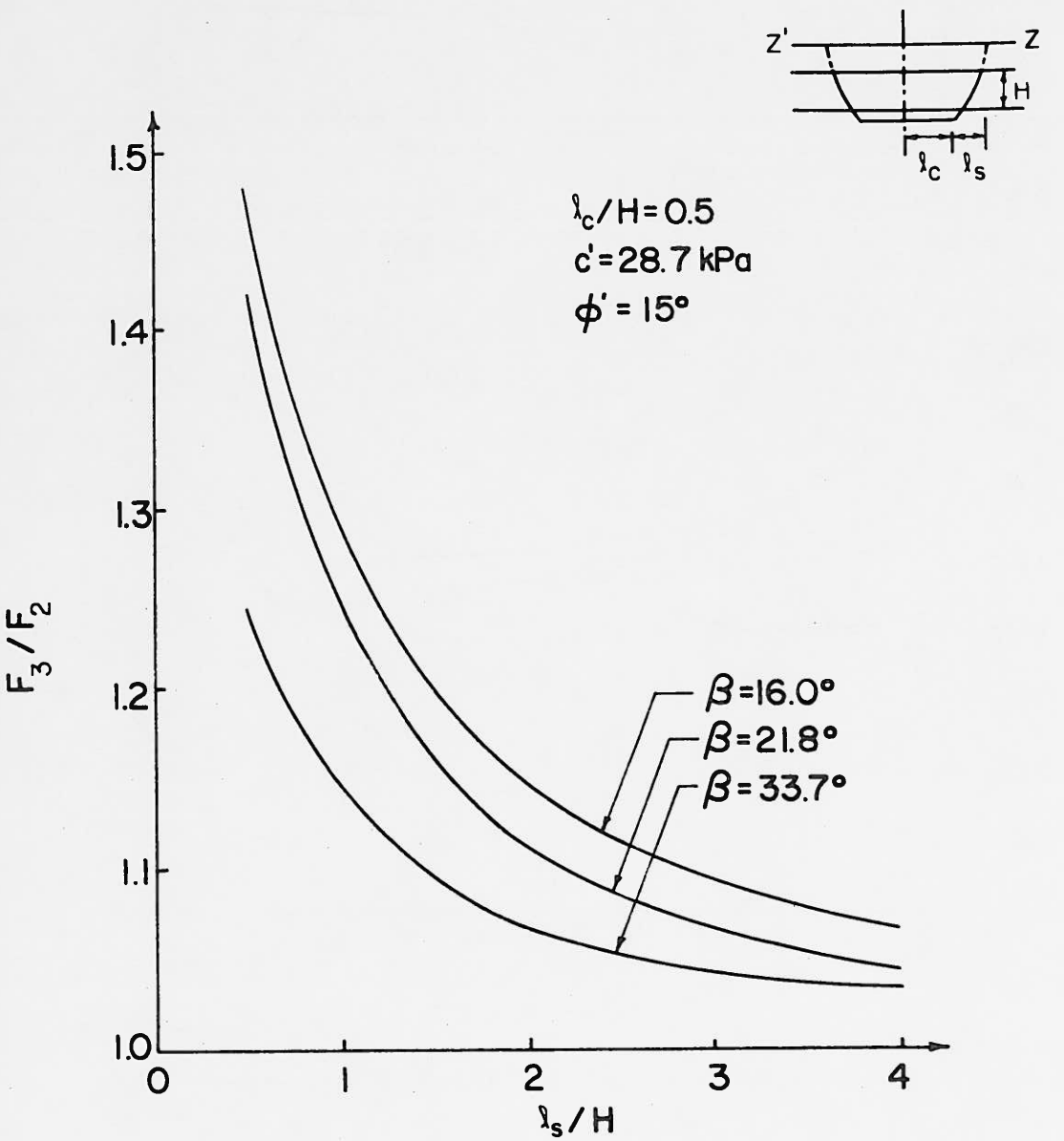

Figure 8 F_3/F_2 vs. l_s/H for Various Slope Angles (r_u = 0.5)

2. Boutrup, Eva (1977), "Computerized Slope Stability Analysis for Indiana Highways." Joint Highway Research Project Reports 77-25 & 77-26, School of Civil Engineering, Purdue University, W. Lafayette, Ind. 512 pp.

3. Goodman, Martin (1982), "Design of Compacted Clay Embankments for Improved Stability and Settlement Performance." Joint Highway Research Project, School of Civil Engineering, Purdue University, W. Lafayette, Ind. (publication pending).

4. Siegel, R. A., Kovacs, W. D. and Lovell, C. W. (1978), "New Method of Shear Surface Generation for Stability Analysis." Proceedings, 29th Annual Highway Geology Symposium, Annapolis, Maryland, pp. 295-312.

5. Boutrup, E., Lovell, C. W. and Siegel, R. A. (1979), "STABL2 ... A Computer Program for General Slope Stability Analysis." Proceedings, 3rd International Conference on Numerical Methods in Geomechanics, Aachen, West Germany, pp. 747-757.

6. Boutrup, E. and Lovell, C. W. (1980), "Searching Techniques in Slope Stability Analysis." Engineering Geology, Vol. 16, No. 1/2, July (Special Issue on Mechanics of Landslides and Slope Stability) pp. 51-61.

7. Siegel, R. A., Kovacs, W. D. and Lovell, C. W. (1981), "Random Surface Generation in Stability Analysis." Journal, Geotechnical Engineering Division, ASCE, GT7, July, pp. 996-1002.

8. Rooney, M. F., Howland, J. D. and Molz, R. J. (1982), "Implementing Large Programs on Microcomputers," Journal of the Technical Councils of ASCE, Vol. 108, No. TC1, May, pp. 125-137.

9. Chen, R. H. (1981), "Three-Dimensional Slope Stability Analysis," Joint Highway Research Project Report 81-17, School of Civil Engineering, Purdue University, W. Lafayette, Ind. 297 pp.

LOOSE SAND PIPES IN GLACIAL OUTWASH: HOW DID THEY DEVELOP AND ARE THEY SIGNIFICANT?

William A. Cutter and Bruce Bailey
ATEC Associates, Inc., Indianapolis, Indiana

INTRODUCTION

Background

Unusual soil conditions have been disclosed beneath several terraces situated along the Ohio River and one of its tributaries in Indiana, Kentucky and Ohio. Typically, these terraces are formed on dense deposits of glacial outwash (sand and gravel) capped with a relatively thin layer of alluvium. In most cases, the terraces are located well above the flood plains of the contemporary river systems. Near-vertical and extremely loose sand features or "pipes," of limited plan dimension, have been found within the otherwise dense outwash. These loose sand pipes have been discovered in soil borings, test pits, and construction excavations at five sites within this region as shown in Figure 1.

Purpose and Scope

The purpose of this paper is to identify and document this unusual condition primarily through a description of the findings at one site where the loose sand pipes were closely spaced and to set forth a probable explanation for their development. The second objective is to solicit input from other practitioners who may have encountered similar conditions.

In this paper, the conditions encountered at Site 1, where the loose sand was first encountered by the authors, will be described in detail. The results of soil test borings and field observations made at other sites will also be discussed. Reference to specific locations, owners and the nature of the projects will not be made considering the proprietary nature of the information.

Regional Geology

The bedrock surface throughout western Ohio, Indiana and northern Kentucky is comprised of Paleozoic age rocks which decrease in age westward from a carbonate sequence consisting of limestone, calcitic dolomite with some shale (Ordovician, Silurian and Devonian) to a clastic sequence with shales, sandstones and lesser amounts of limestone (Pennsylvanian).

Segments of the Ohio River from Cincinnati to Louisville have been crossed two or three times by glaciers during the Pleistocene. From Louisville, an unglaciated, constricted valley segment extends to Tell City, Indiana. Downstream, the river emerges into a broad, unglaciated, alluviated valley with extensive bottom lands. The southern extent of the Wisconsin ice sheet and the maximum limits of Pleistocene glaciation are shown in Figure 1.

The Ohio River channel was modified by several episodes of flooding caused by glacial meltwaters and outwash filling. The present-day course of the river was basically established during the Nebraskan glaciation, the oldest Pleistocene ice advance, when drainage was diverted to the southwest across a well-defined, north-trending cuesta of Silurian rock near Madison, Indiana.

Ice of the most recent Wisconsin glaciation did not reach the Ohio. However, extensive alluviation of the valley by glacio-fluvial deposits and tributary ponding did occur. Wisconsin outwash entered the Ohio River Valley at the confluences of the Great Miami and Wabash Rivers in southwestern Ohio and southwestern Indiana, respectively. In addition, extensive alluviation also occurred in tributary valleys in Indiana including the East Fork of the White River to well north of Indianapolis.

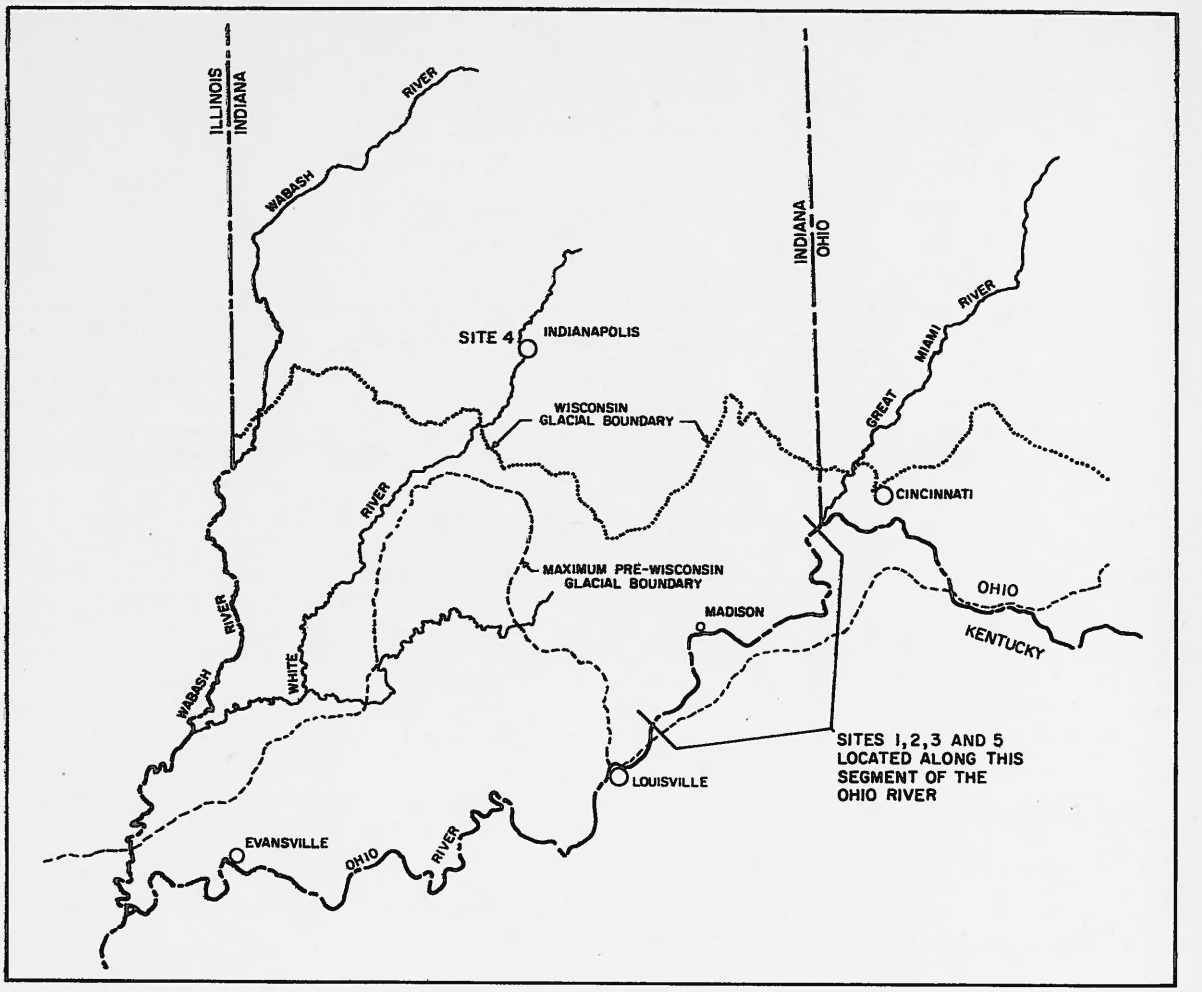

FIGURE 1 LOCATION MAP

Aggradation during advances of the fluctuating Wisconsin ice sheet and degradation during retreats led to the formation of two prominent terraces along the Ohio River developed during the Tazewell and Cary ages. Occasional Illinoian terraces occur locally at higher elevations and remnants of Illinoian and possibly earlier outwash materials are buried beneath the Wisconsin and more recent deposits. These terraces are typically capped with finer-grained silts and clays.

Sand and gravel drift and outwash deposits along the Ohio River commonly contain glacially derived white and brown pebbles of chert, quartz, quartzite, granite, gneiss, schist, and finely-crystalline igneous and metamorphic rocks from Cincinnati to Evansville. Local bedrock lithologies are reflected, to some degree, by the constituent carbonate and clastic assemblages of limestone, calcitic dolomite, siltstone, and sandstone east of Louisville as compared to the clastic siliceous fossil fragments, coal, black shale, and sandstone near Evansville.

CONDITIONS FOUND AT SITE 1

Site 1 is located on a Pleistocene outwash terrace which extends approximately 25 ft above the present flood plain of the Ohio River (Figure 1). At this location and on this side of the river, the outwash terrace is approximately 2500 ft wide while the lower and younger, contemporary flood plain ranges in width from 300 to 400 ft.

The valley walls adjacent to this site extend about 400 ft above the general terrace level. Silurian limestones form the top of adjacent uplands and are underlain by Ordovician shales and limestones. The outwash sand and gravel which forms the terrace is about 120 ft thick and is capped with a veneer of layered and typically fine-grained alluvium. The generalized geologic conditions are shown in Figure 2.

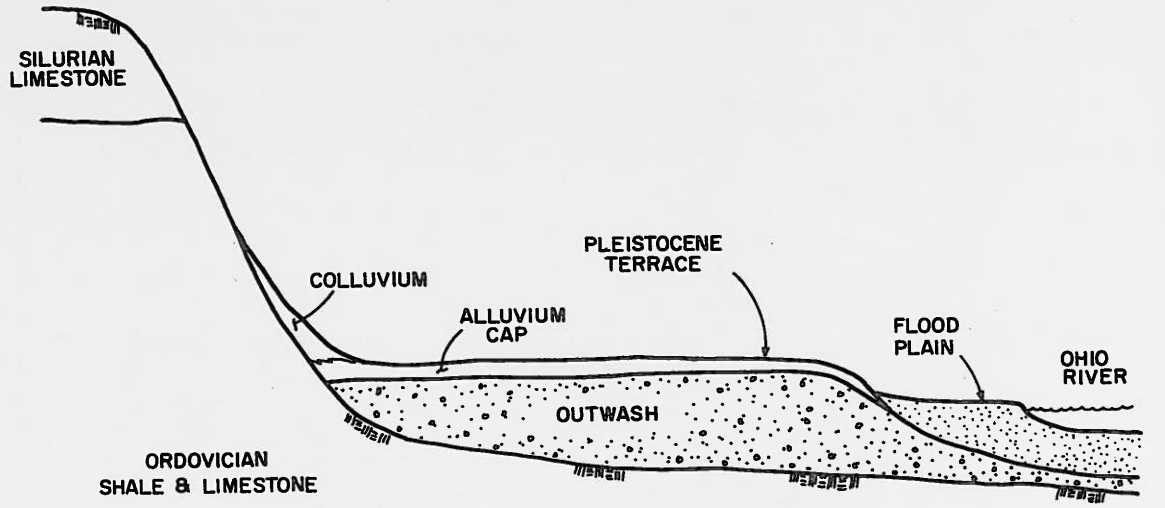

FIGURE 2 GENERALIZED GEOLOGY AT SITE 1

The groundwater level at Site 1 is influenced by the Ohio River level and presently is about 45 to 50 ft below the terrace. The groundwater level has been artificially raised as a result of high lift dam construction. According to Walker (1957), the recorded low river level in 1895 was approximately 65 ft below the Pleistocene terrace level. Considering the manner in which the terraces developed, the groundwater level undoubtedly has been at many different elevations since the outwash was deposited.

Typical Subsurface Conditions

The typical subsurface conditions disclosed in the upper 80 ft at Site 1 are shown in Figure 3. The alluvium generally consists of layers of low plasticity clay, clayey silt, silt and silty fine sand. The sand and gravel varies in gradation with gravel percents ranging from 10 to 70. The percent fines typically is less than 10. Gradation curves for typical outwash materials are shown in Figure 4.

Occurrence of Loose Sand Pipes

A large number of soil borings were made at Site 1, of which approximately 40% disclosed low standard penetration resistances (N-values) of 11 blows/ft or less within the outwash formation. At some locations, only one or two low N-values were disclosed. At other locations, significant depth intervals were involved. In several borings, low N-values were noted for the entire depth from the top of the outwash to near the present groundwater level. Typical plots of N-values versus depth which depict these conditions are shown in Figures 5 and 6. Samples of loose sand from the pipes generally contained less gravel size materials and a larger silt fraction than the denser outwash. Grain size distribution curves of typical loose sand samples are shown in Figure 7.

The frequency of occurrence of the loose sand pipes is depicted in Figure 8. In this illustration, the percentage of low N-values (11 blows/ft or less) disclosed at each sample level is shown graphically. In the same illustration, the percentage of N-values less than or equal to one blow/ft is also shown in a similar fashion. The data shown in Figure 8 represent the results of 53 soil test borings uniformly spaced over a 35-acre area. A similar plot is shown in Figure 9, which represents 39 soil borings made over an area of approximately two acres. Figures 8 and 9 indicate that approximately 35% of the borings disclosed loose granular soils at the top of the outwash (approximately at the 10-ft depth). However, below the 15-ft depth, only 13 to 18% of the borings disclosed low N-values at a given elevation. The data shown in Figures 8 and 9 also indicate that the majority of the very low N-values were encountered between 30 and 45-ft depths. Even though the data illustrated in Figures 8 and 9 were compiled from areas considerably different in size, the two plots are strikingly similar, indicating a regularity of occurrence of the pipes at this site.

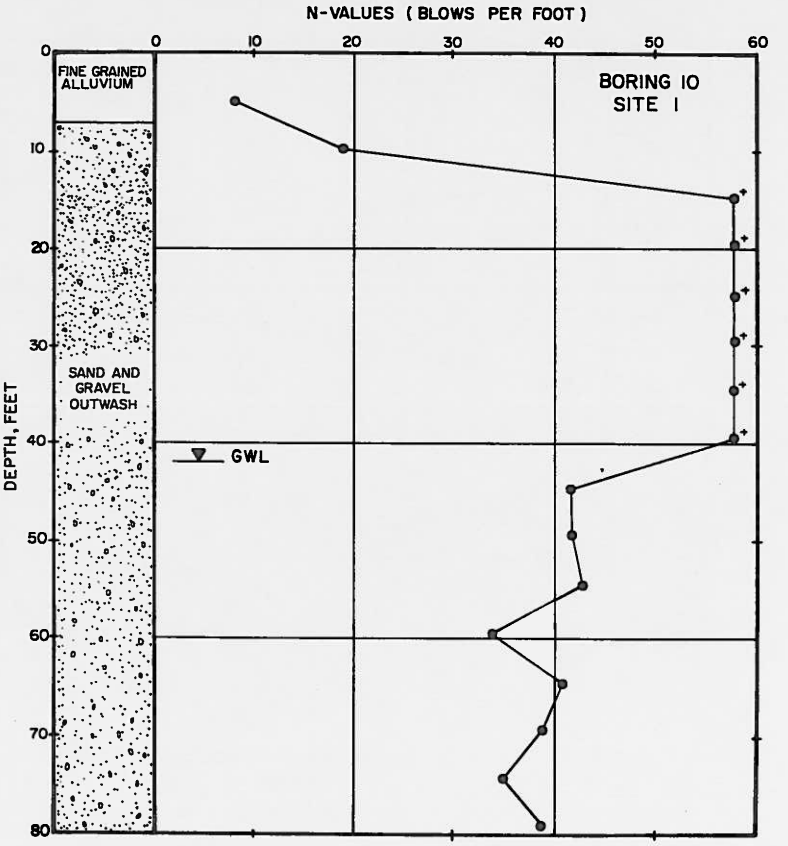

FIGURE 3 TYPICAL BORING WHICH DISCLOSED DENSE OUTWASH

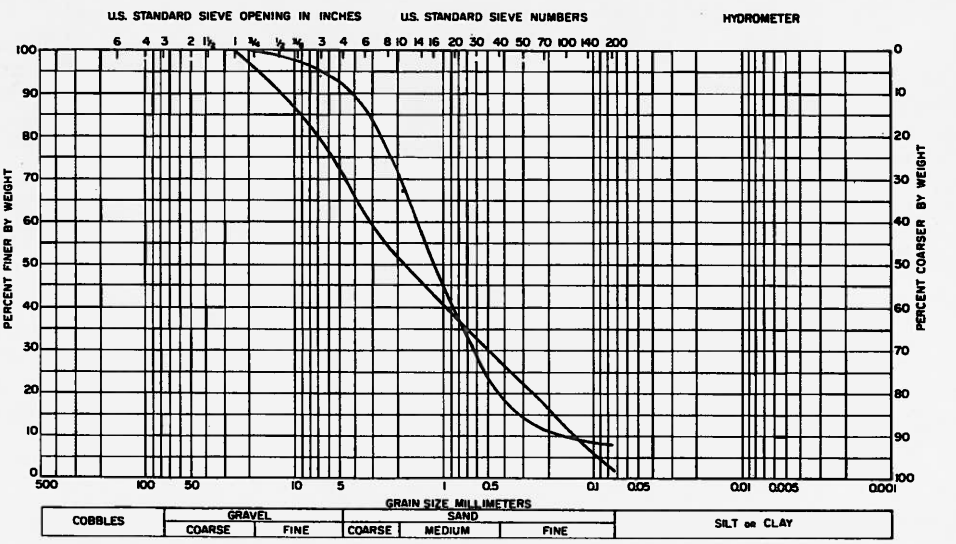

FIGURE 4 TYPICAL GRADATION CURVES FOR DENSE OUTWASH

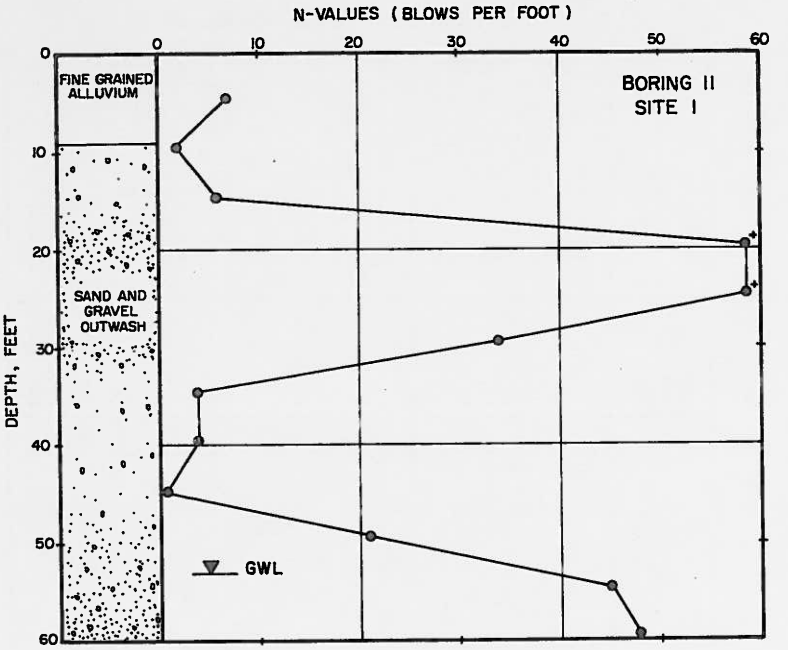

FIGURE 5 TYPICAL BORING WHICH DISCLOSED LOOSE CONDITIONS

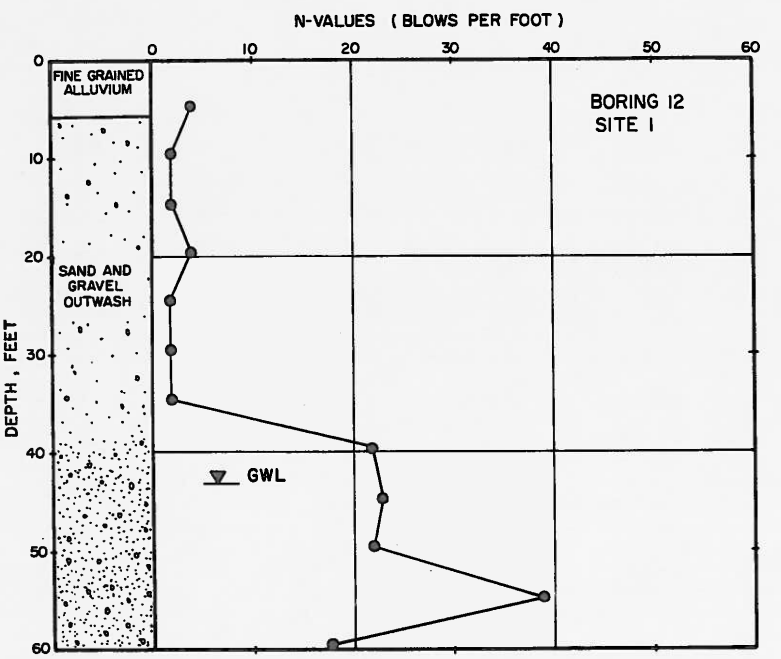

FIGURE 6 TYPICAL BORING WHICH DISCLOSED LOOSE CONDITIONS

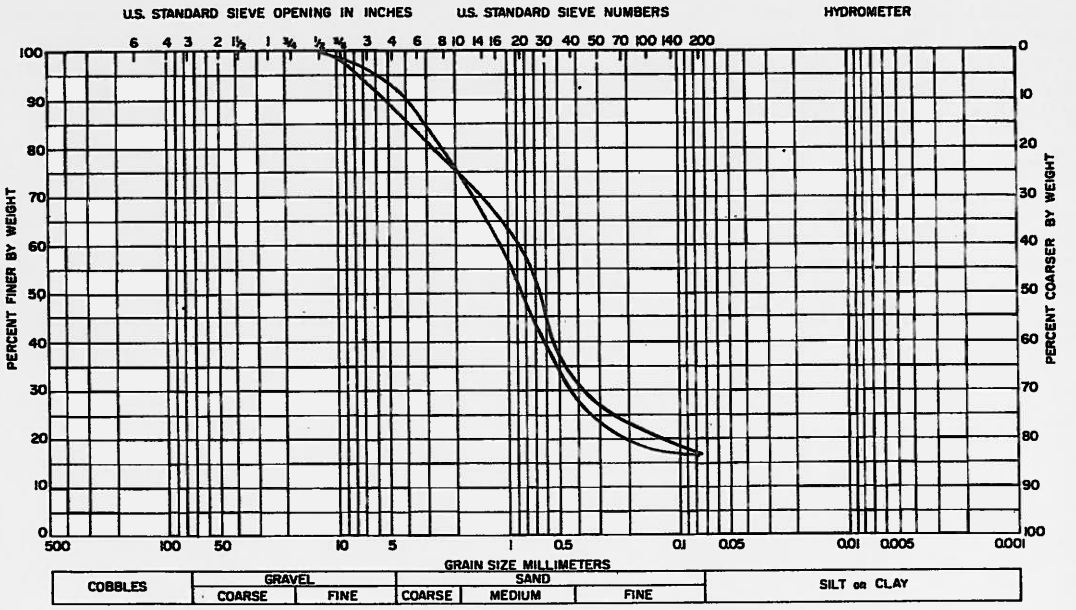

FIGURE 7 TYPICAL GRADATION CURVES FOR LOOSE MATERIAL

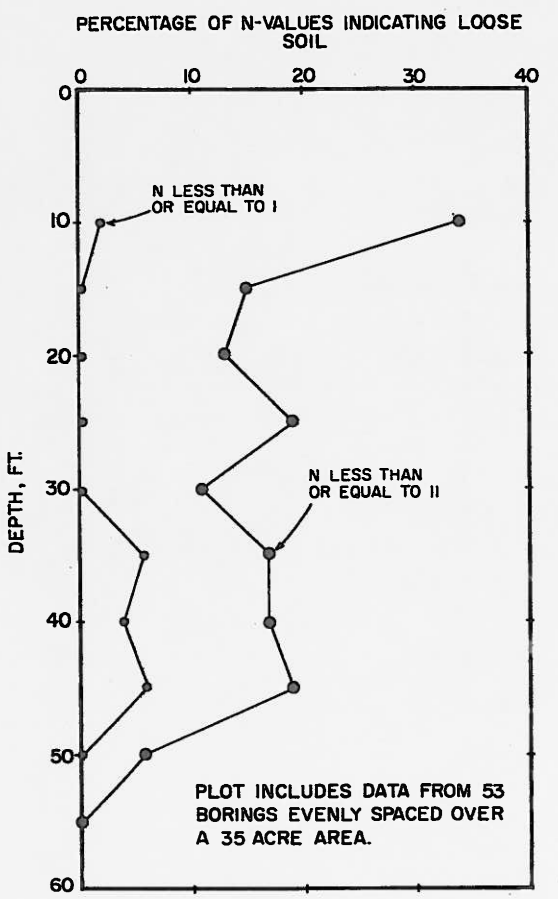

FIGURE 8 PERCENTAGE OF N-VALUES INDICATING LOOSE SAND VERSUS DEPTH

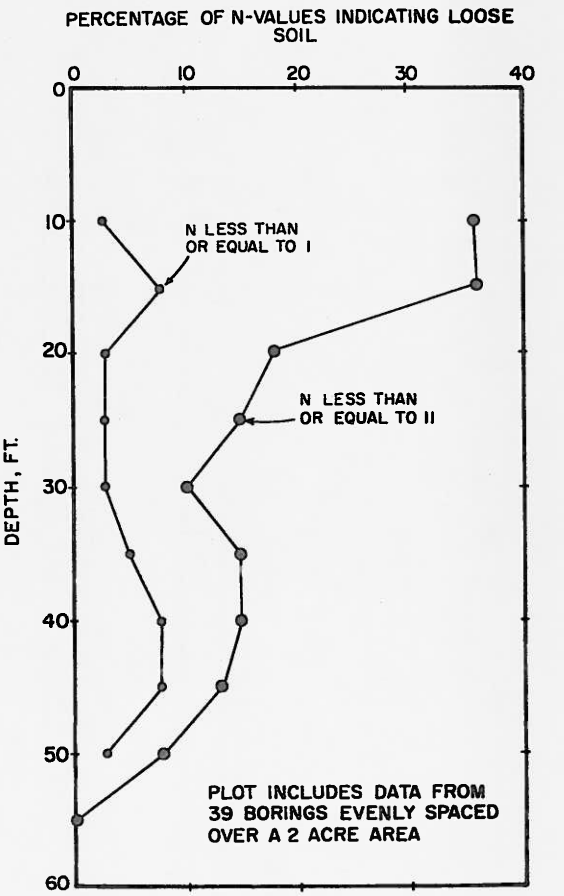

FIGURE 9 PERCENTAGE OF N-VALUES INDICATING LOOSE SAND VERSUS DEPTH

At some boring locations, the sand was extremely loose in condition. On occasion, the sampler and drill rods dropped several feet due to self weight. At one particular boring location, the sampler and rods dropped 5 ft and the hollow-stem auger casing sank approximately 6 in. while preparing to conduct a standard penetration test. It is emphasized that these events generally occurred at elevations above the existing groundwater level.

Plan Dimension of Loose Sand Pipes

The distribution of the low N-values was peculiar in that it did not imply association of the loose material with buried drainage features within the outwash. Rather, the loose sand occurred within a limited plan dimension as indicated in auxiliary test borings drilled at distances of four ft from borings which disclosed loose sand. The results of two auxiliary boring sets are shown in Figures 10 and 11. The variation in N-values over very short horizontal distances displayed in each figure is apparent.

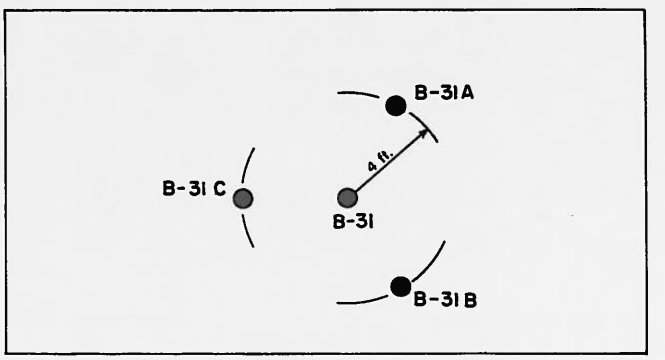

a) PLAN

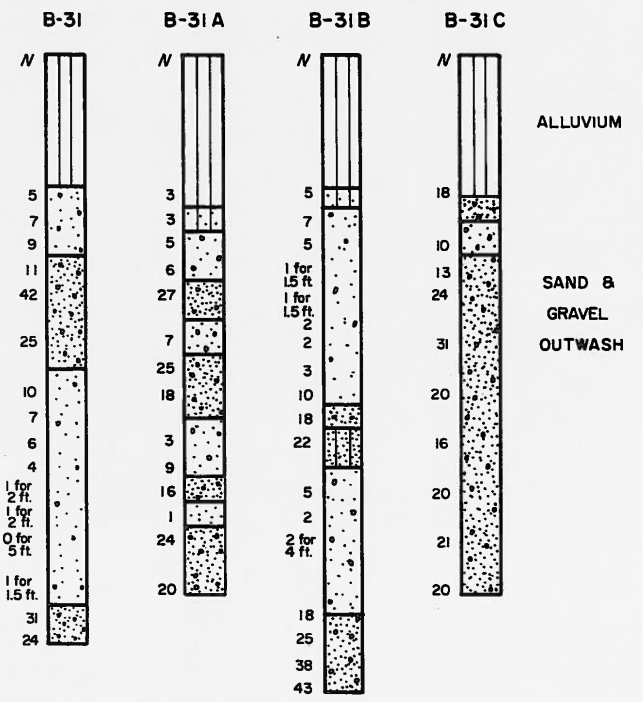

b) STRATIGRAPHY

FIGURE 10 RESULTS OF CLOSELY SPACED SPT BORINGS AT BORING 31 LOCATION

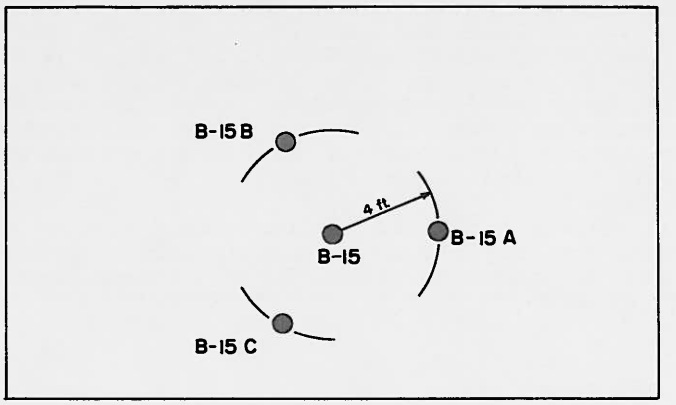

a) PLAN

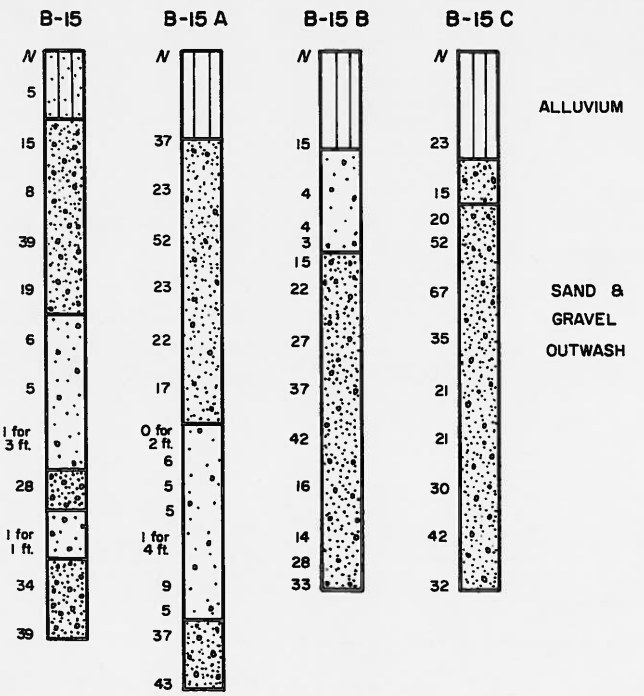

b) STRATIGRAPHY

FIGURE 11 RESULTS OF CLOSELY SPACED SPT BORINGS AT BORING 15 LOCATION

Test Pit Observations

A shallow excavation was made near one of the boring locations where low N-values were disclosed. The excavation was made by removing the upper soils to a depth of six feet over a large area and then continuing the excavation by backhoe over a much smaller area, providing a deep, benched, test pit excavation.

The loose sand features were very apparent in the walls of the pit. To aid in describing the conditions encountered, sketches showing the sampling and testing locations and the visible loose sand features are shown in Figures 12 and 13. These illustrations show profile views through the center of the excavation; the east and west walls of the excavation are shown in Figures 12 and 13, respectively. The locations of five dark brown and relatively wet areas are shown in these figures. In addition, a dark, wet and soft pocket was noted in the bottom of the excavation. Water content and in-place density tests were conducted at several locations within the pit. The results of these tests are shown in Figures 12 and 13. The contrast is most evident when comparing tests R-1, R-2 and R-3 in Figure 13, where the dry unit weights range from 128 to 103 lbs/cu.ft over a distance of about three ft. The loose materials were generally more silty than the surrounding materials and typically contained less gravel. A layer containing light colored gravel, which appeared to be highly weathered, was located near the boundary between the dark-colored loose sand pipe and the adjacent undisturbed outwash.

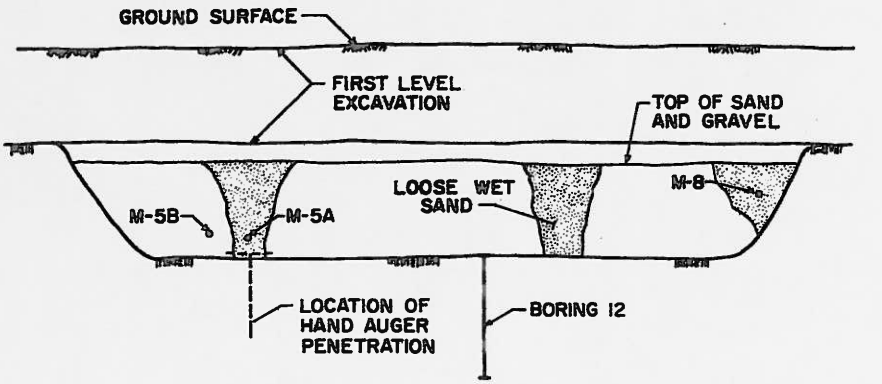

FIELD TEST RESULTS

No.	WATER CONTENT, %
M-5A	13.4
M-5B	5.6
M-8	8.2

FIGURE 12 PROFILE THROUGH TEST PIT SHOWING EAST FACE

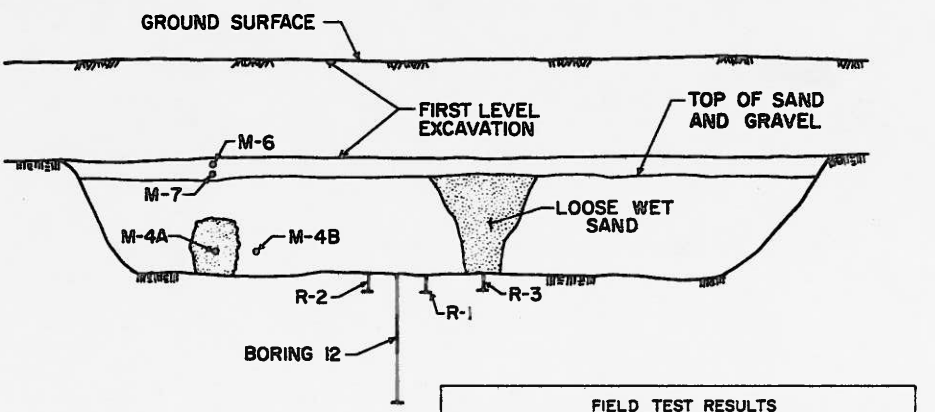

FIELD TEST RESULTS

No.	WATER CONTENT, %	UNIT DRY WEIGHT, pcf
R-1	16.1	103
R-2	5.9	128
R-3	10.0	102
M-4A	11.6	
M-4B	4.2	
M-6	11.3	
M-7	10.1	

FIGURE 13 PROFILE THROUGH TEST PIT SHOWING WEST FACE

The wetter zones were decisively weaker than the matrix outwash materials. At one location, it was possible to push a hand auger four ft into the base of the excavation with very little resistance. Where visible, the loose sand pipes were widest near the outwash surface and decreased in width to about two ft at the bottom of the excavation. The one loose sand pipe exposed in the base of the excavation was generally circular in plan.

Field Observations During Construction

During construction at Site 1, a general excavation was made in the main building areas to a depth of 15 ft. The loose sand pipes could be identified along the walls of the excavation as dark colored materials which typically were widest at the outwash surface and decreased in width with depth. At some locations, thin organic seams, less than one in. in thickness, were observed along the outwash surface. These seams dipped and appeared to form a lining for the loose sand pipe. Where present, the organic seam formed a smooth surface and the loose sand pipe took on a funnel-shaped appearance. At locations where organic seams were not observed, the shape of the darker colored sand was more irregular but typically was largest at the top of the outwash and decreased in width with depth.

Numerous circular zones of dark colored sand could be observed in the base of the excavation where disturbance had been kept to a minimum. A typical near-circular pipe is shown in Figure 14. A second feature is shown in Figure 15. The white spot shown in the center of the dark area is lime, used for marking. The light colored aggregate particles, situated just outside the dark area, were typically very soft, or chalky. In some cases, these aggregate particles could be cut with a pocket knife, as illustrated in Figure 16. For reference, the small pocket knife shown in these photographs is 2-3/4 in. in length.

Hydrochloric acid was applied to materials in the base of the excavation both inside and slightly away from the dark colored sand. At each point tested, a mild reaction was noted outside of the feature and virtually no reaction at all was noted within the circular area.

A reference section approximately 175 by 70 ft in plan area was marked such that an estimate of the distribution of visible features could be made. Each of the 43 pipes identified within this area was circled with a white line of lime. Attempts were made to penetrate these identified pipes with hand augers. A penetration of more than 6 in. could not be made at any location exposed in the base of the excavation, demonstrating that not all of these pipes contained excessively loose materials at this elevation.

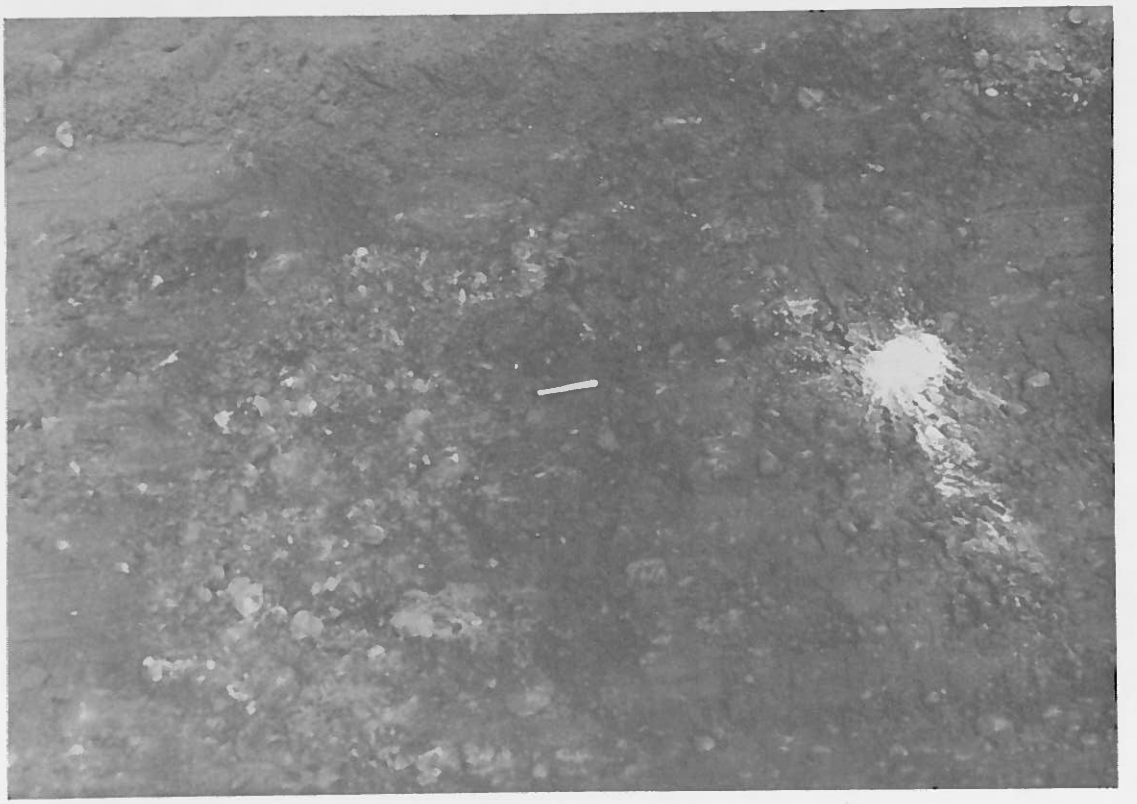

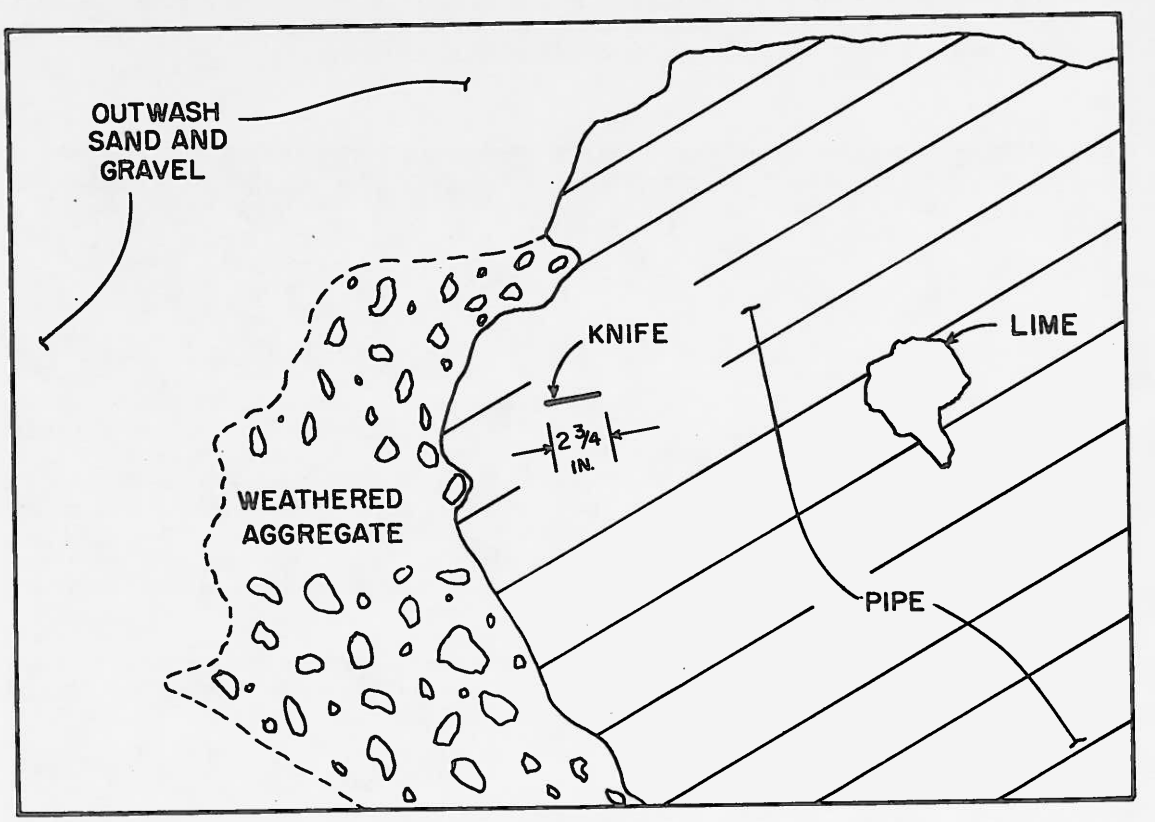

FIGURE 15 LOOSE SAND PIPE EXPOSED ON A HORIZONTAL SURFACE SHOWING CONCENTRATIONS OF LIGHT COLORED WEATHERED COARSE MATERIAL

FIGURE 16 SOFT HIGHLY WEATHERED AGGREGATE

The majority of the pipes were approximately two to three ft in diameter. One large pipe, over seven ft in diameter, was also noted. At this location, a backhoe excavation was made such that one face of the cut exposed the center of the pipe. The edge of the pipe was clearly marked by a thin organic seam as shown in Figure 17. At a depth of two ft, the diameter of the funnel was 3.4 ft. At a depth of 4.3 ft, the diameter had reduced to 3 ft. From this elevation, the base of the backhoe excavation was also probed. After several attempts, a loose area was detected near the center of the pipe and the hand auger was pushed by hand to a depth of approximately four ft below the base of the backhoe excavation.

Flat and sometimes angular pieces of limestone were present in the base of the general excavation. Several pieces taken from the excavation are shown in Figure 18. The surfaces of these limestone pieces were typically weathered and soft.

Occurrence of Soluble Carbonate Materials

Laboratory tests to measure the percent soluble material (primarily carbonates dissolved in acid) were conducted on samples of loose sand and undisturbed outwash soils. The results are shown in Table 1. Each sample tested was bathed in a 0.1N hydrochloric acid solution until additional reaction was insignificant. The N-values for samples obtained from standard penetration test borings are also shown with the appropriate test results in Table 1. These tests indicate that the samples of dense sand typically contain 30 to 40% soluble material. On the other hand, samples of the looser material showed considerable variation in percent soluble material with percentages ranging from almost 0 to 40%.

TABLE I RESULTS OF SOLUBILITY TEST

Sample Depth, ft	N-Value	Material Soluble in HCL, %
41-42 1/2	2/24"	42.7
18.5-20	98	31.5
26-27.5	0/60"	0.3
41-42 1/2	1/12"	18.7
28 1/2-30	48	42.3
23.5-25	59	43.3
46-47.5	2	8.7
9-11	Test Pit Sample (M-5A)	2.1

FIGURE 17 LOOSE SAND PIPE EXPOSED ON VERTICAL SURFACE

FIGURE 18 FLAT AND ANGULAR PIECES OF LIMESTONE TAKEN FROM THE EXCAVATION AT SITE 1

Additional Exploration

Attempts were made to delineate the loose sand features using the geophysical methods of soil resistivity and seismic refraction. In addition, infra-red aerial photography was used on a trial basis. In general, these methods proved to be inconclusive and were not instrumental in the evaluation of the presence or significance of the loose pipes.

LOOSE SAND PIPES OBSERVED AT OTHER SITES

Circular areas of dark colored granular soil were also observed in the base of an extensive area excavation at Site 2 (Figure 1). In addition, at this site, a well-defined feature was observed in the walls of an excavation which extended well below the general excavation. The top of the near vertical face which disclosed this pipe was situated approximately five ft below the outwash surface. As observed on the face of this cut (Figure 19), the pipe was approximately 12 to 18 in. in width and was near-vertical. The center or core of the pipe was extremely soft. It was possible to push a hand auger approximately nine ft below the bottom of the lower excavation. It was estimated that the tip of the auger was approximately 25 ft below the original outwash surface. The owner reported that no loose sand was encountered in the test borings at this site.

Standard penetration test soil borings from another site along the Ohio River (designated Site 3) were examined. Two of the nine soil borings drilled disclosed very loose granular soil within depth zones above the ground water level. These nine borings were part of a preliminary geologic study of this site and it was elected not to develop the site based on these findings.

The tops of rather well-defined loose sand pipes have also been observed at the outwash surface in excavations made at Site 4 which is located in downtown Indianapolis, Indiana. The top of the pipe was only about three ft in width at the outwash surface and was well defined by a thin organic seam. Gravel size materials located within inches of the organic seam on the outside of the feature were extremely weathered and chalky.

Extremely low standard penetration test results were also observed at Site 5. Based on conversations with other practitioners, the loose sand was disclosed above the prevailing ground water level within the otherwise dense sand and gravel outwash formation.

Loose sand features apparently of the same type have also been observed in gravel pit excavations along other rivers. Carroll (1979) reported the probable presence of this phenomenon beneath terraces along the Wabash, Illinois and Great Miami Rivers.

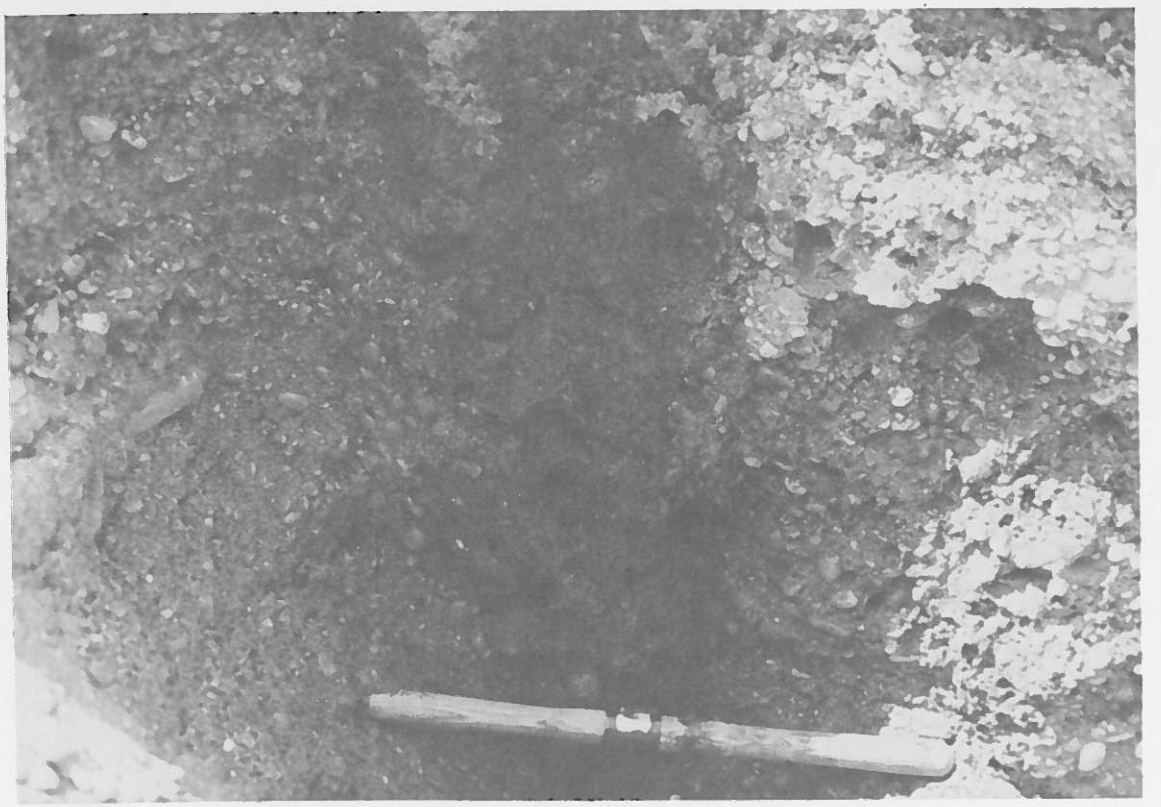

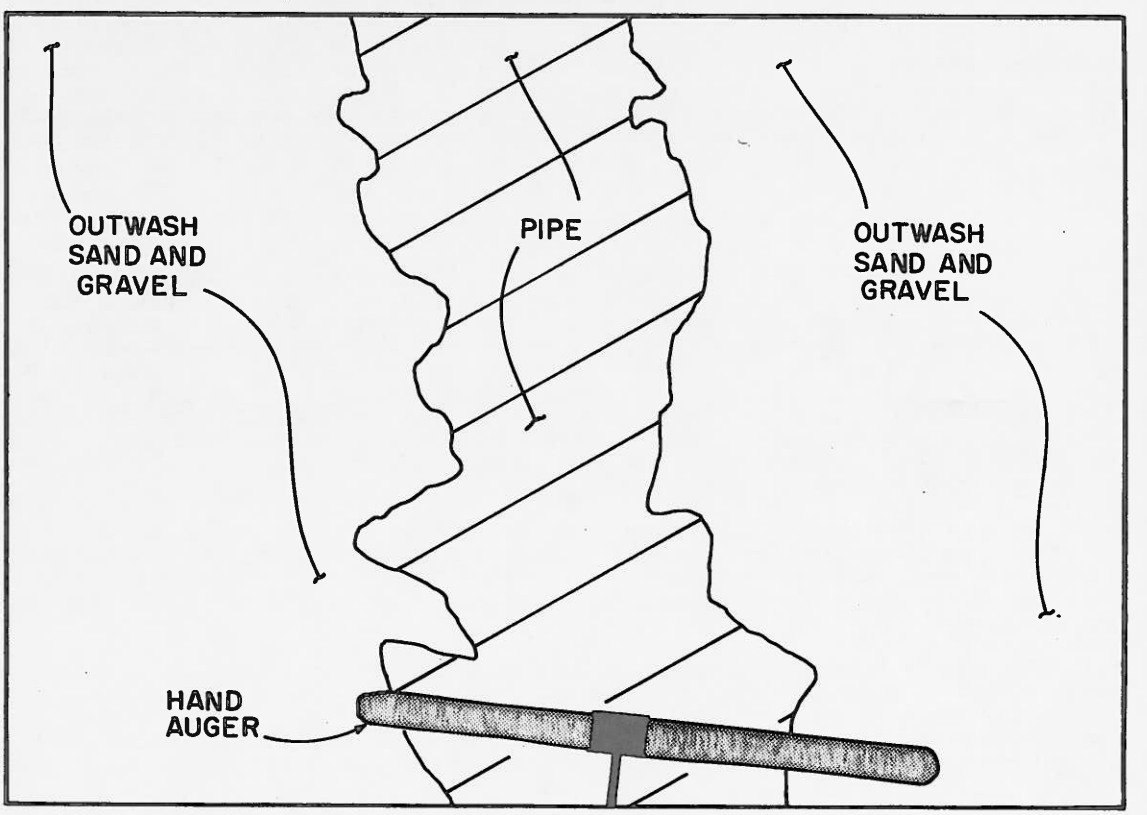

FIGURE 19 LOOSE SAND PIPE EXPOSED ON VERTICAL SURFACE AT SITE 2

EVALUATION OF OBSERVATIONS AND SUBSURFACE DATA

Summary of Pertinent Observations

Loose sand pipes have been discovered beneath terraces along the Ohio River within otherwise strong and dense sand and gravel outwash materials. At sites where the condition was extensively explored, virtually all evidence indicates that the loose sand pipes are of limited plan dimension and that they often exist in the shape of near-vertical cylinders or tubes which are funnel-shaped near the outwash surface. The plots which show frequency of occurrence of the loose sand pipes at various depths below the ground surface (Figures 8 and 9) imply that the total plan area of the site affected by this phenomenon at a given elevation remains relatively constant below the conical tops. The loose sand pipes examined to date have been found almost exclusively above the present groundwater level.

Where encountered, the loose sand pipes have been associated with sand and gravel outwash deposits which are rich in soluble materials. At Site 1, where numerous loose or very loose zones were observed, large gravel and cobble-size aggregate and large plates of limestone and dolomite are present with the outwash. The loose sand pipes observed in the excavations contain a variable percentage of soluble material and in many cases are free of carbonates. Highly weathered, gravel-size materials, which are very soft and chalky, are prevalent especially around the perimeter of the near-circular features. The granular material within the pipes, in some cases, contain higher percentage of fines than the adjacent matrix material. However, in some cases, especially where loose materials were encountered at substantial depths, the sand and gravel was nearly free of fines. In all cases, the materials inside of the pipes were considerably wetter than the surrounding outwash soils.

At some locations, the funnel-shaped tops of the pipes are well defined by thin organic seams. In addition, at certain locations, generally horizontal seams of alluvium above the outwash surface appear to have sagged slightly when situated over well-defined funnel-shaped pipes.

Probable Origin of Loose Sand Pipes

It is the authors' opinion that the loose sand pipes developed through a process of chemical weathering whereby the soluble materials were leached from within the originally dense sand and gravel outwash. The weathering process initiated from the outwash surface under the influence of surface water infiltrating through the alluvial cover and the permeable sands and gravels. The presence of organics resulting from the decomposition of surface vegetation may have produced a mildly acidic surface water which attacked the soluble carbonate particles in the outwash. Visible evidence indicates that the weathering was general and affected most of the outwash surface, possibly when it was exposed. Below this relatively thin zone of general surface weathering, preferred paths of groundwater percolation developed through the more pervious but unsaturated underlying outwash. This process produced a combination of an irregular weathering surface at the top of the outwash and the near-vertical pipes of leached granular soil which extended down to the prevailing groundwater level. This model is illustrated in Figure 20.

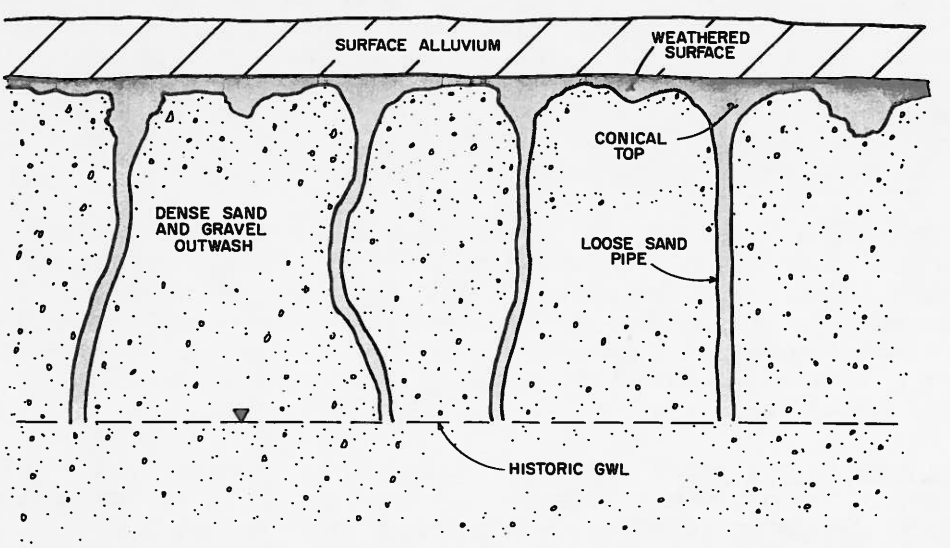

FIGURE 20 AUTHORS' CONCEPTUAL MODEL OF CHEMICAL WEATHERING PRODUCING LOOSE SAND PIPES

The continued infiltration of surface water may have expanded the affected zone (the pipes) and produced the larger funnel-shaped zone of weathering at the top of the pipe. After thousands of years of leaching, the granular soils within the funnels and pipes underwent measurable losses in density resulting in a loose and sometimes near metastable condition.

Considering that the outwash material was typically deposited as braided stream systems, initially the groundwater level was near the surface of the outwash. During later interglacial periods, the groundwater level existed at levels well below the present outwash surface. The leaching action described above most likely proceeded within the unsaturated outwash deposits throughout these periods of low groundwater level up to the present time.

Laboratory studies were conducted by Dr. Jay Lehr (Lehr, 1977), in which water was permitted to percolate down through a two-layer soil system where the lower stratum was more pervious than the overlying soil. These tests indicated that perferred paths of seepage developed in the deeper layer and that seepage continued through these near vertical paths. This laboratory observation is shown in Figure 21. These model test conditions are cited in support of the hypothesized flow conditions through the unsaturated outwash zone which lead to the development of the pipes as described above.

Conditions for Pipe Development

Why the occurrence of these loose sand pipes is more prevalent beneath some terraces is not totally understood. There is some evidence at Site 1, however, that this terrace may be older than Wisconsin age. The presence of large, slab-shaped limestone fragments indicate that these materials did not travel down the Ohio River Valley for extended distances but more likely originated from the adjacent valley walls. This would have been more likely to have occurred when ice fronts were close to the Ohio River Valley at this location, which was not the case during the Wisconsin glaciation. If the terrace materials were deposited during an earlier glaciation, the leaching action would have continued for a much longer period and could account for the significant and frequent development of the pipe features beneath this terrace.

The presence of organic seams and the zone of general weathering at the outwash surface suggest that the surface of the outwash may have been exposed for years. With the absence of an alluvium cap, the rate of surface water infiltration and, therefore, the rate of chemical weathering would have been greater than for a covered deposit. The probability of the outwash surface being exposed for long periods likely would have been greater for the higher terrace levels.

In summary, it seems reasonable that the most extensive development of this type of leaching or the greatest occurrence of the loose sand pipes would be found beneath the highest and oldest terraces, terraces with a thin and relatively pervious alluvium cap and a deep groundwater table and terraces formed on outwash with a high percentage of coarse carbonate materials.

Solicitation of Additional Case Histories

It is of the utmost interest to the practitioner to be able to identify the presence of the loose sand pipes if they exist at a project site and to subsequently assess their engineering significance with respect to foundation design. To date, the existence of this phenomenon has been reported only in Carroll's (1979) thesis which represents research conducted at the University of Illinois under the guidance of A.S. Neito. No case histories disclosing foundation failures or damage attributed to unusual loose sand occurrences in otherwise sound outwash have been reported.

The objectives of this paper were first to identify and document the problem and secondly to solicit input from other practitioners who may also have encountered these conditions. It is intended by the latter objective to consolidate these experiences in an effort to confirm or modify the model set forth herein and thereby develop a better understanding of the engineering significance of the loose sand pipes.

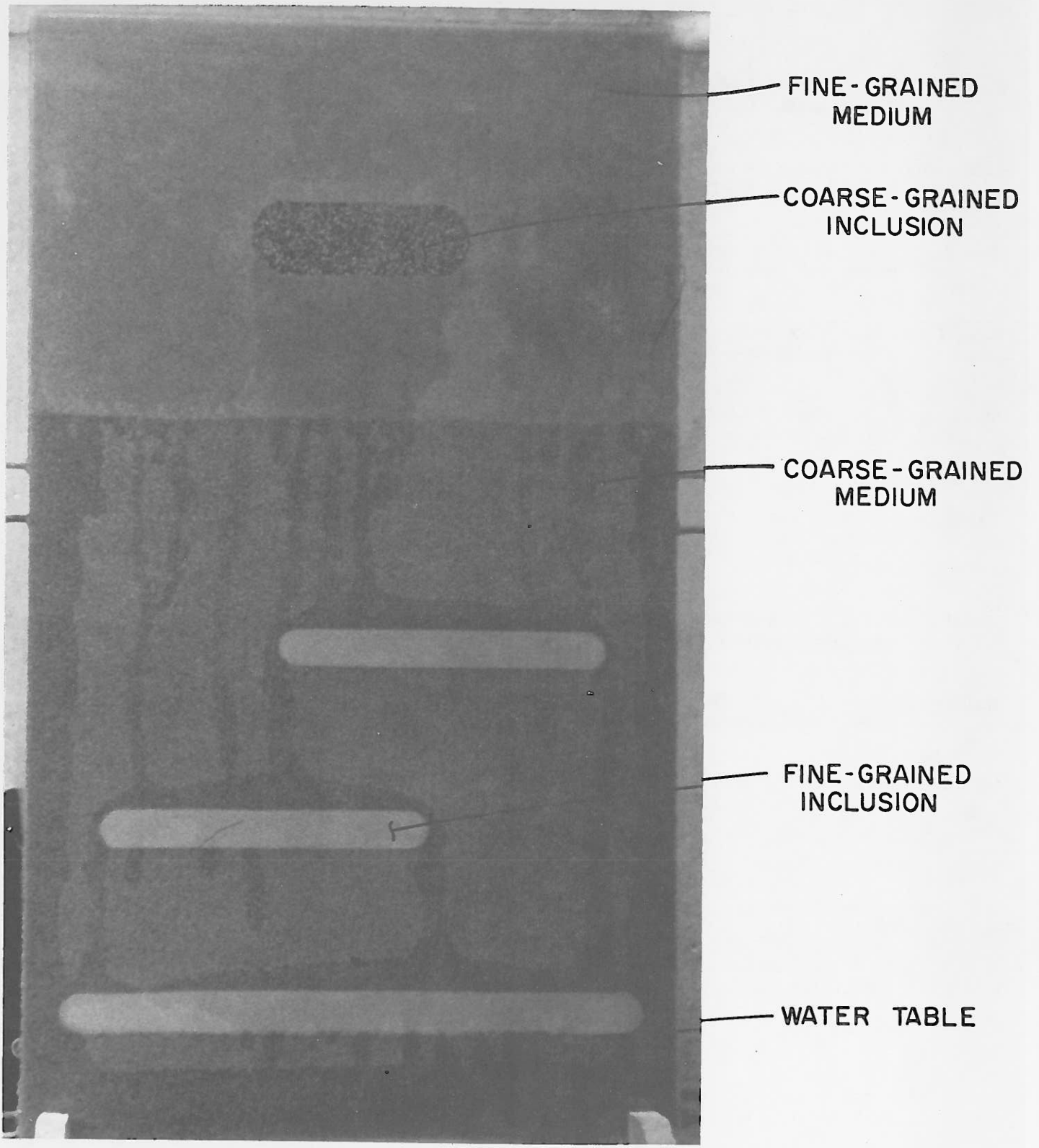

FIGURE 21 LABORATORY MODEL OF GROUNDWATER FLOW THROUGH UNSATURATED TWO-LAYER SOIL MEDIA (PHOTOGRAPH COURTESY OF NATIONAL WATER WELL ASSOCIATION)

REFERENCES

Carroll, Michael T., "A Model for Karst-Like Development in Calcareous Outwash Deposits," M.S. Thesis, University of Illinois, 1979, 130 pp.

Lehr, Jay H., "Ground Water Movement in Living Color: A Slide Show, The National Water Well Association, 1977.

Powell, Richard L., "Geology of the Falls of the Ohio River," Indiana Department of Natural Resources Geological Survey Circular 10, 1970, 45 pp.

Ray, Louis L., "Geomorphology and Quaternary Geology of the Glaciated Ohio River Valley--A Reconnaissance Study, U.S. Geological Survey Paper 826, 1974, 77 pp.

Swadley, W.C., "New Evidence Supporting Nebraskan Age For Origin of Ohio River in North Central Kentucky," Shorter Contributions to Stratigraphy and Structural Geology, 1979, 7 pp.

Teller, James T., "Early Pleistocene Glaciation and Drainage in Southwestern Ohio, Southeastern Indiana, and Northern Kentucky," Ph.D. Thesis, University of Cincinnati, 1970, 115 pp.

Teller, James T., "Significant Multiple Pre-Illinoian Till Exposure in Southeastern Indiana," Geological Society of America Bulletin, Vol. 83, 1972, 8 pp.

Walker, Eugene H., "The Deep Channel and Alluvial Deposits of the Ohio Valley in Kentucky," U.S. Geological Survey Water Supply Paper 411, 1957, 25 pp.

Wayne, William J., "Pleistocene Evolution of the Ohio and Wabash Valleys," Journal Geology, Vol. 60, No. 6, 1952, 10 pp.

USE OF CYLINDER PILE RETAINING WALL TO STABILIZE EXCAVATION SIDES AND PROTECT EXISTING STRUCTURES

P. DEO AND D. NONA
PROJECT ENGINEER AND PRINCIPAL, RESPECTIVELY
NEYER, TISEO & HINDO, LTD., CONSULTING ENGINEERS
FARMINGTON HILLS, MICHIGAN

SYNOPSIS

Steel-reinforced auger-placed and grout-injected concrete pile walls can serve as retaining walls to stabilize excavation sides and constitute the foundations and basement walls for new construction close to existing structures. These walls will yield to lesser extent than sheet pile walls with bracing. The pile walls may be designed as rigid cantilever walls for short to intermediate depths. Lateral earth pressure distribution for the walls will depend upon the soil type and is considered to be similar to the distribution for a rigid embeded pile subjected to lateral loads.

INTRODUCTION

With increased emphasis on urban development, more construction projects are located within a few feet of existing buildings. Often, this requires construction excavations to extend several tens of feet below existing foundations, grade beams, and floor slabs. Accordingly, special measures are required to protect these structures against movement or damage and, at the same time, stabilize the excavation sides to enable construction operations to proceed. Some of the commonly used methods include: a) underpinning of existing structures and retaining the excavation sides such as with sheet piling; b) construction of diaphram walls using heavy slurry of bentonite and tremie concrete. For small and medium-sized projects, these methods may be very expensive. Furthermore, in granular soils, driving of sheet piles could disturb and densify the soils and result in the settlement of existing stuctures.

YIELDING OF SHEET PILE WALLS

The most common method of supporting excavations by sheet piles, walers and tie rods, no matter how carefully designed and constructed, cannot eliminate inward yielding of the face of the excavation. Peck (1) states that the amount of yielding for any given depth of excavation is a function of the characteristics of the supported soil and not the stiffness of the supports. Steel structural members, even of heavy section, are not stiff enough to reduce yielding by any significant amount. Peck summarizes the results of a number of excavations in clay soils in the graphical form shown in Figure 1.

The published and unpublished results regarding observations of inward yielding of deep excavations were summarized by Tomlinson (2) and are presented in Table I. According to Tomlinson, the inward movement may be on the order of as much as 2.5 percent of the excavation depths in soft clays, to 0.05 percent in dense granular soils or hard clays. This inward movement is accompanied by corresponding settlement of the ground surface.

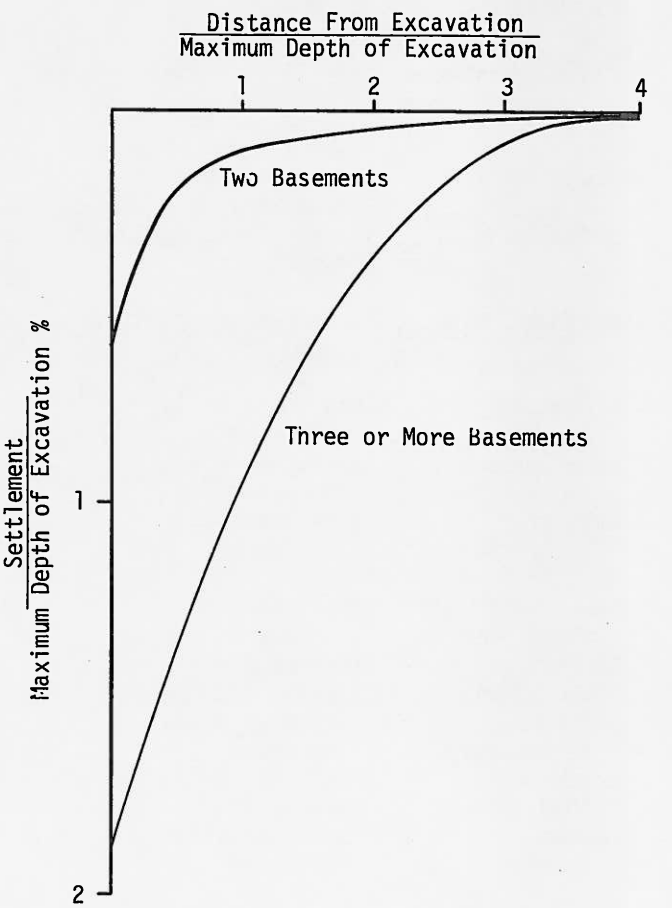

FIGURE 1 - RELATIONSHIP BETWEEN EXCAVATION DEPTH AND SETTLEMENT OF GROUND SURFACE FOR EXCAVATIONS IN SOFT TO FIRM CLAYS (AFTER PECK)

TABLE I

OBSERVATIONS OF MAXIMUM INWARD DEFLECTION OF SIDES OF DEEP EXCAVATIONS (AFTER TOMLINSON)

LOCATION	METHOD OF SUPPORT	EXCAVATION DEPTH (m)	MAXIMUM INWARD DEFLECTION (mm)	DEFLECTION / DEPTH x 100	SOIL TYPE
Chicago	Sheet piling, strutted	11.4	58	0.51	Soft clay
Oslo, Vaterland Subway	Sheet piling, strutted	9	23	0.25	Soft clay
St. Louis	Sheet piling, strutted	11.4	13	0.11	Firm to stiff clay
North London	Sheet piling, strutted	11.5	25	0.22	Stiff clay
Moorgate, London	Diaphragm wall, strutted	18	57	0.32	Stiff clay
South Africa	Diaphragm wall, anchored	14.7	76	0.52	Firm, fissured clay
South Africa	Diaphragm wall, anchored	14.7	38	0.26	Firm fissured clay
South Africa	Diaphragm wall, anchored	22.9	38	0.16	Firm fissured clay
South Africa	Diaphragm wall, anchored	14.7	19	0.13	Very stiff fissured clay
South Africa	Diaphragm wall, anchored	18.3	25	0.14	Weak jointed rock
Buffalo, N.Y.	Timber sheeting tied back	6.4	10	0.16	5.4 m loose sand over dense sand and gravel
Buffalo, N.Y.	Timber sheeting tied back	11.2	53	0.47	5.4 m loose sand over dense sand and gravel
Bloomsbury, London	Diaphragm wall, strutted	16	12	0.07	Gravel over London clay
Westminster Palace Yard	Diaphragm wall, strutted	12	20	0.17	Gravel over London clay
Zurich	Diaphragm wall, strutted	20	36	0.18	Lake deposits and glacial moraine
New York, World Trade Center	Diaphragm wall, anchored	17.7	66	0.37	Sand
London, Guildhall	Diaphragm wall, anchored	9.7	10	0.10	Gravel over stiff clay
London, Bloomsbury	Diaphragm wall, anchored	10	4	0.04	Gravel over stiff clay
London, Victoria St.	Diaphragm wall, anchored	8	3	0.04	Gravel over stiff clay
London, Vauxhall	Diaphragm wall anchored	14.5	22	0.15	Gravel over stiff clay

CAST-IN-PLACE CONCRETE WALLS

Yielding also takes place with cast-in-place concrete walls but to a somewhat lesser extent than with conventional steel sheeting (2). Concrete cylinder pile walls have been successfully used in arresting movements of unstable slopes. Several examples of successful use are in cases where the cylinders were added to stabilization after movements were detected but before any significant decrease of the strength of slope materials had occurred. Gould (4), and Nicoletti and Keith (3) report several case histories relating to arresting the slope movement with cylinder pile walls.

AUGER-PLACED GROUT-INJECTED PILE WALLS

The writers have utilized cylinder pile walls in conjunction with the construction of additions to existing buildings where the basement floor level of the addition was to be deeper than the invert elevation of the foundations or floor slabs of existing adjacent structures.

The method described here involved the use of steel-reinforced auger-placed grout-injected pile wall, which served as retaining wall to stabilize the excavation sides and protect the adjacent foundations, and constituted the foundations and basement wall for the new addition.

Construction Procedure

The auger-placed piles, which are installed by rotating a continuous flight hollow-stem auger to a predetermined depth and then pumping high-stength mortar under pressure as the auger is withdrawn, were placed in a line to form a cut-off wall. The center-to-center spacing was 1 inch larger than the diameter of the pile being placed. The reinforced concrete grade beam was extended for the full length of the wall along the top of the piles. The purpose of the grade beam was to tie the piles together at the top and act as a waler if bracing would be required to hold the wall in vertical position. Reinforcing steel bars were placed in each pile. At the top, this steel extended at least 1 foot into the grade beam.

Design Considerations

The auger-placed pile retaining walls may be structurally designed as rigid cantilever walls for short to intermediate depths. A rigorous analysis of the lateral resistance mobilized upon development of the ultimate soil resistance of a laterally loaded pile is a complex problem involving a progressive failure mechanism and soil reaction intensities well beyond the range of elastic behavior. Considering the analytic difficulties and the inexactness involved in expressing soil behavior, approximate methods have been presented by Woodward, Gardner and Greer (5), Ivey and Hawkins (6), and others. Based upon a review of these methods and based upon the work of Broms (7 and 8) and Hansen (9), the following simplified approximate method of analysis is considered appropriate.

For cohensionless soils, lateral bearing capacity (q_h) can be expressed as:

$$q_h = 3 \, Kp \, \sigma_o \qquad \text{where}$$

Kp = Coefficient of passive earth pressure

σ_o = Effective overburden pressure

The ultimate resistance of cohesive soils in terms of undrained shear strength (Su) is generally accepted to increase from 2 Su at the surface to a maximum of approximately 10 Su at a depth equivalent to about three pile diameter. Following Broms' recommendations, the ultimate unit resistance of cohesive soils below a depth of 1.5 pile diameter can be expressed as:

$$q_h = 9 \, Su$$

The most probable and idealized lateral earth pressure distribution against the pile wall are shown in Figures 2 and 3 for cohesionless and cohesive soils, respectively.

The ultimate passive resistance should be determined on the basis of Figures 2 and 3. It is recommended that a factor of safety of 3 be utilized to obtain allowable lateral bearing capacity. The depth of needed embedment should be determined by trial and error based on the principles of statics.

The maximum bending moment should also be determined from the above discussed pressure distribution diagrams. Because of the lack of well established methods of analyzing walls of this type, the design moment may be increased by 20 percent.

REFERENCES

(1) Peck, R.B., Deep Excavations and Tunneling in Soft Ground, Proc. 7th Int'l. Conf. Soil Mech., State-of-the Art, Pp. 225-290, Mexico, 1969.

(2) Tomlinson, M.J., Foundation Design and Construction, Pitman Publishing Co., Pp. 785.

(3) Nicoletti, J.P. and J.M. Keith, "External Shell Stops Soil Movement and Saves Tunnel", Civil Engineering, Pp. 72, April 1969.

(4) Gould, J.P. "Lateral Pressures on Rigid Permanent Structures", 1970 ASCE Speciality Conference on Lateral Stresses in Ground and Design of Earth-Retaining Structures, Pp 219-269.

(5) Woodward, R.J., Gardner, W.S., Greer, D.M.,, Drilled Pier Foundations, McGraw Hill Book Co., 1972.

(6) Ivey, L. Don and L. Hawkins, Signboard Footings to Resist Windloads, Civil Engineer, ASCE, 1966, No. 12, Pp. 34-35.

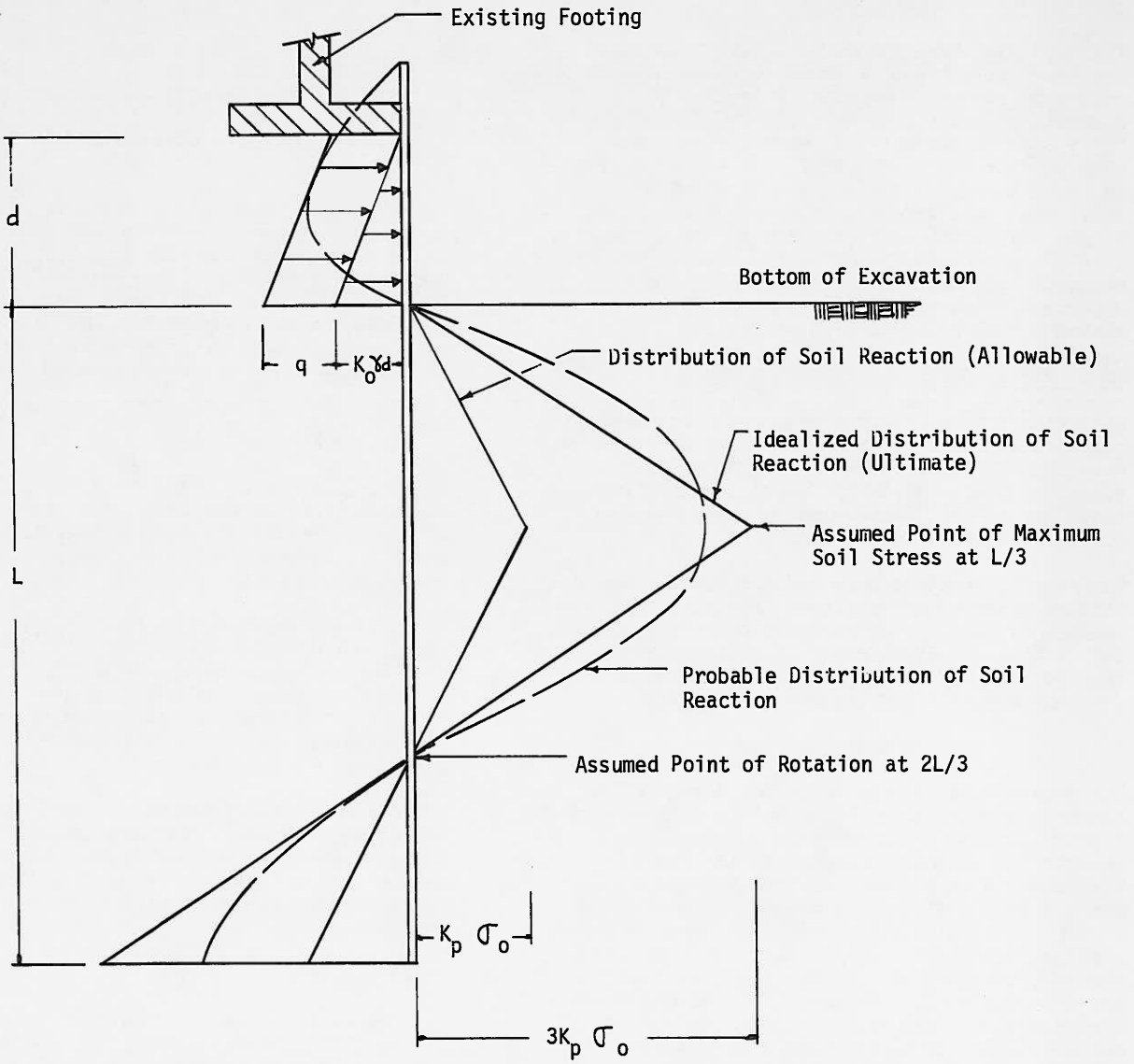

Lateral Pressure (Per Foot of Wall Length)

Ultimate Passive Lateral Bearing Capacity = $3K_p \sigma_o$ where σ_o = Overburden Pressure.

Use a Factor of Safety of 3 to Obtain an Allowable Lateral Bearing Capacity of $K_p \sigma_o$.

Determine Maximum Moment at Point of Zero Shear.

K_p = Coefficient of Passive Earth Pressure
K_o = Coefficient of Earth Pressure at Rest
γ' = Effective Unit Weight of Soil
q = Lateral Pressure of Surcharge Footing Load
D = Pile Diameter
L = Embedded Length of Pile

FIGURE 2 - LATERAL EARTH PRESSURE DISTRIBUTION FOR PILE WALL
(COHESIONLESS SOIL)

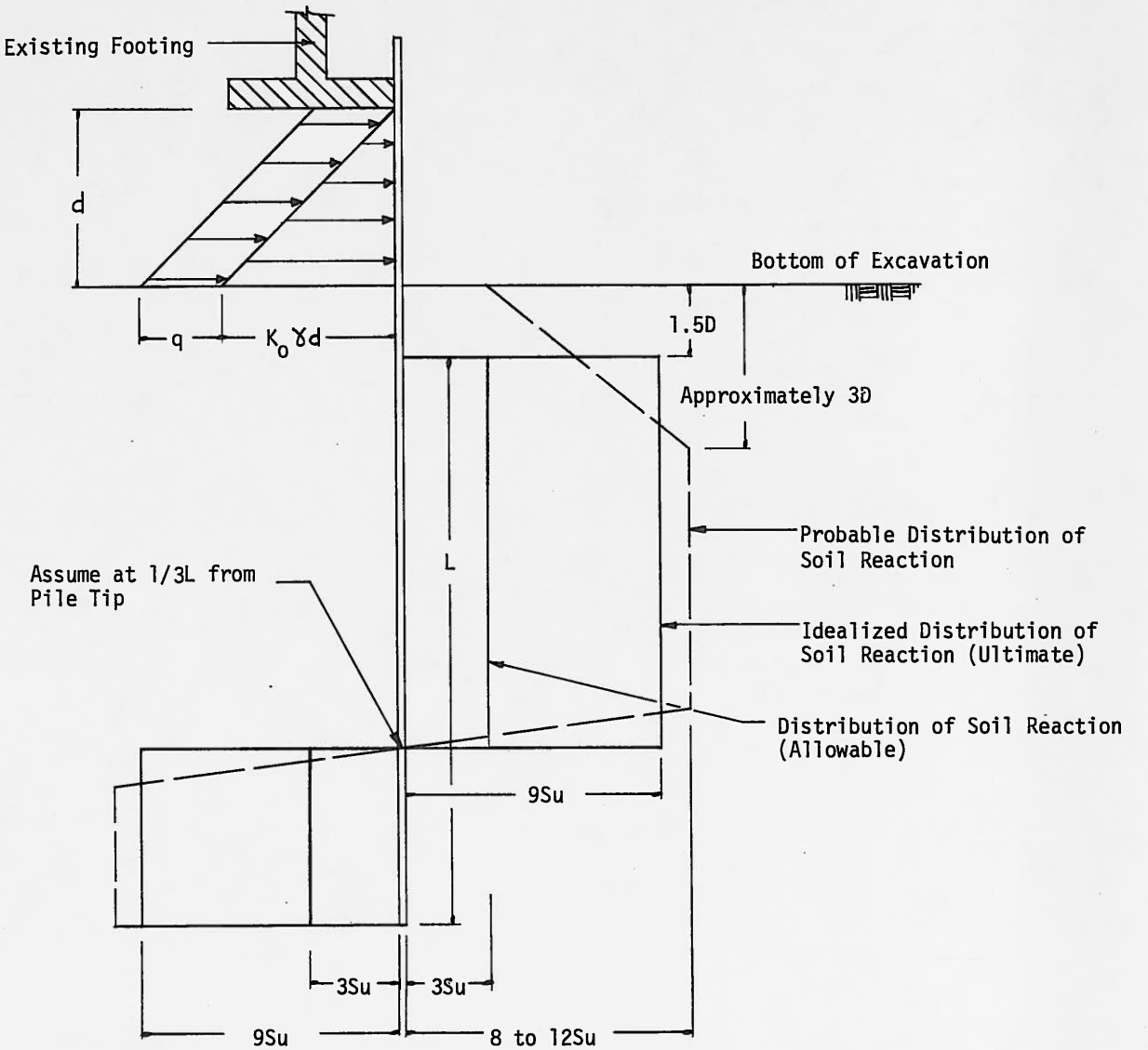

Lateral Pressure (Per Foot of Wall Length)

Ultimate Passive Lateral Bearing Capacity = 9Su.

Use a Factor of Safety of 3 to Obtain an Allowable Lateral Bearing Capacity of 3Su.

Determine Maximum Moment at Point of Zero Shear.

K_o = Coefficient of Earth Pressure at Rest

γ' = Effective Unit Weight of Soil

q = Lateral Pressure of Surcharge Footing Load

D = Pile Diameter

L = Embedded Length of Pile (Neglect Upper 1.5D Below Excavation Bottom)

FIGURE 3 - LATERAL EARTH PRESSURE DISTRIBUTION FOR PILE WALL (COHESIVE SOIL)

(7) Broms, B.B., Lateral Resistance of Piles in Cohesionless Soils, Proc. ASCE, Vol. 90, No. SM-3, 1964, Pp. 123-156.

(8) Broms B.B., Design of Laterally-Loaded Piles, Proc. ASCE, Vol. 91, No. SM-3, 1965, Pp. 27-63.

(9) Hansen, B., The Ultimate Resistance of Rigid Piles Against Transversal Forces, Danish Geotech Inst. Bull 12, 1961.

SAMPLING AND TESTING OF THE MAQUOKETA SHALE IN NORTHWESTERN ILLINOIS

by
Terje Preber *

Undisturbed sampling of shale has always been difficult. As part of a comprehensive subsurface investigation for a nuclear power plant in northwestern Illinois the Maquoketa shale, which contains seams of argillaceous dolomite, was sampled using different coring techniques. Since the Maquoketa shale is extremely fissile, careful sample preservation by both lateral and vertical confining was utilized. The samples were tested to determine both dynamic and static properties, and dynamic properties obtained in the laboratory were compared with those obtained from short distance crosshole shear wave surveys. Correlation was found between the dynamic properties and both undrained shear strength and confining stress. Strength and deformation properties for unconfined and triaxial compression tests compared well with the modulus-strength ratios published for similar materials. Based on the results of the sampling and testing programs, recommendations for sampling and sample preservation techniques are given.

INTRODUCTION

Undisturbed sampling and preservation of samples of weathered, fissile shale is often a very difficult task. The often erratically varying degree of weathering with depth complicates sampling and makes reproducability of testing results difficult. Therefore, the testing of weak, weathered rock very often yields a wide variety of test results with large data scatter. The reproducability of test results usually associated with water-deposited soils are seldom, if ever, obtained.

The testing and sampling program described in this paper was part of a comprehensive subsurface investigation for a nuclear power plant in northwestern Illinois. The sampling, preservation and testing program of shale samples taken from the Maquoketa shale are described, and, in particular, the different sampling techniques and sample preservation procedures are evaluated with respect to their effectiveness. The samples obtained by these procedures were subjected to a comprehensive testing program, including both static and dynamic testing in order to provide input for soil-structure interaction analysis. However, since very limited information has been published on the dynamic properties of shale, the results of the dynamic testing are highlighted.

GEOLOGY

The Maquoketa Shale Group is of Ordovician age, and is part of the Cincinnatian Series. The area where the shale samples were taken was in a broad sea far from sources of clastic sediments during most of Ordovician time. However, during Cincinnatian time when large deltas in the Appalacian region were being formed, clastic sediments from the east dominated the sedimentation in Illinois, resulting in formation of the shale and dolomite shales of the Maquoketa Shale Group (Willman et al (1)).

The geologic unit sampled consists of a greenish-gray to gray silty shale, containing numerous 1 to 12 inch thick interbeds of argillaceous dolomite. The dolomite comprises up to 40 percent of the profile studied. The shale unit studied for this paper ranges from highly to slightly weathered, with the highly weathered portions having the consistency of a stiff clay. The highly to moderately weathered portions of the shale have a low slake durability, and are extremely fissile. For example, when exposed to air for only a few minutes, the core tended to separate parallel to the bedding planes into discs 1/8 to 1/2 inches in thickness.

The shale clay-minerology analysis revealed that the most abundant clay minerals were illite (70-80%), chlorite (10-20%), and kaolinite (0-10%). The liquid limits range between 30 and 35 percent while the plastic limits were typically close to or slightly less than 20 percent.

EXPLORATORY PROGRAM

Sampling

The shale samples were obtained by either 4 inch I.D./5 1/2 inch O.D. double or triple tube (high recovery) core barrels or 3 inch Pitcher Samplers. A Denison sampler was also used, however, due to poor sample quality and high core loss the use of this sampler was discontinued.

Based on visual examination in the field, the double and triple core barrels were judged to produce equally good recovery. Both type core barrels were used with diamond and tungsten carbide bits, and after some initial experimentation, it was decided that the triple tube core barrel with a tungsten carbide bit gave most satisfactory results in the highly to moderately weathered shale, while the double tube core barrel with a diamond bit gave best results in the slightly weathered shale. Effective use of both bit types, however, was hindered by plugging of the water portals by the shale cuttings. This was especially troublesome, because it resulted in the water being forced inside the bit, causing water to flow alongside the sample core and to the interior of the recovery tube. With the low slake durability of the shale, this in some cases caused softening of the outer portions of the

*Senior Engineer, Dames & Moore

recovered core. Another problem was caused by the tendency of the dolomite inclusions in the shale to get jammed in the bit, resulting in the loss of several core runs. This was occasionally quite troublesome in the highly weathered portions of the shale.

The problems of slake loss and jamming of the bits by the dolomite inclusions were later solved by switching to a Pitcher Sampler in the highly and moderately weathered shales. This procedure was hampered by refusal upon encountering the frequent dolomite inclusions sometimes after only an inch of recovery. However, after refusal, a tricone bit was used to advance the borehole through the dolomite layer, and as soon as it was felt that the larger (gravel size) cuttings were cleaned from the borehole, the Pitcher Sampler was again inserted into the borehole and coring proceeded until refusal at the next dolomite inclusion. Due to the high variability of the thickness of shale between the dolomite inclusions (one inch to over two feet), this resulted in a high percentage of damaged tubes and variable sample recovery. It was also undoubtedly expensive, but the procedure, at the time of sampling, was considered highly successful in terms of the good quality samples that were obtained.

Sample Preservation and Storage

Due to the highly fissile nature of the shale, it was necessary to prevent moisture loss and to keep a small confining and axial pressure on the samples to prevent deterioration. Immediately following removal of the core from the inner core barrel or lining, samples judged suitable for testing were wrapped in cellophane (Saran-wrap) and thereafter aluminium foil. The necessity for immediate wrapping of the samples was demonstrated in the field by discing of the core within minutes after exposure to the air. Samples wrapped in cellophane did not show signs of discing.

Following wrapping of the core sample, it was inserted into a plastic tube slit along one side. The tube diameter was slightly less than that of the core, which allowed the samples to remain firmly in the tube. Metal (hose) clamps were thereafter placed around the tube. The ends of the sample was then evened by wax or liquid stone, and wood discs and blocks placed on the evened ends. A device consisting of two bolts was thereafter used to provide axial confinement. A section view of the sample container is shown on Figure 1. However, it was found that wax yielded under the axial load which resulted in loss of the axial confinement. The Pitcher Samples were not removed from the sample tubes in the field, rather, the excess tube was cut off and each end cleaned and sealed by waxing. The tubes were then closed with plastic caps which were taped with duct tape.

In order to prevent damage and disturbance from transportation, the samples were wrapped in fabric carpeting and transported to the laboratory in a station wagon. Following arrival at the test laboratory, the sample containers were immediately placed in a storage facility under nearly 100 percent humidity.

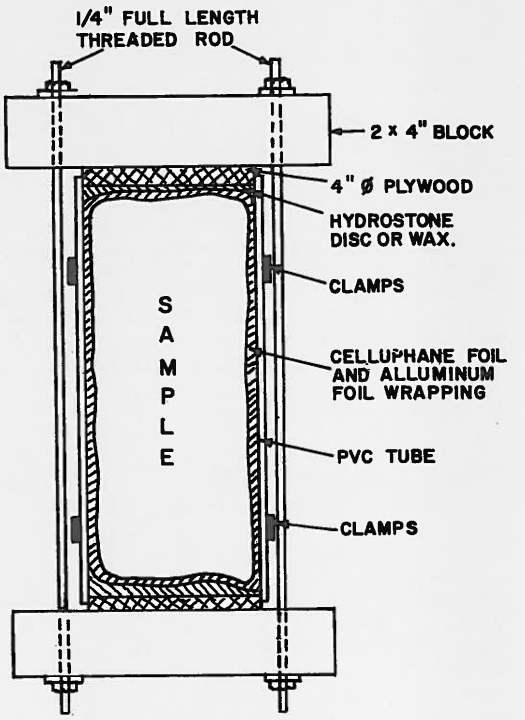

FIGURE 1
SAMPLE CONTAINER
SECTION VIEW

Sample Preparation

Most samples required little or no trimming except for preparation of the end surfaces. Trimming of the end surfaces was done while the sample was under lateral restraint in a split mould. This was necessary in order to avoid risk of separation along bedding planes by the shear forces and bending moments caused by the cutting and levelling of the ends, and to control the levelness of the end surfaces. Following trimming, a rubber membrane was placed around the samples to be subjected to triaxial testing and the sample placed in the triaxial cell.

Sample saturation was not attempted on samples subjected to consolidated undrained tests since testing by the author of highly overconsolidated clay samples have shown a tendency to swell. The tendency of the Maquoketa shale to swell when exposed to free water was also substantiated during oedometer tests, as shown on Figure 2. The maximum swell pressure recorded for this particular sample was 3,100 p.s.f., which was in excess of the effective vertical overburden pressure.

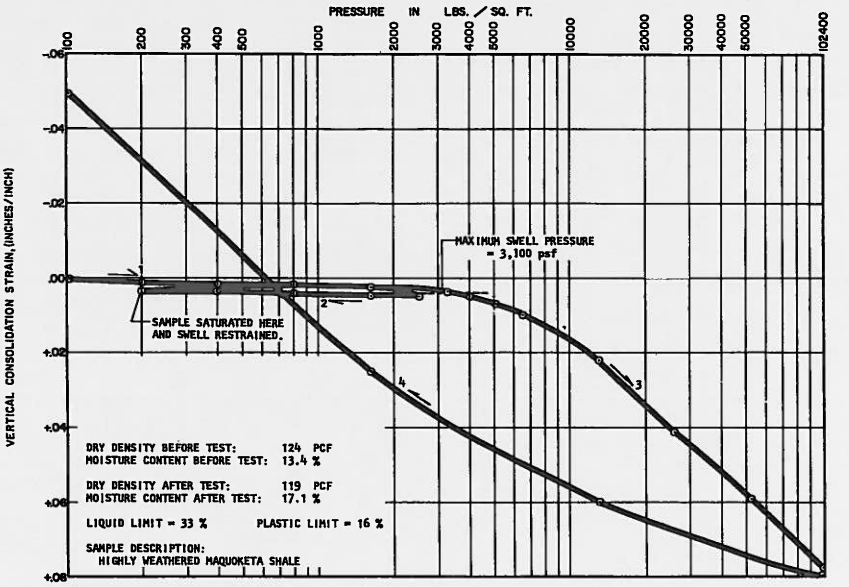

FIGURE 2
EXAMPLE OF SWELLING FROM SATURATION

Since saturation was not attempted, consolidation was monitored by changes in the cell volume. Due to the large sample volume to cell volume ratio (roughly a 1:2 sample to cell volume ratio), a constant temperature environment and the use of de-aired water; it was felt that the cell-water volume change could be used as a reliable indicator of sample volume change.

STATIC TEST RESULTS

The static strength and deformation characteristics of the shale were determined by unconfined, unconsolidated undrained, and consolidated undrained triaxial tests. The test procedures were in accordance with ASTM standards or other generally accepted test procedures. As previously described, saturation was not attempted due to fear of swelling which would have affected the deformation characteristics and could have lowered the shear strength of the samples.

The test results are shown on Figures 3 and 4. It should be noted that the degree of weathering is in accordance with geologic description and based on visual observation. The state of weathering is therefore not directly tied to engineering properties. Figure 3 shows the relationship between peak compressive strength and water content. For completeness, tests on fresh shale are also included on this figure. Although there is considerable data scatter, there is a clear trend of increase in compressive strength with decreasing moisture content. The relationship between compressive strength and water content

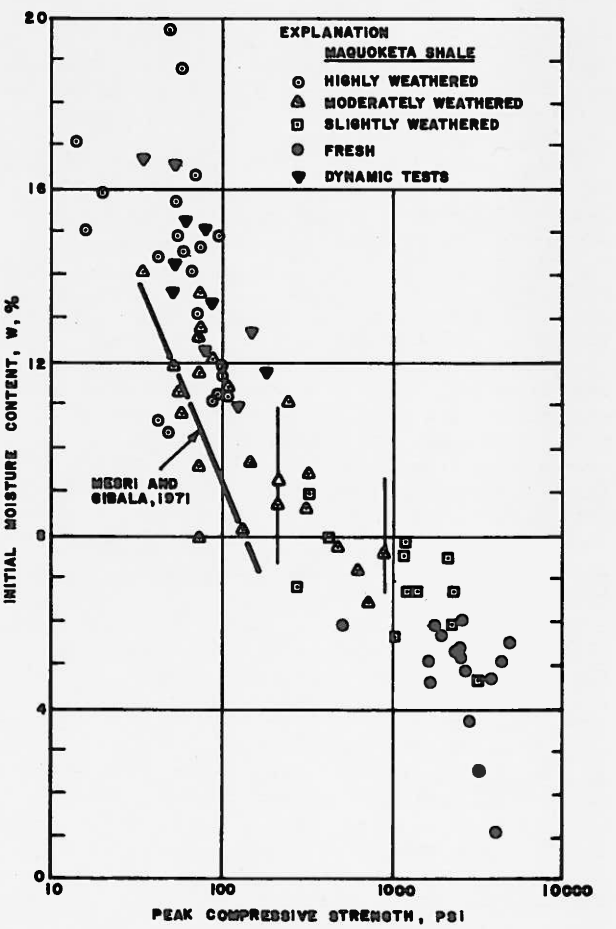

FIGURE 3
MOISTURE CONTENT VERSUS COMPRESSIVE STRENGTH

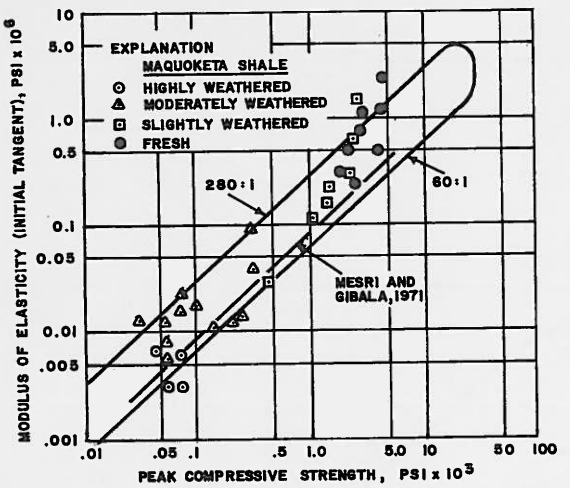

FIGURE 4
YOUNG MODULUS VERSUS
COMPRESSIVE STRENGTH

as observed by Mesri and Gibala[2] for a shale material quite similar in mineralogical composition and plasticity is also shown. Although the two shales materials are quite similar, considerably higher compressive strength was observed on the Maquoketa shale. This could be caused by natural differences in the properties of the two shales, however, since the shale samples tested by Mesri and Gibala were subject to saturation, this may also be a factor.

Figure 4 shows the relationship between the Modulus of Elasticity (initial tangent modulus) and compressive strength. Although there is significant data scatter here also, the mean deformation modulus to compressive strength ratio is approximately twice that reported by Mesri and Gibala. However, the range obtained correspond well with that given by Deere et al.[3]

RESULTS OF DYNAMIC TESTING

General

The dynamic properties were evaluated in the laboratory by means of strain-controlled dynamic triaxial tests. As previously described, the samples were not saturated prior to testing, but were consolidated at "as received" moisture contents under confining pressures related to their overburden effective stress. However, to get a better spread of confining pressures, some samples were consolidated at pressures that exceeded their overburden effective stress. The samples were tested in accordance with the procedures outlined by Silver and Park[4] with shear strain levels generally between 1 x 10^{-3} and 1.0 percent. Based on these test results, a shear modulus and damping value was calculated for each strain level. The damping values, however, are not presented in this paper. Post-cyclic shear strength was obtained by shearing the samples to failure after consolidating the samples following the last cyclic strain level. The resulting shear strength are presented on Figure 3 for comparison with the static test results. In essence, the shear strength obtained following dynamic testing fit within the same pattern as the static testing. Moisture content on the two samples with highest shear strength was inadvertently not obtained, however, it is estimated that the moisture content for these samples generally would be between 7 and 11 percent, hence these tests are only shown as vertical lines on the figure.

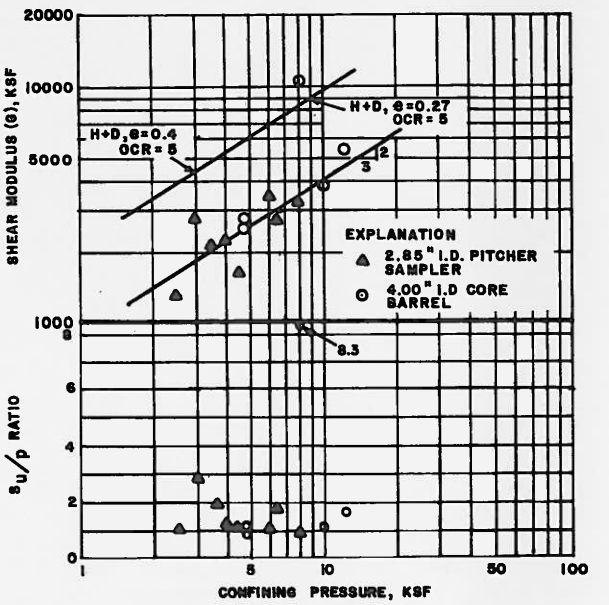

FIGURE 5
VARIATION OF SHEAR MODULUS
WITH CONFINING PRESSURE

Correlation with Confining Pressure

In order to analyse the test results, an attempt was made to correlate maximum dynamic shear modulus (G_{max}) with both confining stress and undrained shear strength. However, the dynamic triaxial tests were only performed for shear strains greater than approximately 1 x 10^{-3} percent. In order to get a reasonable estimate of G_{max}, a best fit curve was drawn through the strain degradation data and the shear modulus (G) value obtained at 1 x 10^{-3} shear strain was taken as 0.9 G_{max}. The factor of 0.9 was based on strain degradation characteristics obtained by others on stiff to hard clay. (Grant and Brown,[5] Arango et al[6]). The obtained G_{max} values were plotted against confining pressure and the results are shown on Figure 5. Although there is some data scatter, most data seem to indicate that G_{max} can be related to the two-thirds power of the confining stress. However, some data points definitely do not fit is pattern. Neither does the Hardin and Drnevich[7] equation using a decreasing

overconsolidation ratio (OCR) with increasing confining pressure predict the obtained slope. However, looking closely at the shear strength data and the void ratio variation with depth, a better correlation can be obtained. The test data obtained during the consolidation and swell tests on the Maquoketa shale (not presented in this paper) indicate a decrease in void ratio with decreasing degree of weathering. Also, increased weathering and the corresponding increase in water content associated with either swelling or mineralogy changes or both, indicates that there is no significant variation in OCR with depth (or increasing confining pressure). This can be seen by plot of ratio of undrained shear strength to confining pressure (s_u/p - ratio) as shown on Figure 5. The plot shows little variation in s_u/p - ratio over the range of confining pressures, and hence, since OCR is closely related to the s_u/p - ratio, there should be little variation in OCR. Using the observed variation in void ratio and a constant OCR (OCR = 5 as a reasonable estimate for the s_u/p ratios obtained), the Hardin and Drnevich equation gives a curve with approximately the same slope as that obtained from the test data. However, the value of shear moduli predicted by the Hardin and Drnevich equation are about 2.5 times those obtained from the triaxial testing.

Considering the s_u/p - ratio, two of the data points falling above the general pattern also seem to fall in place. For the tests represented by these two points, s_u/p - ratios of 2.8 and 8.3 were obtained, indicating OCR values of possibly an order of magnitude above the rest of the tests.

Correlation with Shear Strength

The obtained G_{max} - values were also attempted correlated with undrained shear strength. This is shown on Figure 6.

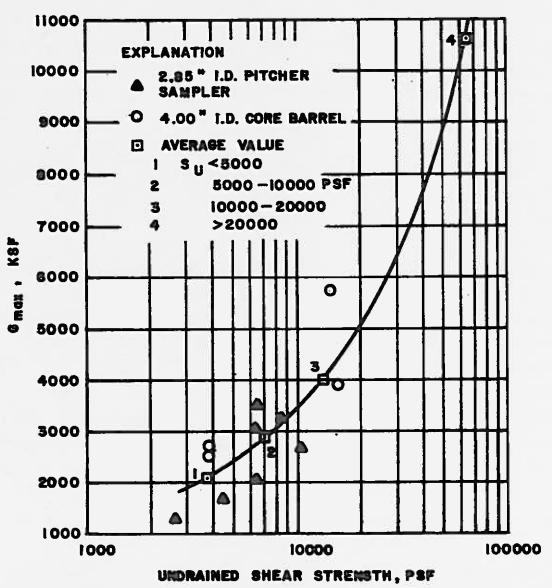

FIGURE 6
G_{max} VERSUS UNDRAINED SHEAR STRENGTH

Although there is some scatter, a trend towards increasing G_{max} with increasing undrained shear strength is clearly present.This is even more pronounced when the G_{max} values are arranged within the shear strength brackets shown.

Since the overconsolidation ratio cannot be evaluated for the shales, the often normalised shear modulus G_{max}/s_u was plotted versus s_u/p - ratio. However, it is a known fact that the OCR is related uniquely to the s_u/p - ratio for a particular material, hence the s_u/p - ratio was used as a measure of OCR, and the resulting plot is shown on Figure 7. As should be expected for this material, there is considerable scatter, but a definite trend in decreasing G_{max}/s_u with increasing s_u/p - ratio (hence also with OCR). Similar trends have also been reported by Koutsoftas and Fisher[8] for overconsolidated clays.

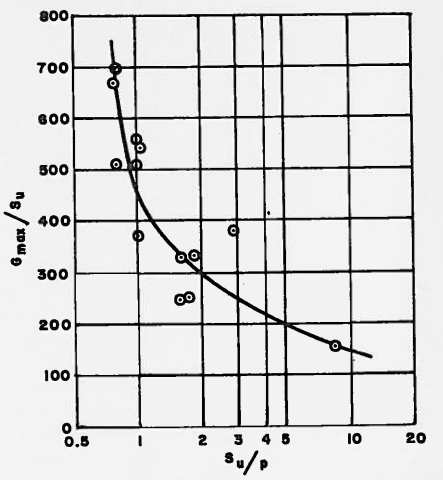

FIGURE 7
NORMALIZED SHEAR MODULUS VERSUS S_u/p RATIO

STRAIN DEGRADATION CHARACTERISTICS

The data points for all the dynamic triaxial tests after normalisation to 0.9 G_{max} at 10^{-3} percent shear strain are shown on Figure 8. From this figure it can be seen that the strongest sample has a somewhat lesser degradation with increasing shear strain than the remainder of the samples. However, as shown on Figure 9, when separating the strain degradation curves according to their strength characteristics and calculating the average strain degradation curve for each group, it can be seen that there is a tendency for the shear modulus not to decrease as rapidly with increasing shear strain for the stronger samples as compared to the weaker samples. The trend is weak, however, and more tests will be required to verify such trends.

Also shown on Figure 9 are the strain degradation curves obtained by Seed[9] from laboratory tests and that for hard clays as obtained from field geophysics by Grant and Brown[5]. It is interesting to note that the

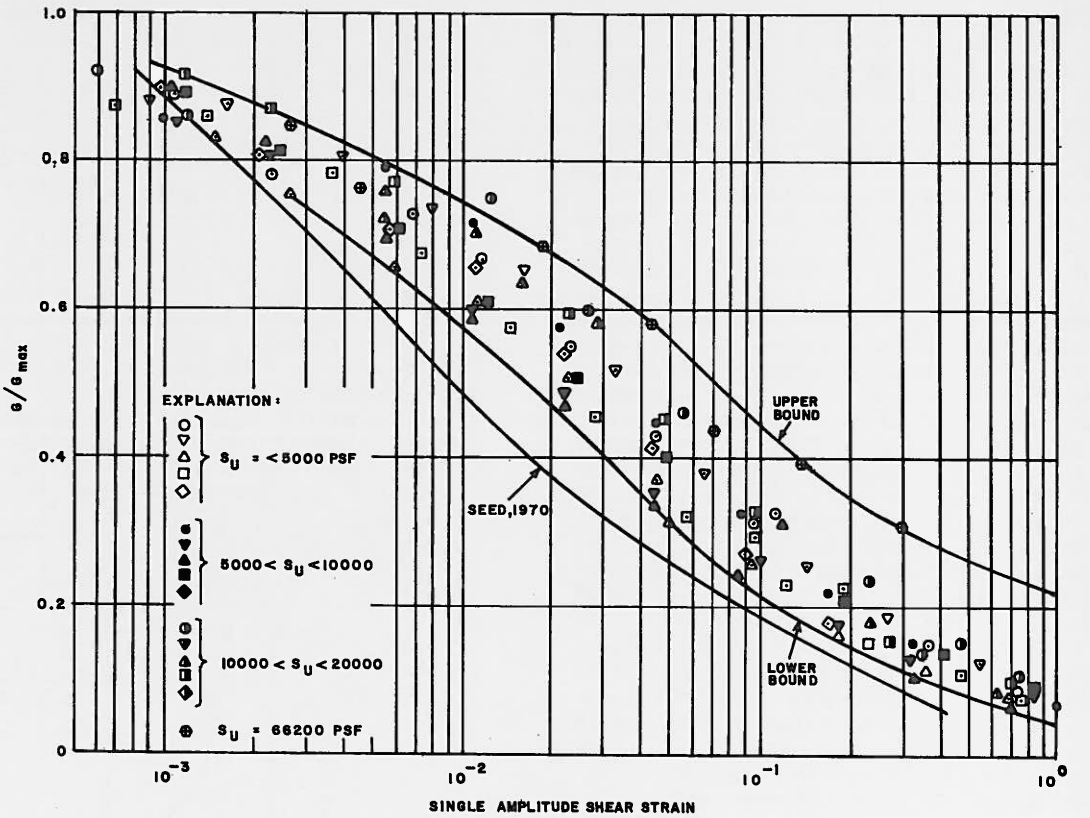

FIGURE 8
STRAIN DEGRADATION CURVES

strain degradation for the strongest sample is almost identical to that presented by Grant and Brown for shear strains smaller than 3 x 10^{-2}%, while the two curves separate considerably for higher strains. It should also be noted, that the strain degradation curves for the Maquoketa shale lie well above that given by Seed. This can also be seen from Figure 8, where Seed's curve even falls below the lower bound for all tests.

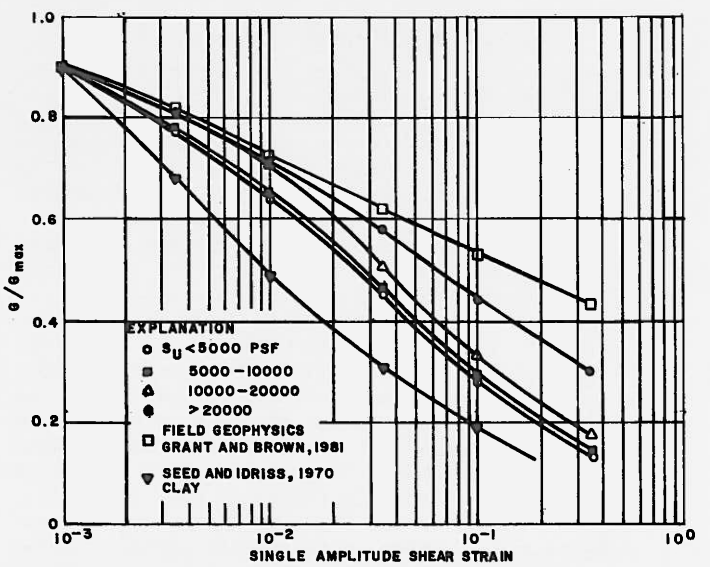

FIGURE 9
MEAN STRAIN DEGRADATION CURVES

FIELD GEOPHYSICAL TESTING

Field Procedures

Geophysical shear wave velocities were measured by conducting a cross-hole survey. Three boreholes were used; one as an energy hole and two as recording hole. A Bison Model 1465 Downhole Shear Wave Hammer provided the energy for the shear wave analysis. The hammer was lowered to the desired depth in the energy hole, and hydraulic pistons were extended to force coupling shoes against the borehole wall and lock the hammer in place. Vertical element, 14-HERTZ borehole geophones were suspended in the recording holes at the same elevation as the hammer. Pneumatic packers were used to lock the geophones against the borehole walls. The zero-reference for wave transit times was obtained from a solid-state triggering switch installed in the body of the shear wave hammer.

At least two sets of recordings were made at each elevation. Each data set consisted of an enhanced record showing two traces from each recording hole. The two traces from each hole represented the wave forms detected by the geophone for a downward and upward series of impacts with the shear hammer.

Evaluation of Geophysical Data

Due to the presence of dolomitic inclusions within the Maquoketa Shale, the geophysical measurement from the field could not be compared directly with the laboratory tests which were conducted on the shale constituent of the subsurface profile only. In order to determine the actual shear modulus of the shale constituents the effect of the dolomitic inclusions on the recorded moduli (velocities) were evaluated. This was performed by using the procedures outlined by White and Angona[10] for laminated material.

For this evaluation it was estimated that the dolomitic inclusions amounted to about 40 percent of the profile, and that the geophysical shear wave velocity of this material was 4,000 feet per second. This velocity was based on that of the fresh shale strata encounterd at a depth of approximately 50 feet. Since the 4,000 feet per second shear wave velocity is representative of the fresh shale-argillacious dolomitic laminate, the dolomitic portions may have a higher velocity, and the shear wave velocity chosen may be on the lower side. Therefore a sensitivity analysis was performed. This analysis showed that an increase in this velocity of 50 percent would only change (reduction) the calculated velocity of the weathered shale by five percent. Also, a reduction in the percentage of argillaceous dolomite inclusions to 30 percent would increase the calculated velocities for the shale a maximum of about seven percent. The velocity profiles before and after adjustment are shown on Figure 10.

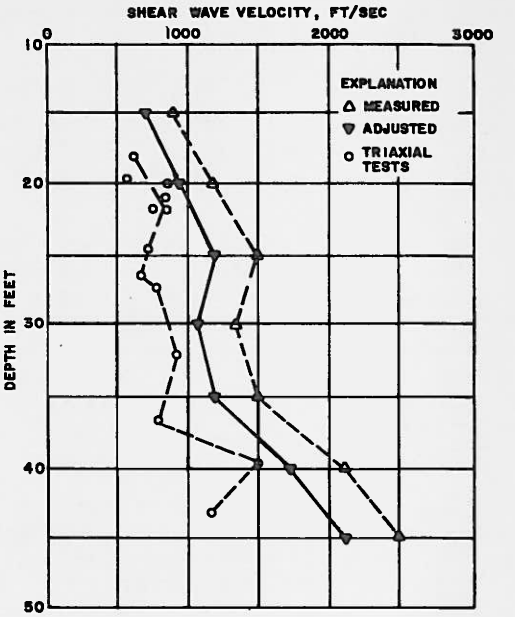

FIGURE 10
GEOPHYSICAL VERSUS LABORATORY SHEAR WAVE VELOCITIES

Comparison of G_{max} from Laboratory & Field Measurements

After the field geophysical shear wave velocities were adjusted and the corresponding shear moduli calculated, a direct comparison of the field and laboratory obtained shear moduli was performed.

The results of the analysis are shown on Figure 11. The results show that the laboratory tests give G_{max} values of only approximately one half of those obtained by the field measurements. On the average, the laboratory results are only 60 percent of the field measurements. Interestingly enough, looking back at Figure 5, this is close to the same ratio obtained between the G_{max} values calculated from the Hardin and Drnevich equation and the laboratory test results. The Hardin and Drnevich equation therefore may be valid for prediction of the G_{max} values for the Maquoketa Shale.

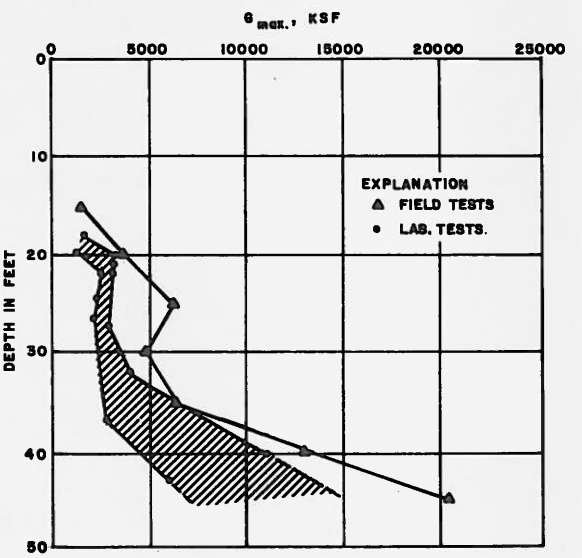

FIGURE 11
G_{max} VERSUS DEPTH FOR LABORATORY AND FIELD TESTS

THE EFFECT OF SAMPLING PROCEDURE ON SAMPLE DISTURBANCE

On Figures 5 and 6, samples obtained by means of a four inch I.D. core barrel and a 2.85 inch I.D. Pitcher Sampler are identified. Overall, although the sample space is limited, it appear that the results obtained by testing samples obtained from the four inch I.D. core barrel are slightly better. This is somewhat surprising, since the samples obtained by the pitcher tube were the least exposed to the eroding and softening effect of the drilling fluid. However, it is possible, that the penetration of the sample tube ahead of the cutting edge may have done more damage than the short duration exposure in the drilling fluid. Another factor may also be the effect of sampler diameter, since

more damage is usually caused by a small than a large diameter sampler.

CONCLUSIONS

The following conclusions may be drawn from this study:-

1. The compressive strength (and undrained shear strength) of the Maquoketa Shale is strongly related to water content.

2. The relationship between initial tangent modulus of elasticity and compressive strength is quite similar to that presented by others (Mesri and Gibala[2], Deere and Miller[3]).

3. G_{max} can be related to both effective confining stress and shear strength, and the rate of increase in G_{max} with confining stress appear to be in accordance with that predicted by the Hardin and Drnevich[7] equation.

4. Normalised shear modulus, G_{max}/s_u decreases with increasing s_u/p - ratio (and consequently also with OCR).

5. Strain degradation may be related to undrained shear strength. However, more studies will be needed to confirm this.

6. The shear modulus for weathered shale does not decrease as rapidly with increasing shear strain as is predicted by the strain degradation curve given by Seed [9].

7. The ratio between the G_{max} values obtained in the laboratory and geophyscially differ by a ratio of about 2.

RECOMMENDATIONS FOR FUTURE STUDIES

Disturbance from sampling appeared to be slightly greater with the smaller diameter Pitcher sampler. It is recommended though, for future sampling of similar material, that a larger diameter Pitcher sampler be tried. It is also recommended when a large diameter core barrel is used, that a tungsten carbide bit be used in highly weathered shales, while a diamond bit be used in less weathered shales.

It is also the opinion of the author that the sample preservation and storage techniques are of utmost importance. The samples should be protected immediately after removal from the core barrel, and subjected to confinment.

The effect of saturation on the properties of weathered shales (residual soils) should be studied closer. As part of such a study, distilled water and groundwater from the site should be considered.

ACKNOWLEDGEMENT

The writer acknowledges with appreciation the efforts and contributions of the laboratory staff at Dames & Moore and the University of Illinois at Chicago Circle. Appreciation also goes to Thomas E. Jensen, Senior Geophysicist at Dames & Moore, for contributions to the evaluation of the geophysical data, and to other Dames & Moore staff for suggestions and encouragement during the writing of this paper.

REFERENCES

1. William, H.B., et al., 1975: Handbook of Illinois Stratigraphy; Illinois State Geological Survey Bulletin 65.

2. Mesri, G., and Gibala, R. 1971: Engineering properties of a Pennsylvanian Shale; Proceedings of the Thirten Symposium on Rock Mechanics, Stability of Rock Slopes, University of Illinois, Urbana, Illinois, August 30 - September 1.

3. Deere, D.U. and Miller, R.P., 1965: Classification and Index Properties for Intact Rock, AFWL-TR-65-116, Air Force Special Weapons Center, Kirtland AFB, Albequerque N.M.

4. Silver, M.L., and Park, T.K. 1975: Testing Procedure Effects of Dynamic Soil Behaviour; Journal of the Geotechnical Engineering Division, ASCE, Vol. 101, No GT10, October.

5. Grant, WP, and Brown, F.R. 1981: Dynamic Behaviour of Soils from Field and Laboratory Tests; Proceedings of the International Conference on Recent Advances in Geotechnical Earthquake Engineering and Soil Dynamics, Vol. II, St. Louis, Mos April 76 - May 3.

6. Arango, I., Muriwaki, Y., and Brown, F. 1978: In situ and Laboratory Shear Velocity and Modulus; Proceedings of the Conference on Earthquake Engineering and Soil Dynamics, Pasadena, Cal, June.

7. Hardin, B.G., and Drnevich, U.P., 1972: Shear Modulus and Damping in Soils, Design Equations and Curves; Journal of The Soil Mechanics and Foundations Division, ASCE, Vol. 98, No. SM 7, July

8. Koutsoftas, D.G. and Fisher, J.A, 1980: Dynamic Properties of Two Marine Clays; Journal of The Geotechnical Engineering Division, ASCE, Vol. 106, No. GT6, June.

9. Seed, H.B., and Idriss, I.M. 1970: Soil Modulus and Damping Factors for Dynamic Response Analysis; RC-70-10, University of California, Earthquake Engineering Research Centre, Berkeley, Calif.

10. White, J.E., and Angona, F.A., 1955: Elastic Wave Velocities in Laminated Media; Journal of The Acoustical Society of America, Vol. 27.

DESIGN CONSIDERATIONS USING SPT'S

by

Yo Y. Cho[1]

1. INTRODUCTION

Many foundations are routinely constructed based on the blow counts from Standard Penetration Tests(SPT's). The blow counts are used to estimate soil properties such as density, modulus and strength. In the evaluation of liquefaction potential of sand deposits, Seed and Idriss(1) conclude that the empirical approach based on SPT blow cunts is the most useful approach available at the present time. Thus the application of SPT blow counts is not limited to routine small foundations but includes the foundations for important structures like nuclear power plants.

The SPT is supposedly a 'standarized test', (ASTM Standard Method D1586), i.e., measuring the required blow count of 140 lb hammer free falling through a distance of 30 inches to push a standard 2 inch O.D. sampler 12 inches into the subsurface test material. However, it is widely recognized that two different drill rigs performing SPT's in an adjacent area frequently yield quite different blow counts. Even though the SPT has the clear advantage over the laboratory testings of small samples for determining in-situ properties, the results are sometimes accepted on a qualified basis.

Schmertmann and Palacios(2,3) have shown that SPT blow count varies inversely with the energy transmitted through the drill rods to the sampler. Field studies conducted on SPT's by Schmertmann et al.(4,5) and Kovacs et al.(6) in the US and Shioi et al.(7) in Japan show that of the theoretical SPT energy of 4,200 inch-lbs (140 lb x 30 inchs) only 30 to 85 percent is actually transmitted through the rod to the sampler. This implies that the blow counts could vary by a factor of almost three in the same soil due to the variable energy transfered.

This paper discusses the implication of such variances in the foundation design for both static and dynamic cases through presenting actual field measured SPT energy and N values applied to typical foundation design configurations. It is followed by simulated liquefaction potential analysis for a half-space under seismic loading condition.

Finally this paper recommends a two-phased solution to improve the current SPT practices, one for immediate remedy and the other for long range solutions.

1 Binary Instruments, Inc., Pittsburgh, PA

2. SPT ENERGY

When the SPT hammer hits the top of the drill rod, a compressional stress wave from the impact travels through the rod. This compressional wave reflects at the bottom of the sampler and travels back as a tension wave. At the top of the drill rod this tension wave separates the drill rod from the hammer. The stress at the top of the drill rod changes from the compression to tension. Figure 1. shows a typical output from a load cell mounted near the top of the drill rod during a single cycle of SPT impact. The time duration of the first compression pulse is the function of the length of the rod, or

$$t = 2 L / c \quad , \qquad (1)$$

where L = length of the rod,
and c = compressional wave velocity in the drill rod(about 16000 ft/sec)

Hall(8) discusses the calculation of the input compression wave energy derived from wave equations. The compression energy is noted as below:

FIG. 1. TYPICAL LOAD CELL OUTPUT, SPT

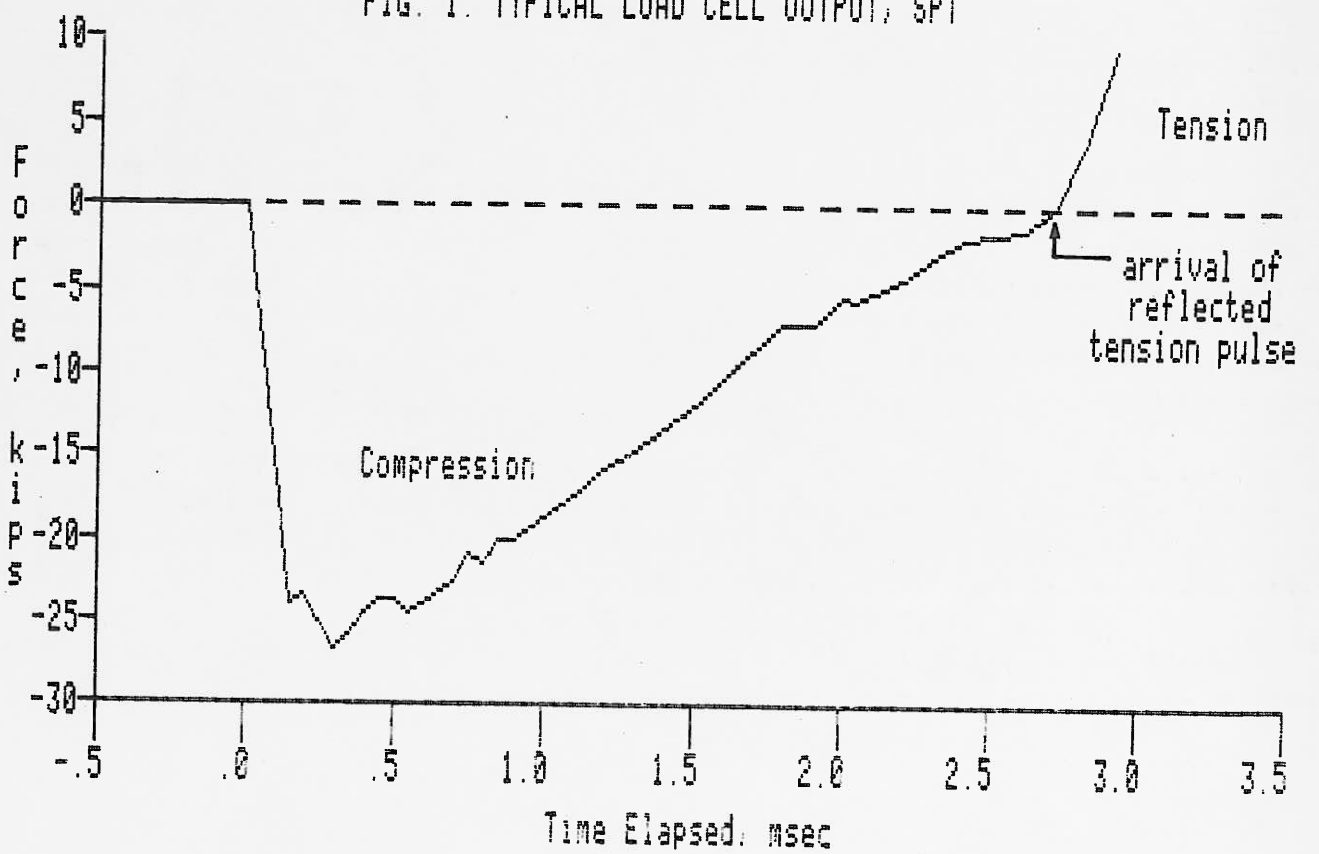

$$E_i = \frac{1}{A\sqrt{E\rho}} \int_0^{\Delta t} [F_i(t)]^2 \, dt$$

where E_i = the energy from the first compression wave,
A = the cross-sectional area of the drill rod,
E = Young's modulus of the drill rod,
ρ = the mass density of the drill rod,
and Δt = the time duration of the first compression pulse.

Equaton (2) indicates that the input compression energy is a function of the rod property but not the soil type.

Shioi et al.(7) have found that even after the hammer and the rod had seperated, the rod continued to penetrate and by the time the hammer and the rod contacted again for the second compression pulse the rod had already completed the penetration. This is clear in Figure 2 which shows the typical motion of the hammer and the rod for loose and dense soils. Please note that this figure is slightly misleading in that the rod lengths of two conditions were different. This is the reason for the difference in the elapsed time for reflected tension wave(time for seperation of the hammer and the rod) and not the difference in soil type.

FIG. 2. TYPICAL MOTION OF SPT HAMMER AND ROD

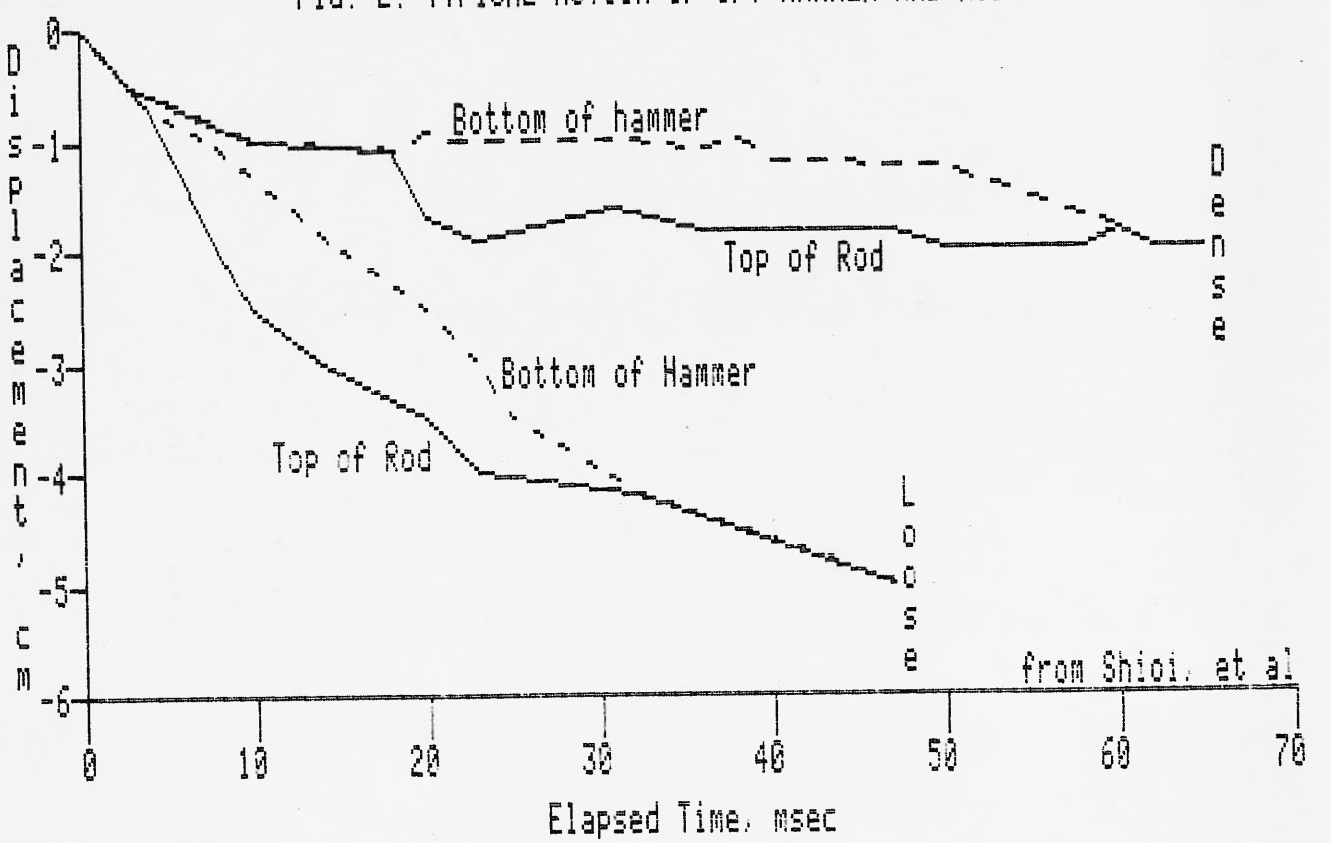

The SPT energy, the energy transmitted to the drill rod, is primarily due to the first compressional energy and can be calculated from equation (2). In practice, adjustments are made to equation (2) to account for the location of the load cell and the finite length of the drill rod.

3. SPT Calibrator

The aforementioned research indicates that the combined effects such as friction in the hammer mechanism, fall height variance, operator habits, etc influence the net energy transmitted through the drill rod. At the present time, there exists no standard on how much this net energy should be. Nevertheless, to obtain reproducible blow counts, a standard energy is required. Schmertmann suggests this standard energy be 50 % of the theoretical energy of 4,200 inch-lbs. Until a value is agreed upon the author suggests that the actual energy be reported along with the blow count.

Figure 3 shows a block diagram of a portable system designed to measure the energy delivered by each SPT blow. Some of the STP energy measurements reported herein have been obtained by this system. The system consists of a load cell mounted near the top of the drill rod, a load cell cable and a portable readout unit. The ciruits in the readout unit include a load cell conditioner/amplifier, a force level detector, arithmetic units, a digital control circuit, a quartz crystal time base, a digital display unit, a digital calibrator and built-in batteries and charging circuits. The digital readouts on the instrument display directly in per cent of the theoretical SPT energy of 4,200 inch-lbs. In addition, readout for peak compressive force is available.

FIG. 3.

BLOCK DIAGRAM OF SPT ENERGY CALIBRATOR

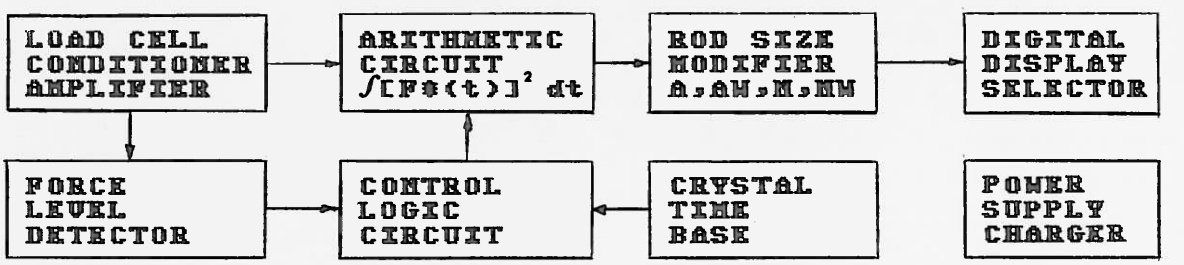

4. FIELD SPT ENERGY MEASURMENT

Field experience indicates that the variance in SPT energy for each rig with the same operator is reasonably small. Table 1 shows Energy Ratio (%) measurements on a Mobile B-34 with Safety Hammer, owned by D'Appolonia Drilling Co. Two sets of SPT energy measurements are presented in the table. The measurements indicate a variation of SPT energy with engine RPM settings. HIGH RPM is the manufacturer's suggested mode of operation for the Safty Driver. Each set shows very little deviation from its average value. These results clearly indicate that the SPT energy for this particular rig and hammer is greatly dependent upon these two engine RPM settings.

TABLE 1. SPT ENERGY MEASUREMENT, MOBIL B-34, SAFETY HAMMER
(courtesy of D'Appolonia Drilling Co.)

	ENERGY RATIO(%)																		
TEST NO	1	2	3	4	5	6	7	8	9	10	11	12	13	14	15	16	17	18	AVG.
HIGH RPM[2]	57	58	59	60	60	57	60	61	60	61	57	58	58	60	60	61	63	60	59.
LOW RPM	34	36	35	35	33	34	36	35	35	36	34	36	36	36	36	34	36	36	35.

Factors affecting SPT energy include the type of drill rig, the type of hammer, use of drilling mud, the operator habits. If the hammer is a cathead and rope type, the number of wraps around the cathead and the direction of rotation have an influence. Schmertman(2,3,4,5) and Kovacs(6) have published comprehensive studies on this subject. To demonstrate the effect of some of these factors on SPT energy, SPT energy measurements were conducted at Soil Testing Services, Northbrook, Illinois. Table 2. summarizes the results from the measurements. It is seen from Table 2. that the type of rig, number of wraps, hammer type, and operator all have an influence or SPT energy.

The average energy ratio of the measurements listed in Table 2. with 2 wraps is 47 %. The lowest energy ratio(average of operators B and C) was 38 % for Mobil B-61 and the highest was 66 %(average of operators D and F) for CME 55. If Schmertmann's suggested standard 50 % yielded a blow count of 16 (N=16) at a location, the average of N values obtained from the rigs listed in Table 2 assuming blow count inversly propertional to energy ratio would yield N=17. The spread in N values would be from 12 to 20. The analytical examples following this section assumes three imaginary rigs producing an energy ratios of 38 %, 50 % and 66 %.

2. manufacutrer's suggested mode

TABLE 2. SPT ENERGY RATIO
(Courtesy of Soil Testing Services, Northbrook, IL)

Rig Type	Hammer Type	No. of wraps	Depth (ft)	Energy Ratio,%	Operator
Mobil	Cathead	3	13.5	32	A
B-61	Rope	2	13.5	40	B
		2	15.5	37	C
Joy	Cathead	2	15.5	42	A
B-12	Rope	1	12.5	55	G
CME	Cathead	2	13.5	71	D
55	Rope	2	13.5	60	F
CME	Cathead	1	13.5	51	E
45 #1	Rope	2	13.5	36	L
CME	Cathead	2	13.5	45	I
45 #2	Rope				
Mobil	Safety	-	17.2	46	J

5. BEARING CAPACITY CALCULATION

A commonly accepted method for estimating the bearing capacity of a foundation on sandy soil is from the empirical relationship developed by Meyerhof(9):

$$P_a = N S_a / 8 \quad \text{for } B = 4 \text{ ft or less} \qquad (3)$$

$$P_a = ((B + 1) / B)^2 \times N S_a / 12 \quad \text{for } B > 4 \text{ ft} \qquad (4)$$

where P_a = allowable bearing pressure, tsf
S_a = allowable settlement, in.
N = SPT blow count per ft
and B = foundation width, ft

Using equations (3) and(4), allowable bearing capacity is calculated for S_a=1 inch for a foundation width of 3, 6, 9 and 12 ft and for N=12, 16 and 20. The result is summarized in Table 3.

TABLE 3. ALLOWABLE BEARING PRESSURE, tsf
Using Eq's (3) and (4)

N	Foundation width, ft 3	6	9	12
12	1.50	1.36	1.23	1.17
16	2.00	1.81	1.65	1.56
20	2.50	2.27	2.06	1.96

If a foundation size is to be selected for a load of 150 tons, it would be a 9 ft x 9 ft (81 sq ft) for N=20, or 12 ft x 12 ft (144 sq ft) for N=12.

6. LIQUFACTION POTENTIAL ANALYSIS

After the Alaskan and Niigata earthquakes, research work on liquefaction of saturated sand under seismic loading has been conducted at various organizations. Liquefaction has been one of the most critical items in nuclear power plant licensing. Various laboratory tests are performed including cyclic triaxial tests, cyclic torsional tests, simple shear tests, shake table tests, etc. However, because of the difficulty in obtaining undisturbed samples and simulating field loading conditions, considerable engineering judgement is required in appling laboratory test results to analysis of liquefaction potential for a given site. In a recent publication, Seed and Idriss(1) conclude that the empirical approach based on SPT data is the most useful approach available at the present time.

An imaginary half-space is assumed in the following example. It is further assumed that the water table is 30 ft below the surface. The design earth quake is 0.2g (horizontal) and the peak shear stresses at the depth of 31, 42, 52 and 64 ft have been calculated by previous analysis. The liqufecation potential at this site is analized using the method described by Seed and Idriss(1). This method uses modified SPT, N1, which is the measured penetration resistance corrected to an effective overburden pressure of 1 ton/sq ft and is determined from the relationship:

$$N1 = Cn \times N \qquad (5)$$

where Cn is a function of the effective overburden pressure at the depth where the penetration test was conducted and can be found in the reference (1). The term stress ratio(SR) at a point is defined to be the ratio of the dynamic shear stress to the effective confining stress. For the strength of the material, i.e., the shear stress required to cause the liquefaction divided by the effective confining stress, it is noted (SR)rqd. For the induced seismic loading, i.e., the seismic shear stress divided by the effective confining stress, it is noted (SR)ind. The ratio of these two, (SR)rqd / (SR)ind is interpreted as a factor of safety against the liquefaction. Table 4. lists the results of calculations

for the liquefaction potential using this example. Part II in Table 4 assumes an SPT energy ratio of 50% while parts III and I assume 38% and 66% respectfully. Figure 4. is a plot of the ratio of (SR)rqd / (SR)ind with depth.

TABLE 4. LIQUEFACTION POTENTIAL ANALYSIS

		Point 1	Point 2	Point 3	Point 4
Depth(ft)		31	42	52	64
Effective Vert Stress(ksf)		3.781	4.291	5.362	5.921
Peak Shear Stress Induced in-situ		.753	.939	1.284	1.453
Stress Ratio Induced in-situ		.129	.142	.156	.160
Modification Factor, Cn		.724	.665	.621	.571
I.	SPT, N	12	11	12	19
	Modified SPT, N1	9	7	7	11
	Stress Ratio for Liquef.	0.12	0.10	0.10	0.15
	Ratio of (SR)rqd/(SR)ind.	0.93	0.71	0.66	0.95
II.	SPT, N	16	14	16	25
	Modified SPT, N1	12	9	10	14
	Stress Ratio for Liquef.	0.16	0.13	0.14	0.20
	Ratio of (SR)rqd/(SR)ind.	1.21	0.93	0.87	1.26
III.	SPT, N	21	18	21	33
	Modified SPT, N1	15	12	13	19
	Stress Ratio for Liquef.	0.20	0.16	0.17	0.25
	Ratio of (SR)rqd/(SR)ind.	1.56	1.11	1.11	1.60

From Figure 4. the liquefaction potential for this site could be said from 'very likely' to 'unlikely' depending on which set of blow counts are used.

7. DESIGN CONSIDERATIONS USING SPT'S

The SPT test has advantages over the laboratory testing because it is conducted in-situ. The engineer working with blow counts from the SPT, however, can not verify the reproducibility of blow counts unless his rig is energy calibrated. Thus for critical projects energy measurements provide an indication of the drilling rig characteristics in comparision to Schmertmann's suggested Energy Ratio of 50 %.

The author believes that SPT energy measurements provide a considerable increase in quality of SPT data and should be seriously considered by engineers in the specificaitons for drilling. The blow counts per foot should then include the total drilling energy per foot. It is recommanded that more studies be conducted using SPT energy measurements so that the SPT becomes more standard in its excution.

FIG. 4. LIQUEFACTION POTENTIAL ANALYSIS WITH SPT'S

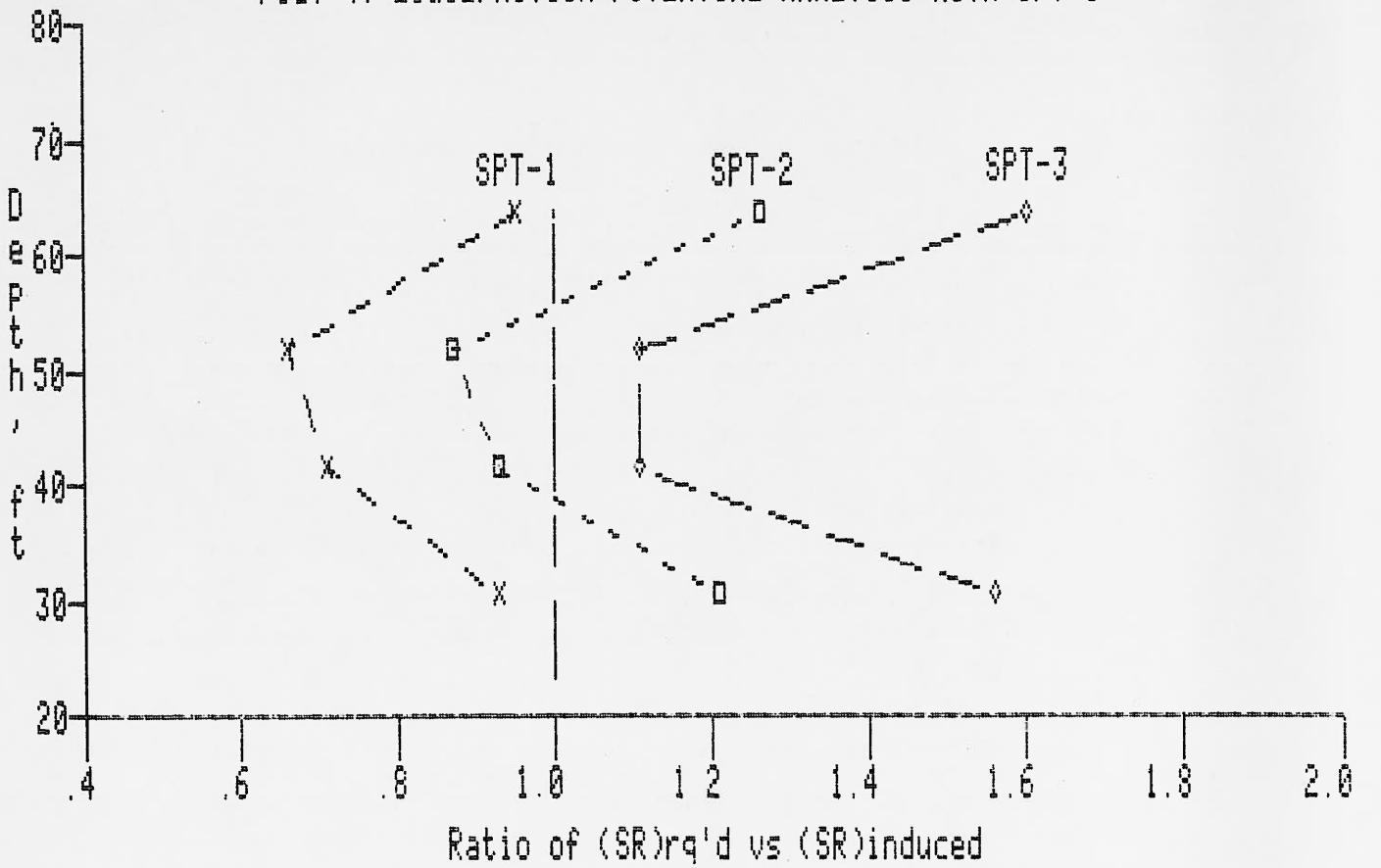

8. REFERENCES

1. Seed, B.H. and Idriss, I.M., "Evaluation of Liquefaction Potential of Sand Deposits Based on Observation in Previous Earthquakes", Site Testing and Evaluation , Proc. ASCE National Conv., St. Louis, October, 1981

2. Schmertmann, J.H. and Palacios, A., "Energy Dynamics of SPT", Journal of the Geotechnical Engineering Division , ASCE, Vol. 105, 1979

3. Palacios, A., "The Theory and Measurement of Energy Transfer During Standard Penetration Test Sampling", dissertation presented to the University of Florida, at Gainsville, Florida, 1977, in partial fullfillment of the requirements for the degree of Doctor of Philosophy.

4. Schmertmann, J.H., "Use of the SPT to Measure Dynamic Soil Properties?--Yes, But ...!", Dynamic Geotechnical Testing , ASTM STP 654, 1978

5. Schmertmann, J.H. and Smith, T.V. and Ho, R., "Example of an Energy Calibration Report on a Standard Penetration Test (ASTM Standard D 1586-67) Drill Rig," Technical Note, Geotechnical Testing Journal , ASTM, Vol. 1, No. 1, 1978

6. Kovacs, W.D., Salomone, L.A. and Yokel, F.Y., "Energy Measurement in the Standard Penetration Test", National Bureau of Standards Building Science Series 135, 1981

7. Shioi, Y., Uto, K., Fuyuki, M. and Iwasaki, T., Standard Penetration Test, Part III, Report by the Japanese Site Investigation Subcommitte on Present State and Future Trend of Penetration Testing in Japan, prepared for Xth International Conference on Soil Mechanics, Stockholm, June, 1981

8. Hall, J.R., "Drill Rod Energy as a Basis for Correlation of SPT Data," Procedings of the Second European Symposium on Penetration Testing-ESOPT II, Amsterdam, The Netherlands, 1982

BY

JOSEPH P. WELSH, P.E.

VICE-PRESIDENT

ROBERT M. RUBRIGHT

PROJECT ENGINEER

HAYWARD BAKER COMPANY

ODENTON, MARYLAND

AND

RUSSEL SNYDER

CHIEF ENGINEER

MARTIN MARIETTA'S

REFACTORIES DIVISION

HUNT VALLEY, MARYLAND

PRESENTED AT

OHIO RIVER VALLEY SOILS SEMINAR

OCTOBER 8, 1982

LEXINGTON, KENTUCKY

CHEMICAL GROUTING USED FOR UNDERPINNING AND WATER CONTROL

BY

Joseph P. Welsh, Robert M. Rubright and Russell W. Snyder

ABSTRACT

Chemical grouting was recently used at an industrial site in Michigan to simultaneously underpin spread footings, act as an excavation support system and provided a watertight barrier against very large ground water flows. The grouting process performed at Martin Marietta's Refactories Plant in Manistee, Michigan, involved the injection of low viscosity chemical grout into the sands where it hardened at a precisely controlled rate, glueing the sand particles together into a sandstone-like material. This project followed the five steps recommended in "Planning and Performing Structural Chemical Grouting;"[1] namely, (1) the establishment of specific objectives for the grouting program, (2) definition of the geotechnical conditions requiring and controlling the treatment, (3) development of an appropriate grouting program design and matching specifications, (4) the planning and execution of a detailed injection work plan, and (5) monitoring and evaluation of the grouting program.

BACKGROUND

During upgrading of a process line in the plant, it was determined that a vibrating cooler located just downstream of a rotary kiln was of inadequate capacity. A rotary cooler was chosen as a replacement to achieve more capacity, greater temperature drop and reduced emission levels. The kiln/cooler arrangement was located between two other parallel units and within a forty year old concrete building. Installation of the new cooler required the construction of a deep machinery pit in the midst of heavily loaded spread footings and operating machinery (Fig. 1). Two spread footing retaining walls flanked the pit site to the east and south and a heavily loaded column sat on the northwest corner.

Test borings taken by Stohl, Evans and Woods in the proposed pit area revealed clean sands with the exception of several thin strata of cohesive soil (Table 1). Borings taken on an adjacent project showed the sand strata extending to a considerable depth below the proposed pit bottom and verified that the water level was at Elevation +12. Whitman, Requardt and Associates, the consulting engineers, investigated various systems to support the footing loads and to control the 10 feet of anticipated ground water head during pit construction. Due to site conditions and the inability to accept any ground movement, it became obvious that conventional techniques such as sheeting and dewatering could not be employed. Sieve Analysis (Table 2) verified that the sand contained less than 20 percent fines and therefore was considered to be chemically groutable and this technique was recommended by the consultant as the surest means of accomplishing all of the design objectives.

CHEMICAL GROUTING PROGRAM

The Owner and Consultant decided on a performance type specification whereby a specialty contractor would submit a detailed lump sum proposal containing a design, procedure and price for the chemical grouting program. The Hayward Baker Company of Odenton, Maryland, was selected to perform the work.

Their plan utilized sleeved grout pipes which allow the injection (and re-injection, if desired) of grout from one-way ports located every foot along the length of the grout pipe. This was accomplished by placing a double-ended packer inside a 1 1/2" diameter PVC pipe and isolating it on the one-way port at the desired injection depth. In this manner, a predetermined quantity of grout was precisely injected at known location. On the Martin-Marietta project, three rows of grout pipes on 2.5' centers were placed around the perimeter of the pit in order to insure that a minimum 5' thick grout wall would be created. The outer rows were injected initially and then the inner row to fill in any gaps in the curtain. On each pipe alternate sleeves were injected and then the remaining sleeves injected to give better control to the flow of the grout. Grout pipes for the floor were also located on 2.5' centers and a 6' thick floor of grouted soil was created (Fig. 1 and 2). Altogether 140 grout pipes were used to form a grouted soil "bathtub" around the outside of the proposed excavation. If only structural chemical grouting was required, the grout pipe spacing would have been spaced at wider centers.

Dr. Roy Borden, Associate Professor of Civil Engineering at North Carolina State University, was retained by Hayward Baker Company to review the design of the chemical grout zone. Dr. Borden's analysis verified the structural stability of the proposed grouting plan.

GROUT PIPE PLACEMENT

A specially adapted Ingersoll Rand LM-100 airtrack drill was used to work in the less than 14-foot headroom. Initially, a 3" steel casing was drilled and driven into place. A weak cement mortar was then poured into the casing before the bit and drill steel were extracted. This was the only way to keep the "running sand" from intruding inside the casing up to the water table elevation. Needless to say, this type of soil behavior put all parties on notice as to the potential consequences of leaks in the final grout "bathtub."

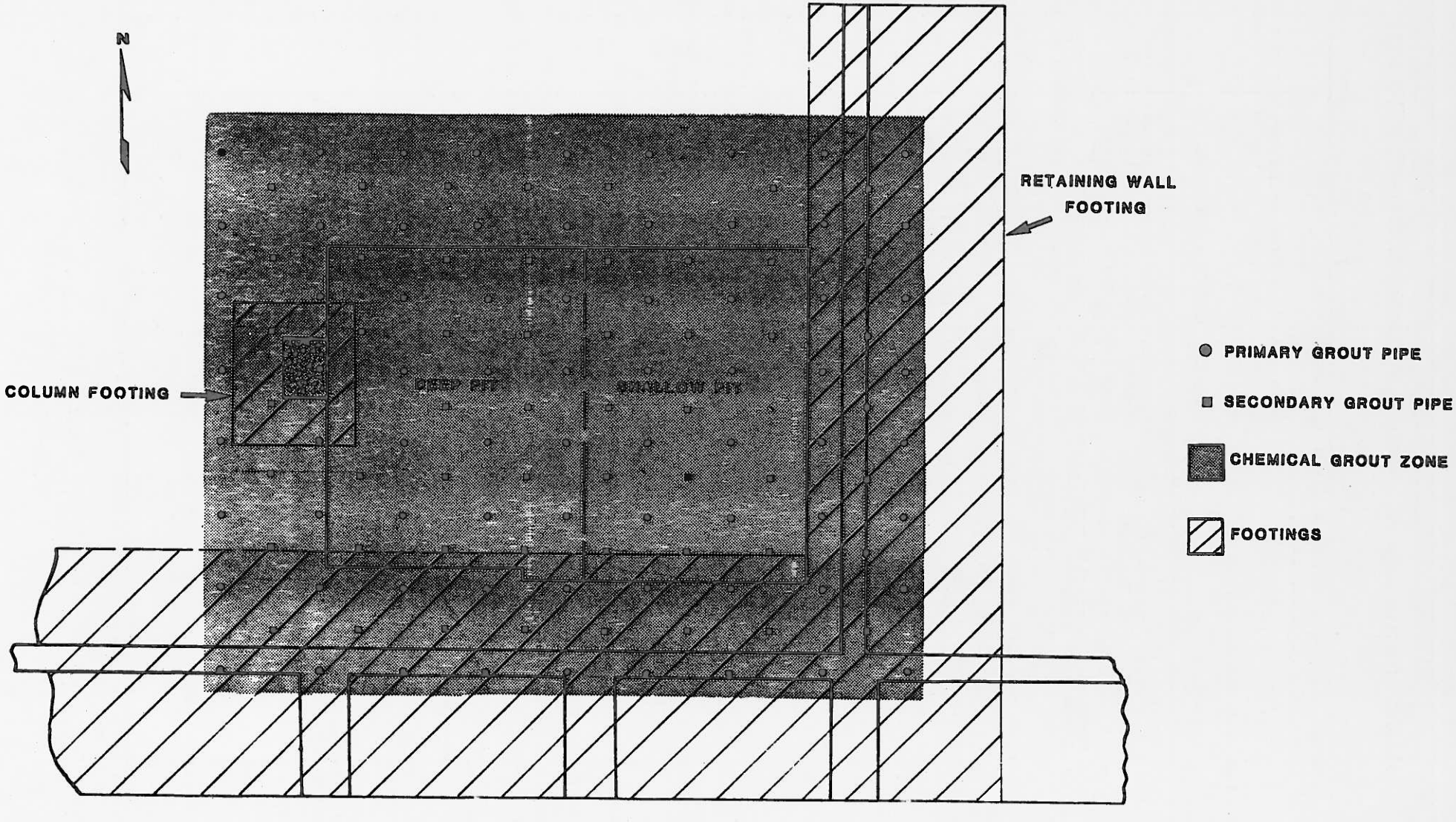

Fig. 1

GROUT HOLE LAYOUT PLAN

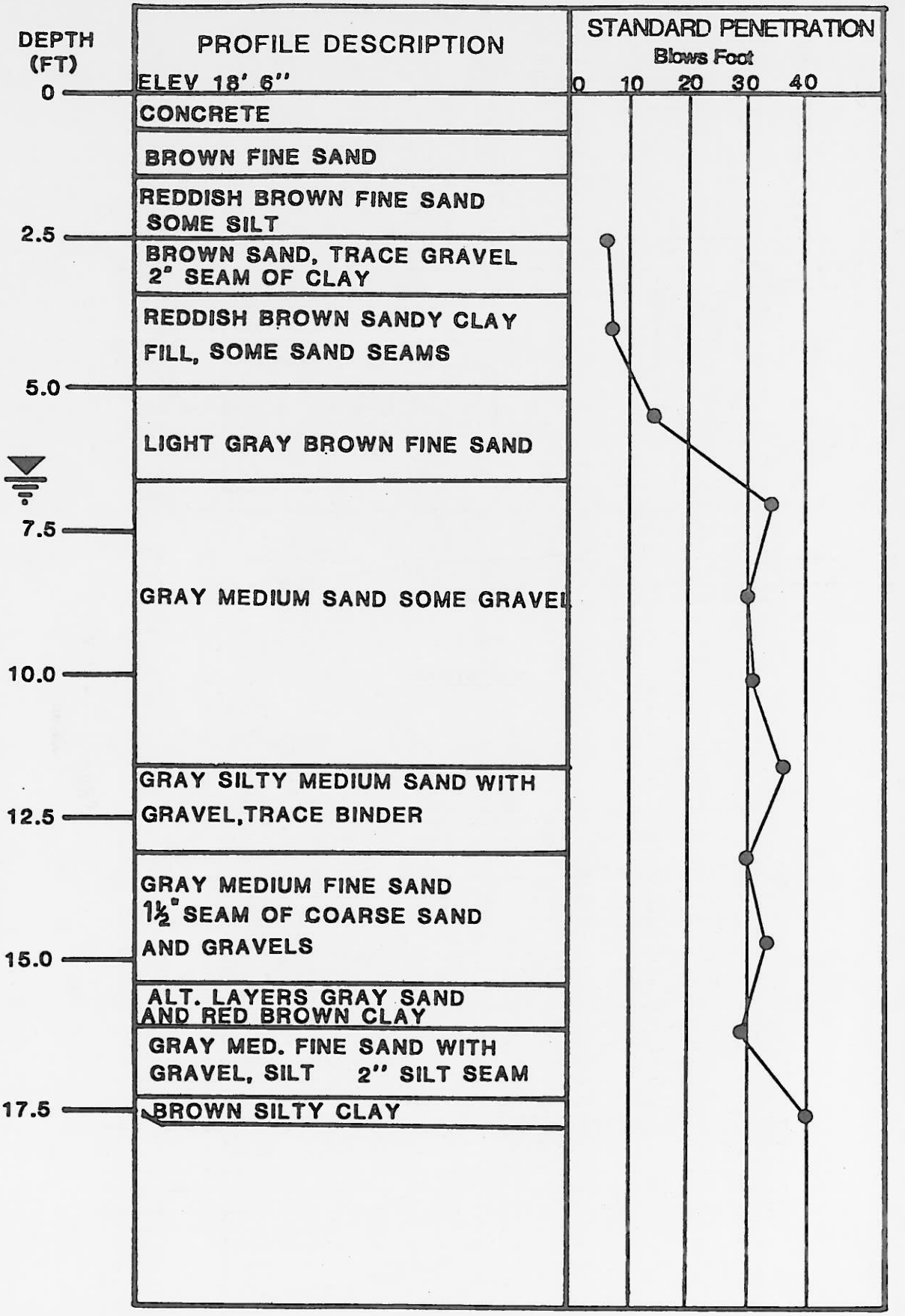

TABLE 1

BORING LOG

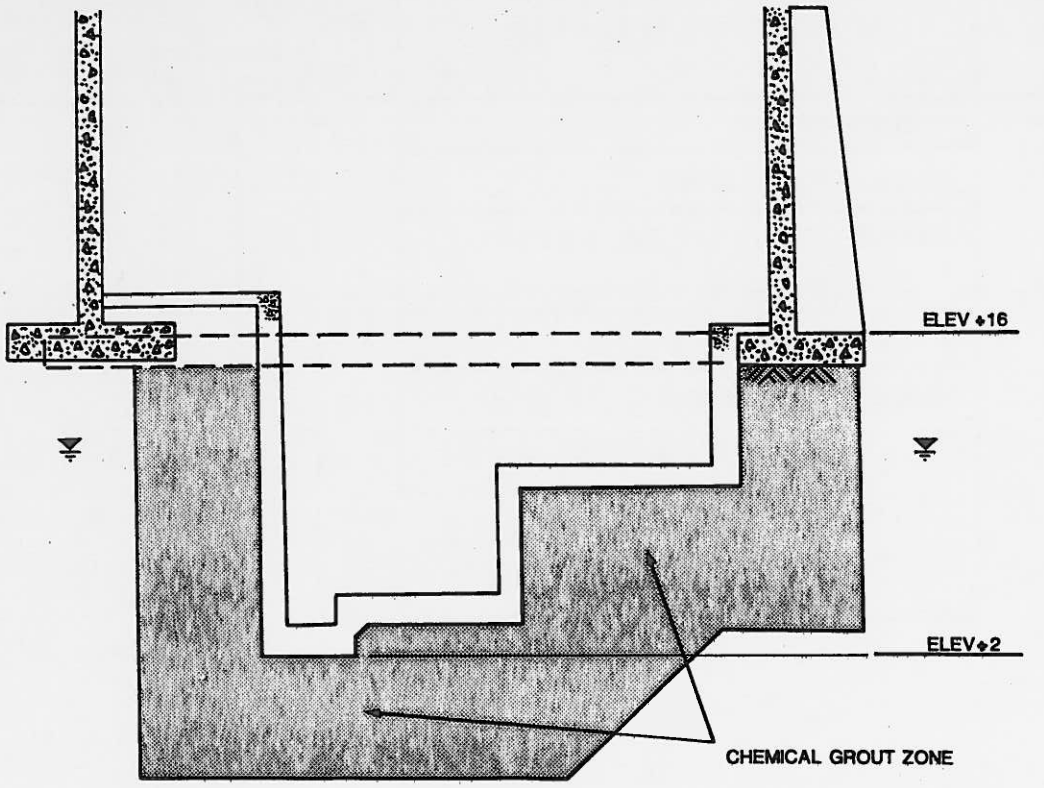

Fig. 2

CROSS SECTION

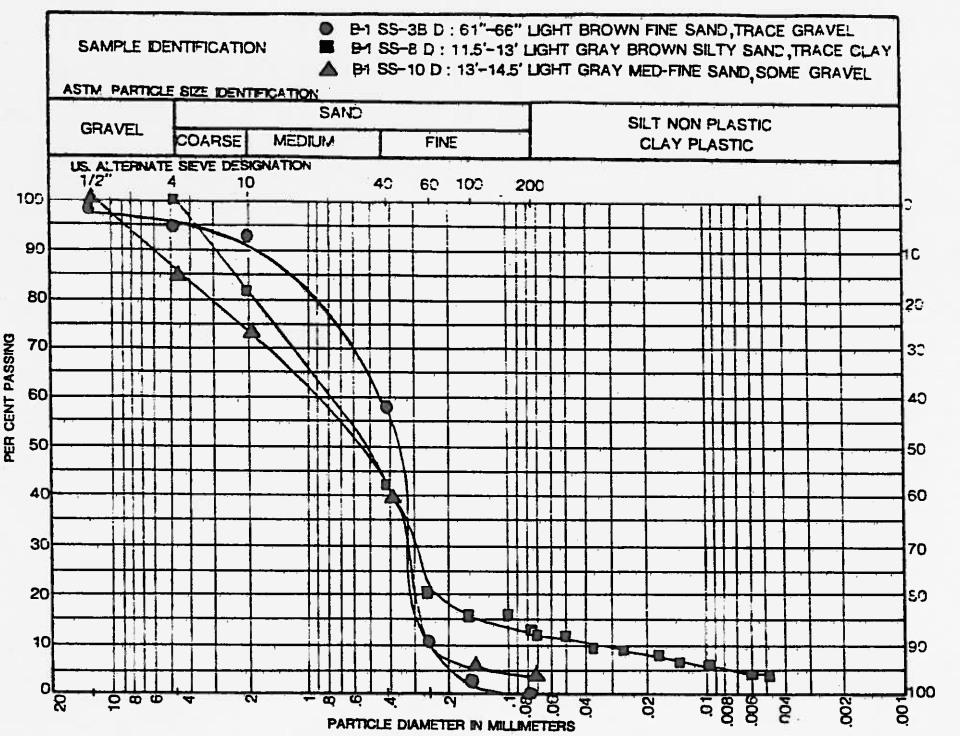

TABLE 2
SIEVE ANALYSIS

The closed end 1 1/2" diameter sleeved grout pipe was then inserted into the casing, and the casing was extracted. The mortar set in the ground forming a tight soil-like seal around the grout pipes which was easily fractured when grouting began.

The grout pipes below the footings to the east and south were placed through pre-drilled core holes in the footing.

CHEMICAL GROUT

As this project required the chemically grouted soil to be both a structural element and a water barrier, it was elected to use a sodium silicate grout which could achieve unconfined compressive strengths over 500 psi and grouted soil permeability values as low as 10-5 cm./sec. Of the many formulations of sodium silicate grout available, GELOC-4 was chosen due to its proven high strength, dependability and its non-odorous and non-toxic characteristics. It consisted of a formulation of 40% Grade N Sodium Silicate, 6% organic ester, and the remainder water with trace accelerators. This grout, as formulated, obtained average in-situ strengths of 150 psi, and had a viscosity of 4 cps with a gel time of 15 minutes at 68 degrees F. The components of GELOC-4 grout were stored in a compartmentized tanker and stream proportioned and mixed by a series of 4 parallel pumps with variable speed transmissions.

ESTIMATION OF LIQUID GROUT VOLUMES

The volume of liquid grout required to chemically solidify a given volume of granular soil is generally calculated based on the assumption that the grout must fill almost all of the soil voids, that the grout flows radially away from the injection points leaving no ungrouted zones in its path, and that some grout will penetrate beyond the idealized flat faces of the grout zone due to the generally spherical shape of the grout bulbs. This is represented in the equation

$$\text{Liquid Grout Volumes} = V\ (n \times F)\ (1 + L)$$

where V is the total volume of the treatment zone, n is the soil porosity, F is the void filling factor, and L is the loss factor for grout placed outside the treatment zone.

The porosity of granular soils may vary from 25% for very dense, well-graded silty sands to almost 50% for loose, uniform sands. The actual porosity depends upon the grain-size distribution and the relative density of the deposit.

In practice, it has been found that typical sodium silicate-based grouts fill from a minimum of about 85% of the void volume up to nearly 100% of the void volume, depending on various factors. Generally, the lower percentage of void filling occurs for well-graded sands with fines, where only a single stage or limited second stage of grouting is performed under low pressures. Some correlation seems to exist between injection pressure gradients and the percentage of void filling.

The grout loss factor may vary from about 5% to 15%, depending upon the shape of the grouting zone, the frequency of injection points per unit volume, and the presence of highly porous layers in the groutable soils.

On this project, a total of 42,000 gallons was injected while treating approximately 18,000 cu. ft. of sand.3/

MONITORING AND EVALUATION

To verify the water tightness of the grouted zone before excavation, Hayward Baker Company installed a 3" diameter well point to elevation 5. Highly concentrated dye solutions were injected outside of the grout zone. A different color was injected beyond each wall of the proposed pit and below the floor. A subsequent 24 hour pump-down test in the well point led to a steadily decreasing water level and no color traces of any kind.

Also considered for testing for this project were three non-destructive testing techniques currently emerging from Research and Development: Cross Hole Radar, Cross Hole Shear Wave Velocity, and Acoustic Emission Monitoring. Although the critical time frame on this project did not allow use on this project, they have subsequently been utilized on the largest chemical grouting project performed in the United States, underpinning on the Pittsburgh Subway project 2/ and the writer would like to digress and report on these systems and their current status.

Cross Hole Shear Wave Velocity

Dynamic shock waves are produced in the hammer hole and they are received by two in line geophones. The travel times are measured and velocities are computed. Medium strength sodium silicate grouts may double or quadruple the shear wave velocities of the impregnated soils. 4/& 5/ With the development of a down the hole hammer small enough to fit inside a sleeve pipe it is now relatively easy and economical to measure before and after shear wave velocities and efforts are now underway to convert this into unconfined compressive strengths.

Cross Hole Radar

Probes have been developed which allow placing a signal sender and receiver down adjacent sleeve pipes. By raising the sender and receiver probes simultaneously prior to grouting a radar picture depicting the various soil stratas, water table or abnormalities is developed. By repeating after grouting the uniformity of grouting is established as properly grouted soil will not permit the radar signal to pass so any radar picture produced normally shows an improperly grouted soil. The advantage of

this system is its speed of operation and therefore relatively low cost. Its major disadvantage other than the relatively high initial cost of the radar equipment and the probes is the high degree of interpretive skills of the radar needed by the operator and like most emerging systems the unexplainable results sometimes obtained.

Acoustic Emission Monitoring

This technique is becoming fairly standard in critical grouting operations to monitor Hydrofracturing. In effect, as the grout penetrates through the voids in the soil or rock, down hole tranducers can pick up the acoustic emissions produced. A sudden drop off in emissions normally indicates that the formation has been fractured and the easier paths taken by the grout is producing less noise. By stopping the grout pumping operation the formation will try to heal itself producing another telltale burst of acoustic emission.[6] Another and more far reaching use of acoustic emission in grouting and other geotechnical applications is to trace the flow of grout. Current research [7] is underway which involves placing down hole transducers in predrilled grout holes and running the grout produced acoustic emissions through an analyzed design to calculate the "x", "y", and "z" coordinates. It is hoped to be able to plot out on a field computer screen the actual path and location of the grout!

Evaluation of the Grouting Program

The excavation was begun by Gerace Construction Company of Midland, Michigan. Paving breakers and clay spades were used to trim the inside of the excavation which the contractor described as "just like sandstone." This stone-like quality led to some over confidence in the integrity of the grouted soil. It was predicted by Hayward Baker Company that come creep would occur under the heavy point loading in the northwest corner. A block of grouted soil approximately 3 cu. ft. in volume did spall off the face of the wall, but no measureable movement took place in the structures. Total ground water intrusion for the entire pit was estimated at less than 5 GPH. The pit remained opened and unsupported for approximately 4 days before the reinforced concrete walls of the pit were poured against the grouted walls of the excavation.

The chemical grout program was carried out despite severe dust, extreme heat and cramped quarters. It proved that chemical grout can be applied under adverse site conditions and performed to standards unusual in the construction industry.

CREDITS

Raymond M. Racey was Project Manager for Martin Marietta and Byron Gibbs was their Site Engineer. Donald Klinger was Project Manager and Henry James, Geotechnical Engineer for Whitman Requardt and Associates. Robert M. Rubright was Project Manager for Hayward Baker Company with Michael Cuer, Project Superintendent and Hawley Peterson, Grout Technician.

AUTHORS

Joseph P. Welsh, P.E., is Vice-President for the ground modification firm of Hayward Baker Company in Odenton, Maryland. Mr. Welsh is a member of the ASCE Committees of Grouting and he is also Chairman of the ACI Committee of Cement Grouting.

Robert M. Rubright is Project Manager for Hayward Baker Company.

Russell W. Snyder, P.E., is the Chief Engineer with Martin Marietta Chemicals Refractories Division in Hunt Valley, Maryland.

REFERENCES

1. Baker, Wallace Hayward, "Planning and Performing Structural Chemical Grouting," ASCE Specialty Conference on Grouting in Geotechnical Engineering, New Orleans, Louisiana, February, 1982, pgs. 515 - 539.

2. "Shoehorning Pittsburgh Subway," Engineering News Record, July 22, 1982, pgs. 30 - 34.

3. Baker, Wallace Hayward, "Engineering Practice" Vol. III of Design and Control of Chemical Grouting, Report No. FHWA/RD-82-038, for U.S. Dept. of Transportation, February, 1982.

4. Woodward-Clyde Consultants, Results and Interpretation of Chemical Grouting Test Program, Existing Lock and Dam No. 26, Mississippi River, Alton, Illinois, Final Report for Dept. of Army, St. Louis District, Corps of Engineers, Contract No. DACM43-78-C-0005, June, 1979.

5. Woods, R.D., Partos, A., (1981) "Control of Soil Improvement by Crosshole Testing," Proceedings X. ICSMFE, Vol. 3, pgs. 793 - 796.

6. Koerner, R.M., McCabe, W.M., Huck, P.J. and Welsh, J.P., "Hydrofracturing Monitoring Using the Acoustic Emission Method," Conference on Geotechnical and Environmental Aspects of Geopressure Energy, Sea Island, Georgia, January 13-18, 1980.

7. Koerner, R.M., Leaird, J.D., "Acoustic Emission Monitoring of Seepage:Grouting: Hydrofracturing" - National Science Foundation Program, Industry/University Cooperative Research Grant and Geotechnical Engineering Program Report due late 1982.

THE FOLLOWING PAPER WAS NOT RECEIVED IN TIME FOR PUBLICATION:

THE STANDARD PENETRATION TEST

By Charles O. Riggs